UNIVERSIDADE ESTADUAL PAULISTA "Júlio de Mesquita Filho"
FACULDADE DE ENGENHARIA DE ILHA SOLTEIRA
PROGRAMA DE PÓS-GRADUAÇÃO EM ENGENHARIA MECÂNICA

MSc. Eli Jorge da Cruz Junior

APPLICATION OF NICKEL AS METAL ADDITION IN THE UNION OF UNS S32750 SUPERDUPLEX STEEL PLATES WITH Nd: YAG PULSED LASER WELDING

Ilha Solteira

2020

UNIVERSIDADE ESTADUAL PAULISTA "Júlio de Mesquita Filho"
FACULDADE DE ENGENHARIA DE ILHA SOLTEIRA
PROGRAMA DE PÓS-GRADUAÇÃO EM ENGENHARIA MECÂNICA

MSc. Eli Jorge da Cruz Junior

APPLICATION OF NICKEL AS METAL ADDITION IN THE UNION OF UNS S32750 SUPERDUPLEX STAINLESS STEEL PLATES WITH Nd: YAG PULSED LASER WELDING

Tese apresentada à Faculdade de Engenharia - UNESP - Campus de Ilha Solteira, para obtenção do título de Doutor em Engenharia Mecânica.
Área de conhecimento: Materiais e Processos de Fabricação.

Prof. Dr. Vicente Afonso Ventrella
Orientador
Profª. Drª. Irene Calliari
Orientadora (Cotutela)

Ilha Solteira

2020

FICHA CATALOGRÁFICA
Desenvolvido pelo Serviço Técnico de Biblioteca e Documentação

C957a

Cruz Junior, Eli Jorge da.
Application of nickel as metal addition in the union of UNS S32750 superduplex steel plates with Nd: YAG pulsed laser welding / Eli Jorge da Cruz Junior. -- Ilha Solteira: [s.n.], 2020
97 f. : il.

Tese (doutorado) - Universidade Estadual Paulista. Faculdade de Engenharia de Ilha Solteira. Área de conhecimento: Materiais e Processos de Fabricação, 2020

Orientador: Vicente Afonso Ventrella
Coorientadora: Irene Calliari
Inclui bibliografia

1. Soldagem laser. 2. Aços inoxidáveis duplex. 3. Adição de níquel. 4. Resistência à corrosão. 5. Propriedades mecânicas. 6. Microestrutura.

Raiane da Silva Santos
Supervisora Técnica de Seção
Seção Técnica de Referência, Atendimento ao Usuário e Documentação
Diretoria Técnica de Biblioteca e Documentação
CRB/8- 9999

unesp

UNIVERSIDADE ESTADUAL PAULISTA

Câmpus de Ilha Solteira

CERTIFICADO DE APROVAÇÃO

TÍTULO DA TESE: APPLICATION OF NICKEL AS METAL ADDITION IN THE UNION OF UNS S32750 SUPERDUPLEX STEEL PLATES WITH Nd:YAG PULSED LASER WELDING

AUTOR: ELI JORGE DA CRUZ JUNIOR
ORIENTADOR: VICENTE AFONSO VENTRELLA

Aprovado como parte das exigências para obtenção do Título de Doutor em ENGENHARIA MECÂNICA, área: Materiais e Processos de Fabricação pela Comissão Examinadora:

Prof. Dr. VICENTE AFONSO VENTRELLA
Departamento de Engenharia Mecânica / Faculdade de Engenharia de Ilha Solteira - UNESP

Prof. Dr. ANTONIO DE PADUA LIMA FILHO
Departamento de Engenharia Mecânica / Faculdade de Engenharia de Ilha Solteira - UNESP

Prof. Dr. JUNO GALLEGO
Departamento de Engenharia Mecânica / Faculdade de Engenharia de Ilha Solteira - UNESP

Profª Drª IRENE CALLIARI
Dipartimento di Ingegneria Industriale / Università Degli Studi di Padova

Prof. Dr. ANDREA ZAMBON
Dipartimento di Tecnica e Gestione dei Sistemi Industriali / Università Degli Studi di Padova

Ilha Solteira, 19 de fevereiro de 2020

ACKNOWLEDGEMENTS

First, thank God, source of all wisdom and knowledge.

To São Paulo State University – UNESP, where I have studied since 2005, for the opportunity to develop my doctorate.

To University of Padua for enabling the cotutelle process and receiving me on PhD program.

To Federal Institute of São Paulo (IFSP) for allowed me to dedicate full time for the doctorate.

To Prof. Dr. Vicente Afonso Ventrella for all help, guidance and support throughout the doctorate.

To Profª. Drª. Irene Calliari for receiving me in the Department of Industrial Engineering - University of Padua, and for the guidance throughout the doctorate.

To Coimbra Group for its financial support as part of the scholarship program “Young professors and researchers from Latin America” that allowed the internship at Department of Industrial Engineering – University of Padua

To my wife Taiele Cruz for always being by my side supporting and encouraging me even in the most difficult times.

To my parents Eli Cruz and Vanda Cruz, for the legacy they left me. Everything I am I owe you.

To my second parents Paulino e Perpétua, for all the support.

To my brothers, sisters-in-law and nephews. Thanks for everything.

To my friends Alessandro and Sandra Zilio and their family for all the help during my stay in Italy, your help was essential. “Grazie mille”.

To Alessio Settimi, Claudio Gennari, Luca Pezzato and Mattia Lago from Department of Industrial Engineering (DII) of University of Padua.

To all those who contributed directly or indirectly to the development of this work and who, by mistake, forgot to mention.

“The fear of the LORD is the beginning of wisdom”

RESUMO

Os aços inoxidáveis duplex (AID) são caracterizados por uma microestrutura bifásica composta por proporções semelhantes de austenita e ferrita, que promovem excelente resistência mecânica e resistência à corrosão. Normalmente, após ser submetido a processos de soldagem, o AID apresenta uma microestrutura desbalanceada, predominantemente ferrítica, que compromete suas propriedades. O objetivo deste trabalho é investigar o efeito do uso de chapas finas de níquel eletrolítico com diferentes espessuras como metal de adição na soldabilidade da junta através da análise da microestrutura, microdureza, resistência à tração e resistência à corrosão do AID UNS S32750 soldado pelo processo laser pulsado Nd:YAG. Foram utilizadas seis condições de soldagem: soldagem autógena e com adição de níquel. Houve uma melhora na soldabilidade com a adição de níquel, permitindo obter porporções iguais de austenita e ferrita no cordão de solda, consequentemente boas propriedades mecânicas e resistência à corrosão. O aumento da adição de níquel aumentou a proporção de fase da austenita e diminuiu a microdureza. A resistência à tração foi pouco afetada adição de níquel.

Palavras-chave*:* Soldagem laser. Aços inoxidáveis duplex. Adição de níquel. Resistência à corrosão. Propriedades mecânicas. Microestrutura.

RIASSUNTO

Gli acciai inossidabili superduplex (SDSSs) sono caratterizzati da una microstruttura bifasica costituita da un'uguale frazione volumetrica di ferrite ed austenite. Ciò porta ad ottenere migliori proprietà meccaniche e di resistenza a corrosione Il processo di saldatura porta ad uno sbilanciamento della microstruttura, con prevalenza della ferrite, che conduce alla compromissione delle proprietà dell'acciaio superduplex. Lo scopo di questo lavoro di tesi consiste nello studio dell'effetto dell'aggiunta di un film sottile di nickel elettrolitico a differenti spessori sulla saldabilità del materiale. Sono state valutate, quindi, la microstruttura, la durezza, la resistenza a trazione e quella a corrosione dell'acciaio UNS S32750 SDSS saldato impiegando un laser Nd:YAG pulsato. Sono state considerate sei condizioni: saldatura autogena e saldatura in presenza del film di nichel a differenti spessori. E' stato dimostrato che l'aggiunta di un film sottile di nichel comporta un miglioramento della saldabilità del materiale, permettendo di ottenere un buon bilanciamento dell'austenite e della ferrite nel giunto saldato, così come una buona resistenza meccanica ed a corrosione. Spessori grossi del film, quindi un'elevata concentrazione di nichel, comportano l'aumento della frazione volumetrica dell'austenite a discapito della ferrite nel giunto saldato. Ciò comporta una minor durezza. La resistenza meccanica è leggermente influenzata dall'aggiunta di nichel.

Parole chiave*:* Saldatura laser. Acciai inossidabili duplex. Aggiunta di nichel. Resistenza alla corrosion. Proprietà meccaniche. Microstruttura.

ABSTRACT

Super duplex stainless steels (SDSSs) are characterized by a biphase microstructure consisting of equal volume fractions of FCC austenite and BCC ferrite, which promotes excellent mechanical strength and corrosion resistance. Welding process results in an unbalanced microstructure, with large amount of ferrite, which compromise SDSS's properties. The aim of this work is to investigate the effect of using electrolytic nickel thin foils with different thickness as an addition metal on the weldability through the evaluation of the microstructure, microhardness, tensile strength and corrosion resistance of UNS S32750 SDSS welded by the Nd:YAG pulsed laser welding. Six welding conditions were used: autogenous welding and with addition of nickel. There was an improvement on the weldability with the nickel addition allowing to obtain well balanced austenite-ferrite microstructure in the weld bead, as well as good mechanical properties and corrosion resistance. Thicker foils, hence nickel amount, have promoted increasing of the austenite volume fraction and the lower microhardness. The tensile strength was slightly affected s with larger nickel addition.

Keywords*:* Laser welding. Duplex stainless steel. Nickel addition. Corrosion resistance. Mechanical properties. Microstructure.

LIST OF FIGURES

LIST OF TABLES

LIST OF SYMBOLS

σ – Sigma phase

χ – Chi phase

α – Alfa ferrite

δ - Delta ferrite

γ - Austenite

LIST OF ABBREVIATIONS

ABINOX – Associação Brasileira do Aço Inoxidável

ABNT – Associação Brasileira de Normas Técnicas

AID – Aço Inoxidável Duplex

AISI – American Iron and Steel Institute

ASS – Austenitic Stainless Steel

BCC – Body-Centered Cubic

CPT – Critical Pitting Temperature

DSS – Duplex Stainless Steel

EB – Electron Beam

EDS - Energy-Dispersive X-ray

FCC – Face-Centered Cubic

FSS – Ferritic Stainless Steel

GTAW – Gas Tungsten Arc Welding

HAZ – Heat Affected Zone

ISSF – International Stainless Steel Forum

Nd:YAG - Neodymium-doped Yttrium Aluminum Garnet

PREN – Pitting Resistance Equivalent Number

SAW – Submerged-Arc Welding

SDSS – Super Duplex Stainless Steel

SEM – Scanning Electron Microscope

UNS – Unified Numbering System

CONTENTS

1 INTRODUCTION

Duplex stainless steels (DSS) are characterized by a biphase microstructure composed by similar proportions of FCC austenite and BCC ferrite, which promotes excellent mechanical strength and corrosion resistance [1]. These alloys are about twice as strong as austenitic steels [2]. Due to their excellent properties, these steels have a wide range of applications in the chemical, oil and gas, petrochemical, pulp and paper, offshore and marine industries [3]

Is not easy to select the DSS welding process for the proportion of austenite and ferrite should not be affect during the welding. Normally, after being subjected to welding processes, DSS presents an unbalanced microstructure, predominantly ferritic, which compromises its properties, especially local pitting corrosion resistance and toughness [4]. Arun et al. [5] have stated that to obtain the optimal phase balance in the fusion zone is a hard and yet unsolved challenge.

The Nd:YAG pulsed laser welding process offers some advantages over conventional processes namely process accuracy, complex shape welding, short cycle time, low heat input [3]. Ventrella et al. [6] concluded that Nd:YAG pulsed laser is the better welding processing when precise heat input control and lower heat-affected zone (HAZ) are required. Low heat input and high cooling rates, which are typical of the process, promote the formation of BCC ferrite which results in an undesired microstructure for most applications [7]. To obtain a balanced microstructure, alternatively (or in combination) a post-weld heat treatment or add strong austenite-forming elements to the welding pool, such as nickel or nitrogen, might prove useful.

In the literature, there are several studies concerning the effects of nickel and its addition on phase balance for certain welding processes, e.g., gas tungsten arc welding, electron beam welding, and plasma welding. Muthupandi et al. [8] studied the influence of nickel and nitrogen addition on the microstructure and mechanical properties of power laser beam processed DSS

weld metals. Migiakis and Papadimitriou [9] made a similar study but applied to plasma welding. Pilhagen and Sandström [10] have investigated the role of nickel on the toughness of lean DSS weld metal prepared by submerged arc welding (SAW). Tahaei et al. [11] studied the effect of nickel and post weld heat treatment applied to gas tungsten arc welding (GTAW). Zhang et al. [12] also have worked with GTAW but given emphasis on nitrogen as the shielding gas. Related to the Nd:YAG pulsed laser process it's hard to find results in literature.

1.1 OBJECTIVES

The Nd:YAG pulsed laser welding characteristics e.g., low heat input, short cycle time, high cooling rates, make adding alloying elements, whether as filaments or shielding gas, very difficult. Find a way to add austenite-promoting is very important to make this laser welding process applicable to duplex stainless steels

Due to the importance of phase balance to the properties of DSS and in its applications, this work studied the effect of using electrolytic nickel foil, as an addition metal, on the microstructure, mechanical properties and corrosion resistance of UNS S32750 DSS welded by the Nd:YAG pulsed laser.

Considering influence of nickel on the properties of DSS and its applications and the fact that the addition of nickel could improve the Nd:YAG pulsed laser welding, the specific objectives of this work are to:

- Perform the microstructural characterization on the weld bead for the different conditions studied;
- Determine the phase balance on the weld bead;
- Obtain the microhardness profile;
- Measure tensile strengths;
- Evaluate the corrosion resistance

2 LITERATURE REVIEW

2.1 STAINLESS STEEL

Stainless steels are alloys that have emerged to meet the demands of corrosion resistant materials. The word steel means that iron constitutes the bulk of the material, while the adjective “stainless” implies absence of staining, rusting or corroding in environments where normal steels are susceptible [13].

To achieve such strength it is necessary that stainless steels have in their composition at least 11% by weight of chrome [14]. In contact with atmospheric air, or another oxidizing environment, chromium oxidizes, forming a corrosive resistant layer. This process is called passivation (Figure 1).

Figure 1 – Passivation process

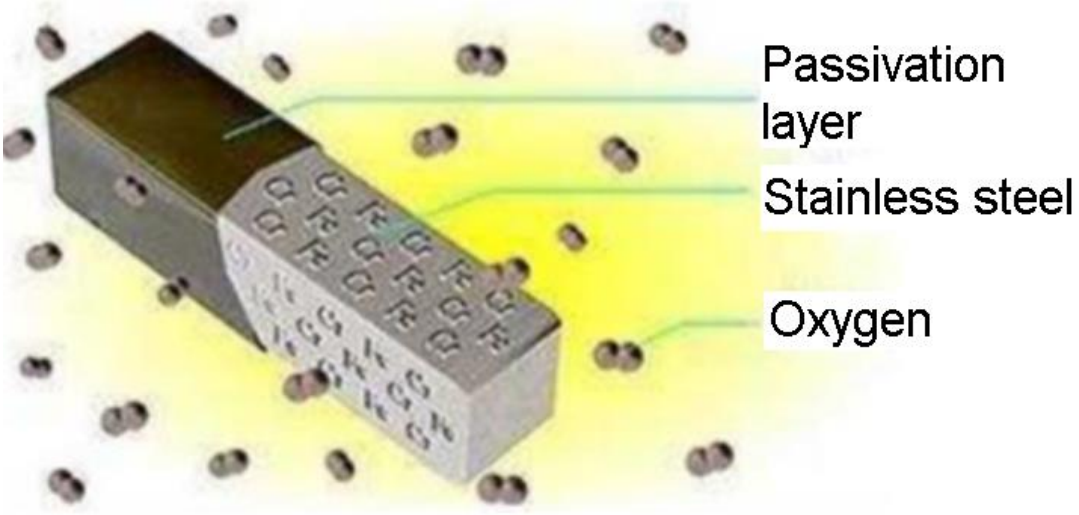

Souce: LIMA [15] modified

According to the International Stainless Steel Forum (ISSF) [16] and the “Associação Brasileira do Aço Inoxidável” (ABINOX) [17], in 2018, the stainless steel worldwide production was about 51 millions of tons and in Brazil 333 thousands of tons, as shown in Figure 2 and Figure 3.

Figure 2 - Stainless steel worldwide production (millions of tons)

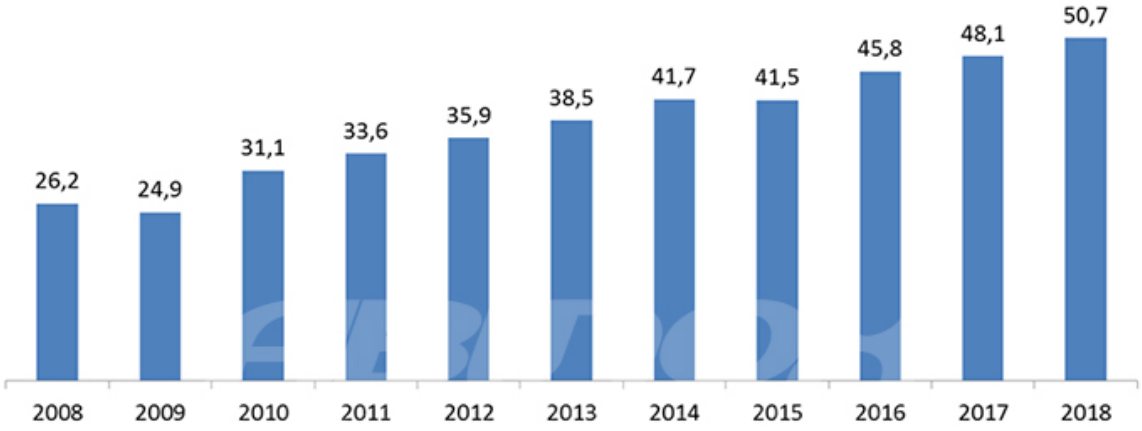

Source: ISSF [16]

Figure 3 - Stainless steel Brazilian production (thousands of tons)

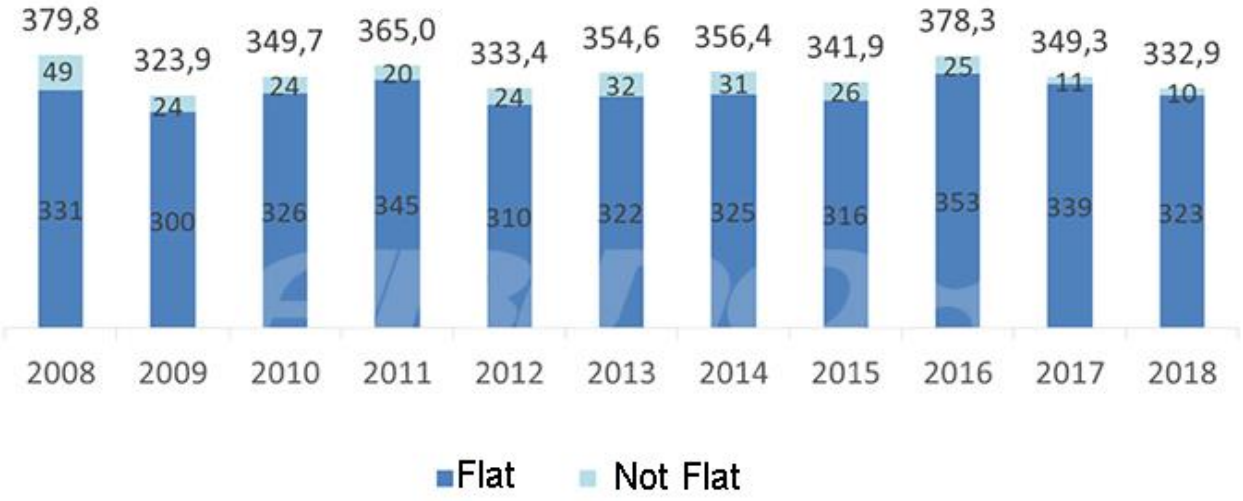

Source: ABINOX [17]

In general, the essential requirements for an alloy used in industries Oil & Natural Gas and offshore industry are mechanical strength, given the various stresses to which materials will be subjected, and corrosion resistance due to the environmental severity to which the materials will be exposed. Components and equipment in these industries are often subjected to high temperatures and contact with extremely corrosive or abrasive-containing fluids. The new

discoveries of Brazilian industry called Pre-Salt represent a group of operations that will require the use of high mechanical performance and corrosion resistant materials, and also welding processes capable of ensuring good quality of the welded joint. DSS is gaining more and more space in the petrochemical industry precisely because of the above requirements [18].

2.1.1 Classification of Stainless Steels

Stainless steels can be classified with reference to their microstructure presented at room temperature. According to this criterion, stainless steels can be divided into four classes: ferritic, martensitic, austenitic and duplex.

Ferritic Stainless Steel

,

Ferritic stainless steel (FSS) is one type of stainless steels developed contemporaneously with austenitic and martensitic stainless steel and it occupies 40%–50% of the whole stainless steel yield. FSS exhibits excellent weldability, corrosion resistance and thermal fatigue performance [19].

They have between 10.5 and 30% of chromium with low carbon (maximum 0.2%), presents a body-centered cubic (BCC) structure. They cannot be austenitized therefore cannot be hardened by quenching. They are considered more economical than austenitic stainless steels because they do not contain high levels of nickel in their composition [20].

They present satisfactory toughness and ductility, but when subjected to welding process, grain growth may occur in the HAZ and precipitation of deleterious phases on grain boundaries, such as chromium carbides and nitrides. The combination of these effects compromises toughness and corrosion resistance.

There are a variety of FSS, and because of their low cost, good formability, and ceramic-like thermal expansion coefficient, they have also been used in the manufacturing of solid oxide fuel cell components [21]. To exemplify the microstructure of FSS, typical polygonal ferrite grains of AISI 444 FSS after cold rolling and annealing at 880 ºC is presented in Figure 4.

Figure 4 – Microstructure of AISI 444 FSS

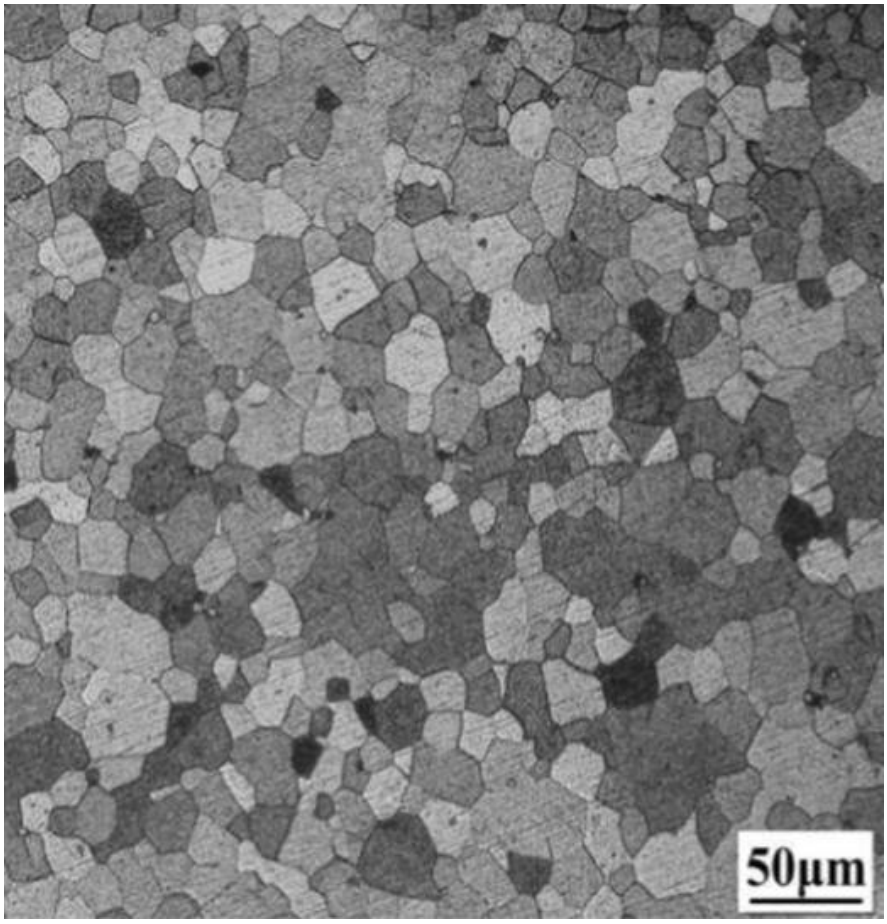

Source: Bai et al. [19]

Martensitic Stainless Steel

Martensitic stainless steels are Fe-Cr-C alloys, which have compositions ranging from 10.5 to 18% chromium, from 0.1 to 0.5% carbon. They may have Mo, W, V, or Ni additions in small quantities to improve creep resistance under

high temperature conditions and also to the addition of other austenite stabilizing elements for partial carbon replacement, improving their corrosion resistance. They are ferromagnetic and can be hardened by quenching [22].

These alloys can be austenized when heated to a suitable (sufficiently high) temperature. The cooling rate is responsible for turning austenite into other products. At low speed cooling conditions, ferrite and carbides are formed, while under high speed conditions the martensite is formed [14]. To exemplify the microstructure of martensitic stainless steels, Figure 5 shows an optical micrograph of AISI S410-L, an equiaxed fine grain structure morphology is observed. The manufacturing processes involved in the production of commercially available martensitic stainless steels include thermo-mechanical treatment with final hot-rolling and annealing, explaining the microstructure

Figure 5 – Microstrucutre of AISI S410-L

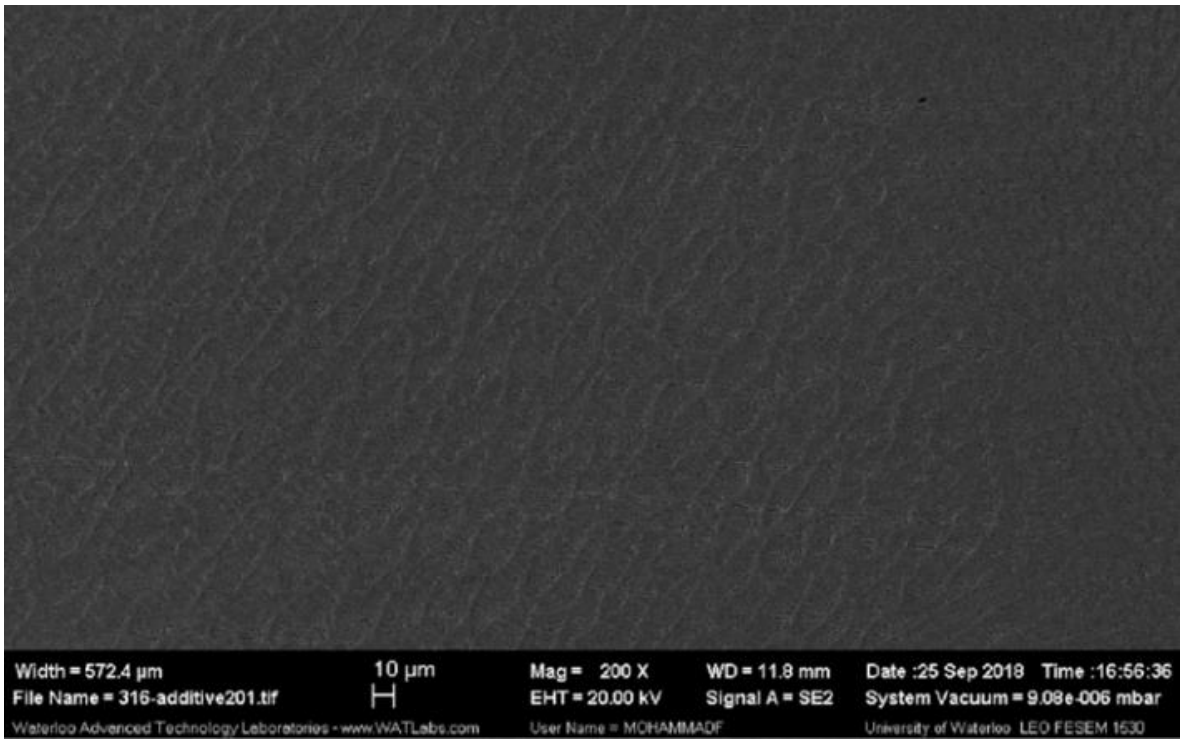

Source: Khodabakhshi et. al. [23]

Austenitic Stainless Steel

Austenitic Stainless Steels (ASSs) are mainly Fe-Cr-Ni alloys, with the predominance of an austenitic microstructure (γ). Cr is responsible for ensuring corrosion resistance, while Ni provides the extension of the austenitic region at room temperature. ASSs exhibit good resistance to corrosion and oxidation at temperatures up to 650 °C or higher. These steels also exhibit excellent ductility and toughness in this temperature range. Corrosion and oxidation resistance is imparted primarily by high chromium content, generally greater than 16 wt% [24]. The addition of austenite-stabilizing elements, primarily carbon and nickel and sometimes nitrogen, promotes an austenitic structure over a wide range of temperatures. In some alloys, austenite is stable from room temperature to the melting temperature range. The predominance of an austenitic structure in these steels gives rise to their excellent ductility and toughness [25].

The wide utilization of plain austenitic stainless steels, due to both their satisfactory corrosion resistance and their cost-effectiveness, has led to studies and researches concerning their applications in a variety of situations and environments, so that a satisfactory amount of data is available concerning their shaping, welding (even with high power density facilities) and eventually post weld heat treatments. Actually, superaustenitic stainless steels are being used because they bridge between relatively cheap austenitic stainless steel and expensive nickel base super alloys, when high corrosion properties are required at moderately high temperatures [26]. To exemplify an austenitic microstructure, Figure 6 shows an SEM micrograph of AISI 316L ASS. Polygonal austenitic grains are identified by greek letter γ.

Figure 6 – Microstrucutre of AISI 316L ASS

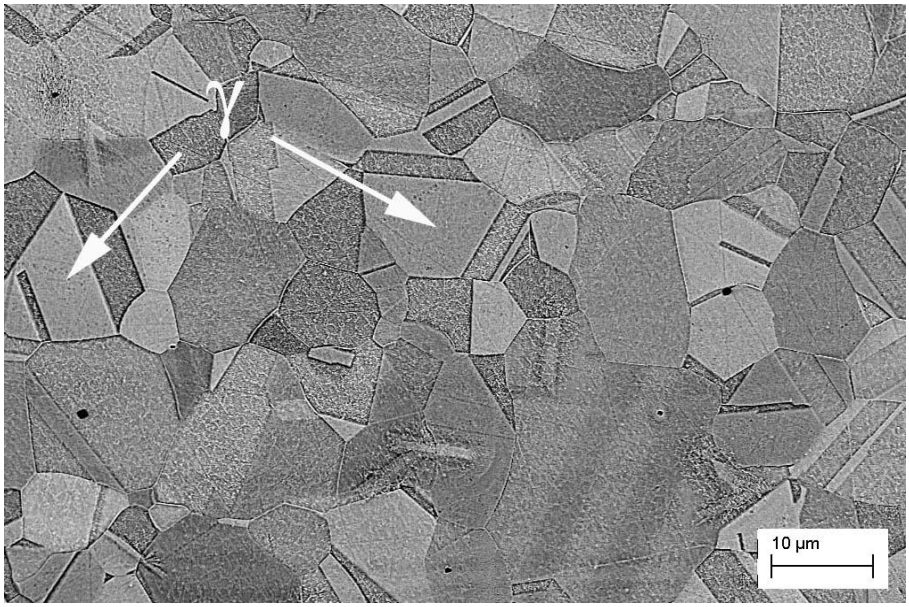

Source: Leite et. al. [26]

Duplex Stainless Steel

Duplex stainless steel (DSS) has a biphasic microstructure with equal proportions of austenite (γ) and ferrite (α), which gives it excellent mechanical strength and corrosion resistance compared with austenitic stainless steel. DSSs are best suited for robust heavy engineering industrial applications viz., mining, petrochemical, engine, marine, pulp & paper industries [3].

Duplex stainless steels, such as UNS S32750 are often used in aggressive corrosion environments where service temperatures are below approximately 350 ° C. These steels contain 24 – 26% Cr, 5 – 8% Ni, 3 – 5% Mo and 0.2 – 0.3% N. They have good resistance to chloride stress corrosion cracking, pitting and crevice corrosion. The corrosion behavior of the weld metal of these steels is largely controlled by the microstructure balance of ferrite and austenite with an approximate 50%–50% balance providing optimum corrosion resistance [26]. To exemplify the microstructure of DSS, Figure 7 shows an SEM micrograph of UNS S32750 DSS. Similar proportions of austenite (γ) and ferrite (α) are observed.

Figure 7 – Microstrucutre of UNS S32750 DSS

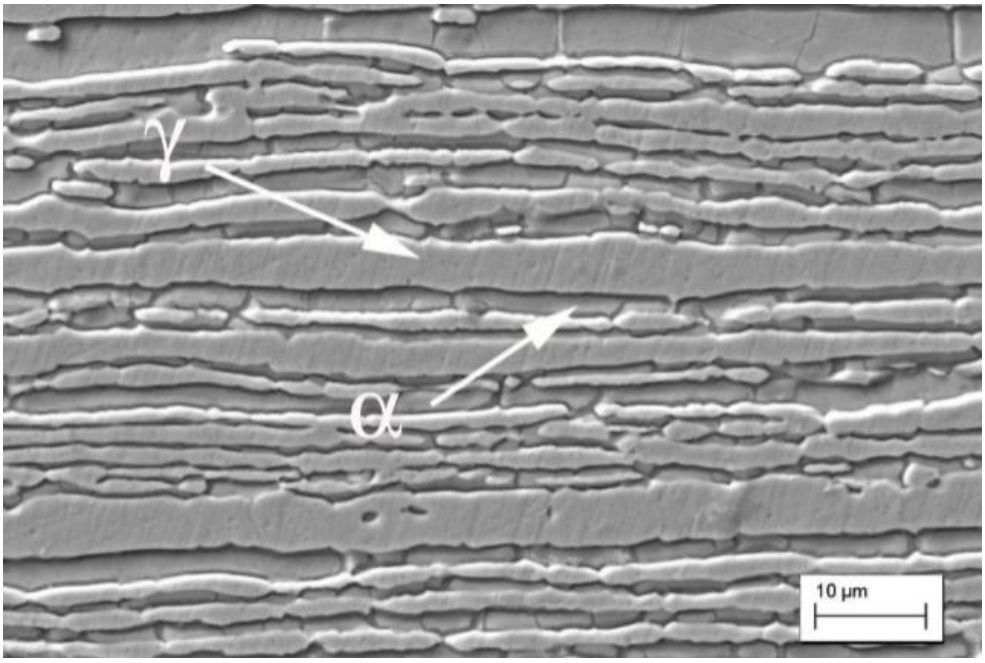

Source: Leite et. al. [26]

A way to rank pitting susceptibility in DSS is using the pitting resistance equivalent number (PREN) as presented in Equation 1 [27].

$$PREN = wt.\%Cr + 3.3\ wt.\%Mo + 16\ wt.\%N \quad \text{Eq. 1}$$

Pitting corrosion is an extremely localized corrosion that leads to the creation of small holes in the metal. The diameter of the pits is less than its depth. A characteristic of pitting corrosion is the presence of pits formed as a result of an interaction between a passive film (cathode) and locally depassivated regions (anodes) on the surface of the material [28, 29].

The role of an anode can be played by internal inhomogeneities (non-metallic inclusions, separations, deformations) and by external inhomogeneities such as, scratches and edges. Low welding energy can lead to nitride precipitation. Chromium nitride particles are also believed to be nucleation for pitting [30, 31].

Chemical composition also has crucial influence on the pitting corrosion resistance of stainless steel [29]. Table 1 summarizes the influence of some alloying elements on pitting resistance.

Table 1 – Influence of alloying element on the pitting corrosion resistance

Element	**Pitting corrosion resistance**
Chrome	Increase
Nickel	Increase
Molybdenum	Increase
Silicon	Decrease; Increase when in combination with Molibidenium
Sulfur and Selenium	Decrease
Carbon	Decrease
Nitrogen	Increase

Source: Elaborated by author

Figure 8 exemplify a pitting corrosion. A laser welded DSS was submitted to Critical Pitting Temperature (CPT) test, and the pitting occurred on the weld bead.

Figure 8 - Pitting corrosion on laser welded DSS

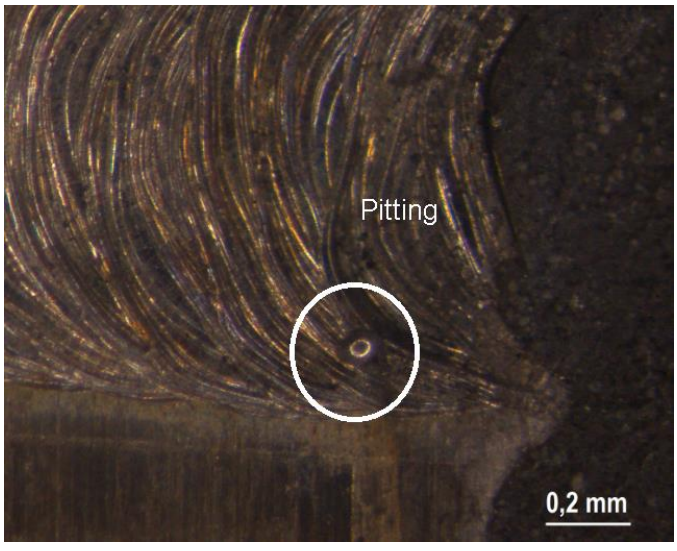

Source: Elaborated by author

The difference between DSS and super duplex stainless steel (SDSS) beyond the concentration of alloying elements is their PREN. DSS has PREN between 30 and 40, while SDSS has PREN above 40 [13].

2.1.2 Alloying Elements in Stainless Steels

The steel chemical composition and environment oxidizing capacity influence its corrosion resistance. Alloying elements modify this resistance and may be associated with increased or decreased of phase formation [32].

Alloying elements present in stainless steels may be associated with the stabilization of ferrite or austenite. Chromium, molybdenum, titanium, silicon, aluminum, niobium, vanadium, tungsten and boron are examples of ferrite-forming elements. Nickel, copper, carbon, nitrogen, manganese and cobalt are austenite-forming elements. Each of these elements may alter the characteristics of stainless steels in a specific way [33]. Figure 9 shows a histogram of the relative strengths of alloying elements in steels in terms of enthalpy (H). Ferrite formers are listed in (a) and austenite in (b).

Figure 9 - Relative force of alloying elements (a) ferrite formers (b) austenite formers

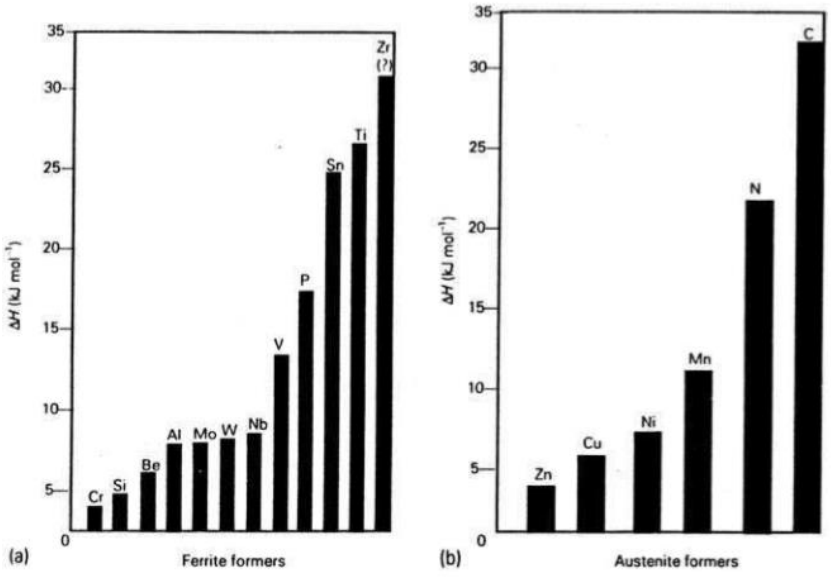

Source: Honeycombe [34]

Modenesi [33] summarized the main effects of alloying elements and impurities on stainless steels. The nickel effect will be discussed in a specific topic.

- Aluminum: Ferrite and nitride former. Used with titanium may cause precipitation hardening;
- Carbon: Austenite former. Increases mechanical strength and hardness but affects corrosion resistance and toughness at low temperature;
- Cobalt: Increases mechanical strength and creep at elevated temperatures;
- Chrome: Ferrite and carbide former. Main element responsible for increased corrosion resistance;
- Manganese: Austenite former. Increases crack resistance of weld with austenitic structure;
- Molybdenum: Ferrite and carbide former. Increases corrosion resistance and creep at elevated temperatures. Improves corrosion resistance in non-oxidizing environ;
- Niobium: Ferrite and carbide former. May cause precipitation hardening;
- Nitrogen: Austenite former. May be responsible for increasing mechanical strength but also strongly degrading the weldability of ferritic alloys;
- Silicon: Ferrite former;
- Titanium: Ferrite, carbide and nitride former. Improves mechanical resistance at high temperature. With aluminum it causes precipitation hardening.
- Copper: Increases corrosion resistance in reducing environ.
- Tungsten: Element considered as strong ferrite former. Increases mechanical strength and creep at elevated temperatures

The Schaeffler-Delong diagram (Figure 10) summarizes the effect of the alloying elements on the structure of stainless steels. The diagram is based on

the fact that the alloying elements can be divided into ferrite-stabilizers and austenite-stabilizers. Relating the austenite-stabilizers to nickel and ferrite-stabilizers to chromium, it becomes possible to calculate the total ferrite and austenite stabilizing effect of the alloying elements in the steel. This gives the so-called chromium and nickel equivalents in the Schaeffler-Delong diagram. In this way it is possible to take the combined effect of alloying elements into consideration.

Figure 10 – Schaeffler-Delong diagram

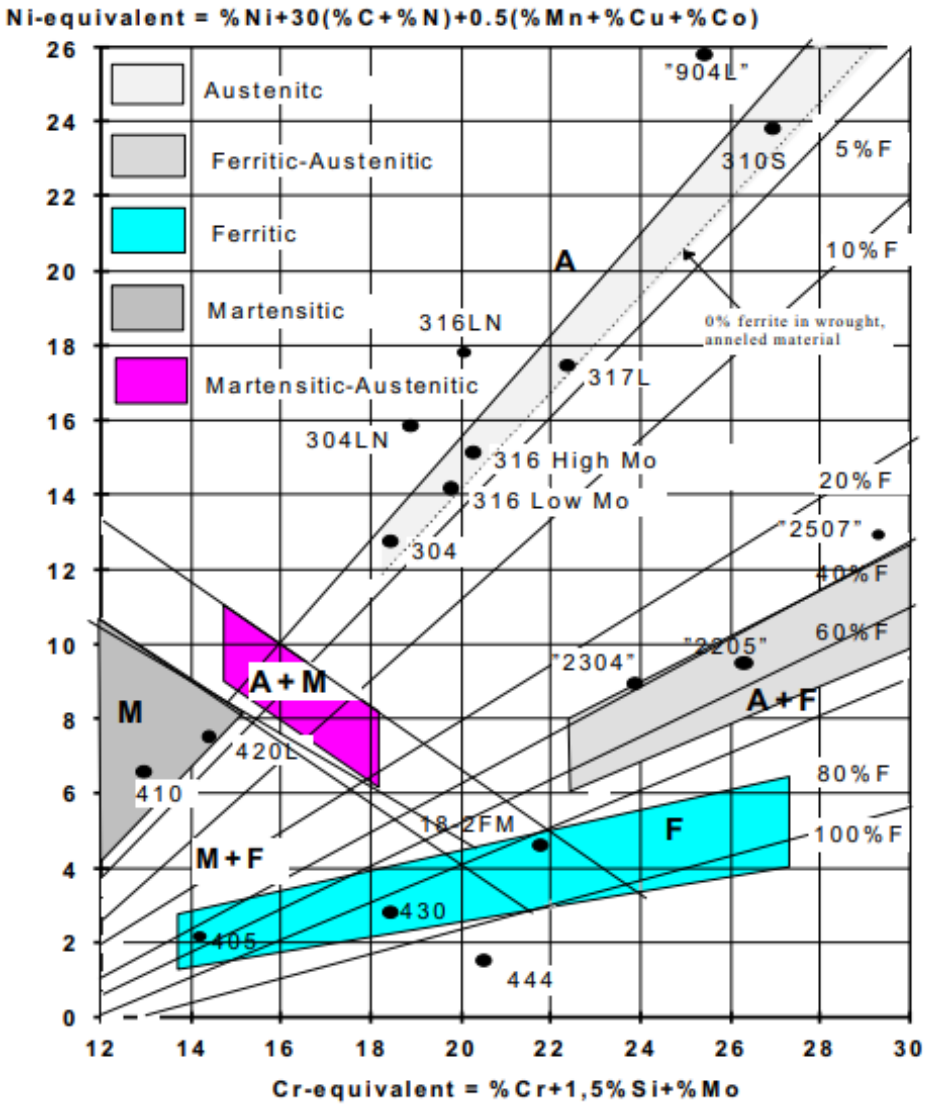

Source: Rostfria [35]

The Schaeffler-Delong diagram was originally developed for weld metal; it describes the structure after melting and rapid cooling. The Schaeffler-Delong diagram is not the only diagram for assessment of ferrite contents and structure of stainless steels.

Nickel

Nickel is an austenite former. Increases corrosion resistance in non-oxidizing environment. Muthupandi et al. [8] stated that the addition of Ni increases the austenite amount in the weld metal by increasing its initial transformation temperature, promoting the equilibrium of its content.

DSS are based on the ternary Fe–Cr–Ni phase diagram (Figure 11). It`s clear that the higher amount of nickel will expands austenite field.

Figure 11 - Ternary Fe–Cr–Ni phase diagram

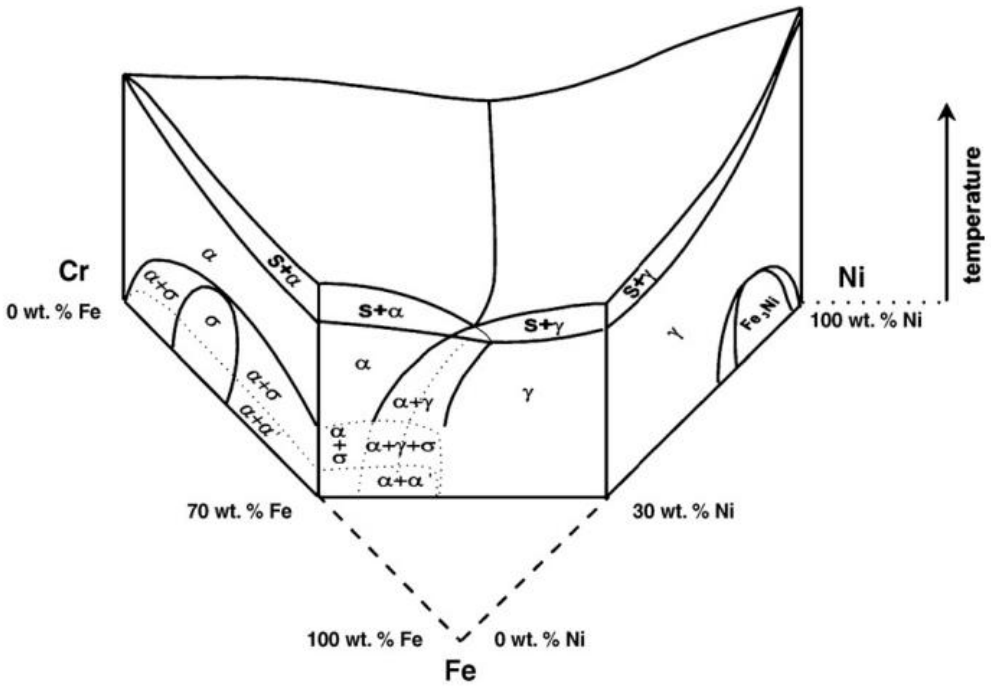

Source: Pohl et al. [36]

2.1.3 Microstructure of welded duplex stainless steels

Welding is a fabrication process of generating a metallurgical joint result from the melting parts to be joined together, with or without the utilization of pressure and a filler material [37]. In general, after being subjected to welding processes, DSS presents an unbalanced microstructure, predominantly ferritic, which compromises its properties [4].

In DSS welding austenite is formed from solid-state ferrite. Welding conditions with low cooling rates favor the growth of ferritic grains in the heat affected zone (HAZ) and the formation of nitrides and carbides. High cooling rates favor a higher amount of ferrite, not having the time required for austenite formation [38]. When high heat inputs and slow cooling rates are applied, the properties of DSS weldment can accurately advance [39].

In DSS weld metals, austenite forms in three morphologies: allotriomorphs, at the prior ferrite grain boundaries; Widmanstätten side-plates, growing into the grain from the allotriomorph grain boundaries; and intragranular austenite. Grain boundary allotriomorphs and Widmanstätten austenite form at high temperatures, while intragranular austenite forms at lower temperatures [8].

Under high cooling rates, typical for Nd:YAG laser welding process, there is no time for austenite formation, which results in a predominantly ferritic microstructure. Figure 11 shows the unbalanced microstructure of UNS 32750 welded using Nd:YAG pulsed laser process. To obtain a balanced microstructure, we must use a post-weld heat treatment, or add austenite-forming elements, such as nickel or nitrogen.

Figure 12 - SEM micrographs of transition region between base material and fusion zone for UNS 32750 Nd:YAG pulsed laser welded

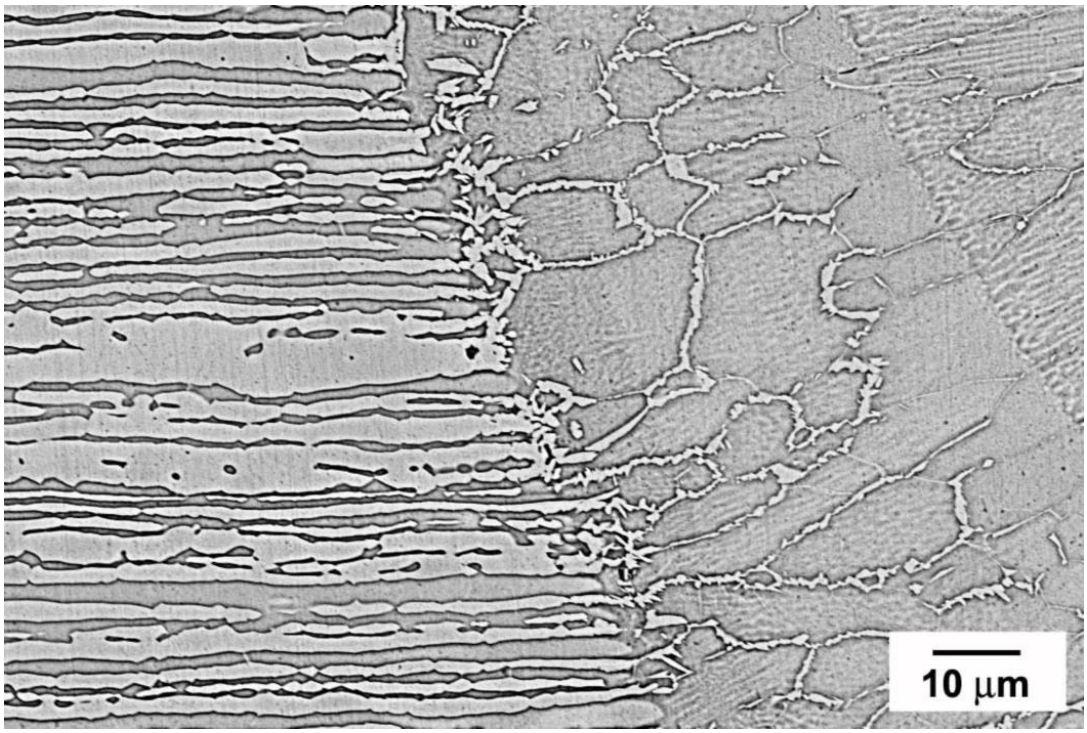

Source: Da Cruz Junior et. al. [40]

2.1.4 Second phase precipitation in duplex stainless steel

Due to the high amount of alloying elements, the duplex stainless steels show a rather complex second phase precipitation and phase transformation behavior. The effect on the mechanical and corrosive properties of several precipitations might be extensive. In DSS welding processes secondary phases can precipitate in a temperature range between 700ºC and 950ºC [41]. Knowledge of the quantity, distribution and type of phases is critical to predicting the mechanical properties and corrosion resistance of stainless steels [32].

The section at 70% iron shows the quasi-binary phase diagram (Figure 13), which represents the duplex stainless steels. They solidify primarily as ferritic alloys and transform at lower temperatures by a solid state reaction

partially to austenite. Hence, the austenite ferrite ratio is adjusted in a temperature above 1000 °C.

Figure 13 - Pseudo-binary Fe–Cr–Ni phase diagram at a 70% Fe section

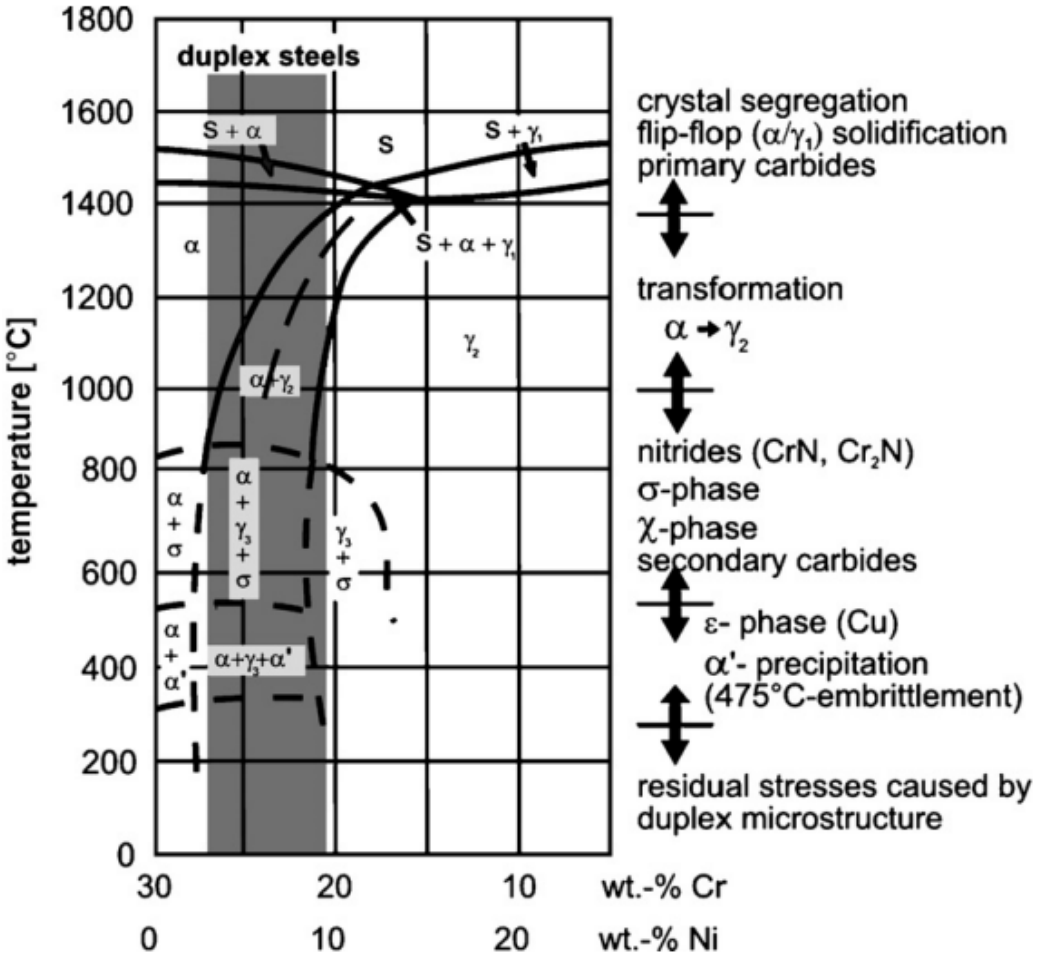

Source: Pohl et al. [36]

Carbides

In stainless steels, different types of carbides may be formed, having different stoichiometries such as $M_{23}C_6$, MC, M_6C and M_7C_3.

- $M_{23}C_6$: Forms by the association of carbon atoms in clusters in the interstices, at temperatures between 600 and 950ºC. They are the most common in stainless steels.
- MC: Have low interfacial energy therefore they are less harmful to mechanical properties such as creep resistance. In AIS at temperatures between 600 and 800 ° C, MC growth rate is lower than $M_{23}C_6$.
- M_6C: Usually present in AIS containing Mo. This carbide accommodates a little nitrogen in its structure due to Mo. Therefore, it is very likely to be present in superaustenitic stainless steel that generally contains Mo as well as Nb at high levels.
- $M_7C_{3:}$ These carbides are found only when carbon levels are too high.

Nitrides

Due the high amount of nitrogen in some classes of DSS, nitrides like Cr_2N can precipitate embrittling the material. Figure 14 shows the typical appearance of nitride precipitation in the duplex microstructure after rapid cooling.

Figure 14 - Optical micrograph of heat treated UNS S32750

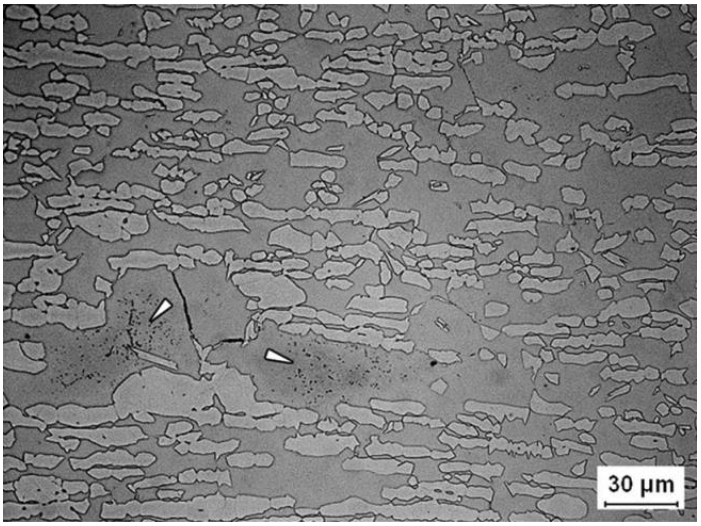

Source: Pettersson et al.[42]

Sigma phase σ

This phase presents in its chemical composition mainly the elements Fe and Cr [36]. It is considered a non-magnetic Fe and Cr intermetallic that is hard and brittle. The brittle phase σ is the most precipitated intermetallic phase in ASS and DSS. It has a negative effect on creep properties when precipitated on grain boundaries and it becomes a serious problem when these stainless steels are used at elevated temperatures as this phase not only reduces corrosion resistance due to the removal of chromium and molybdenum, but also deteriorates the mechanical properties of these steels.

Cr diffusion can be considered as one of the factors controlling its precipitation. In addition to Cr, the diffusion of another substitutional element such as Mo could also be important for sigma phase formation. High cooling rates are necessary to prevent sigma phase formation [13]. Figure 15 shows the sigma phase in UNS S32205 aged at 950 °C for 15 minutes, coarser particle is Sigma phase.

Figure 15 - Sigma phase in UNS aged at 950 °C for 15 minutes.

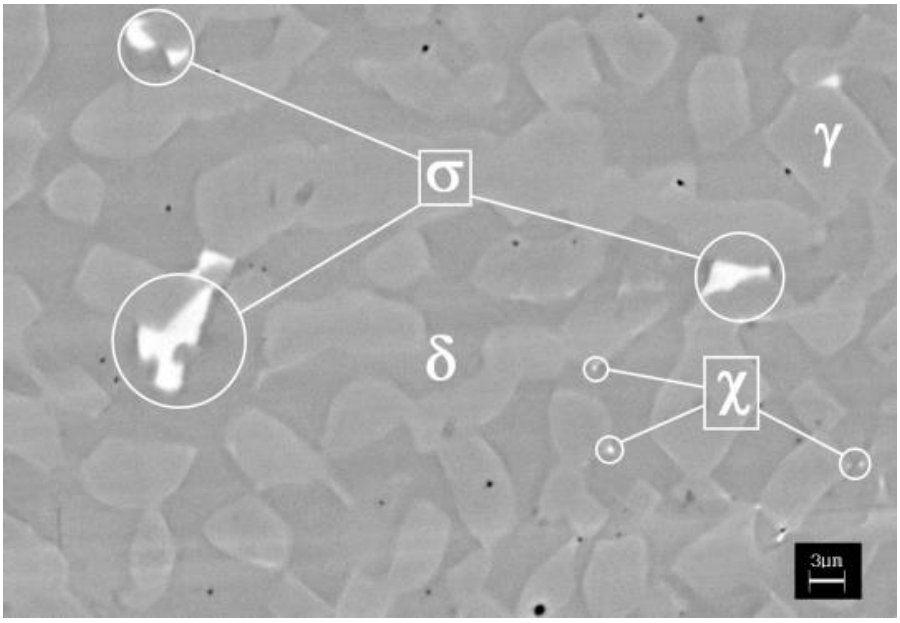

Source: Gennari et. al. [43]

Chi phase χ

The chi χ phase is relatively the smallest phase, forming at temperatures between 700 and 900ºC mainly at the ferrite-austenite interface. It is a body-centered cubic phase, hard and fragile. In general, for its formation needs molybdenum. Tungsten is responsible for stimulating the formation of the chi phase while inhibiting the formation of the sigma phase. Intermetallic chi phase formation leads to a loss of toughness. Figure 16 shows the chi phase in UNS S32750 DSS

Figure 16 - Chi phase on grain boundaries of UNS 32750

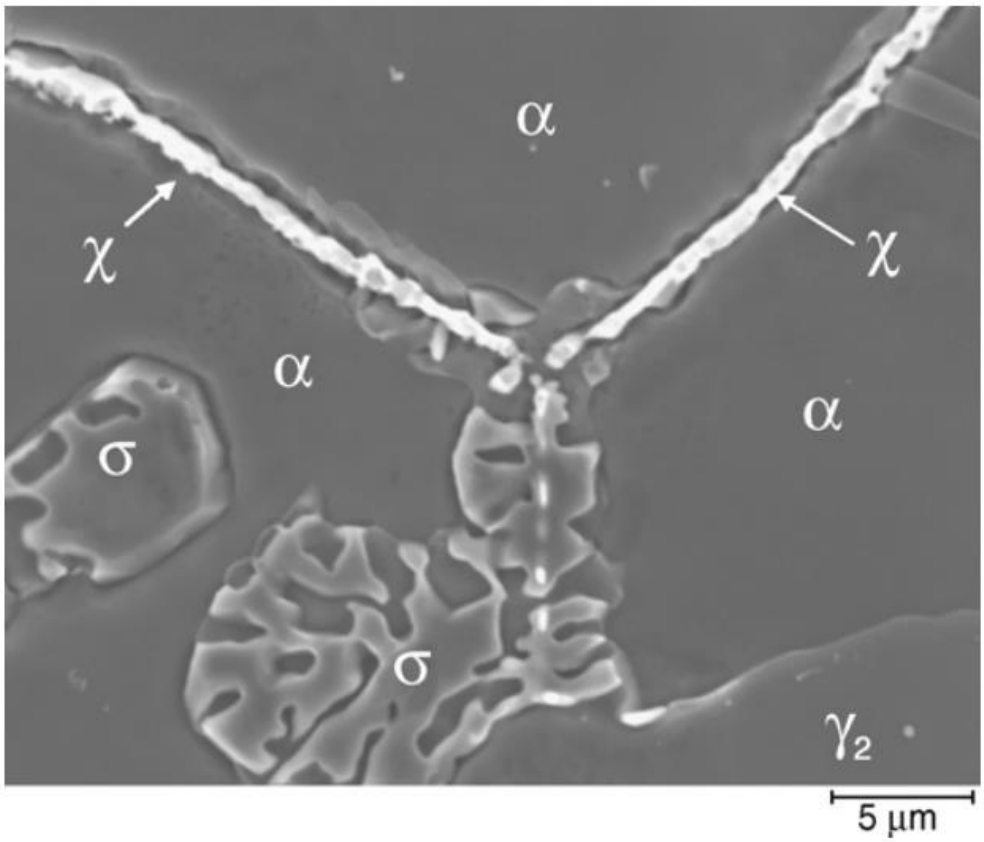

Source: Pohl et al.[36]

2.2 Nd:YAG PULSED LASER WELDING

The Nd: YAG laser is inserted among the solid state lasers. The term YAG means Yttrium Aluminum Garnet ($Y_3Al_5O_{12}$), is a grenade group material commonly used as the basis for various solid state lasers. The triple ionized neodymium dopant replaces a small fraction of yttrium ions in the host crystal structure as their sizes are similar. Neodymium ions provide the laser activity in the crystal [44]. Figure 17 shows Nd:YAG crystals used in laser welding.

Figure 17 - Nd:YAG crystals

Source: MSE SUPPLIES [45]

Figure 18 shows the laser generating cavity schema. Nd:YAG crystal is transparent and is considered the most common in industrial applications. It provides radiation with a wavelength of 1.06 micrometres, easily transmitted by flexible quartz optical fibers and the active medium can be excited by either xenon or krypton light. Compared to gaseous laser (CO_2), the system is considerably simple and the wavelength of radiation is easily absorbed by metals, making it more efficient [46]. The Nd:YAG laser operates in both continuous and pulsed modes

Figure 18 - Laser generating cavity schema

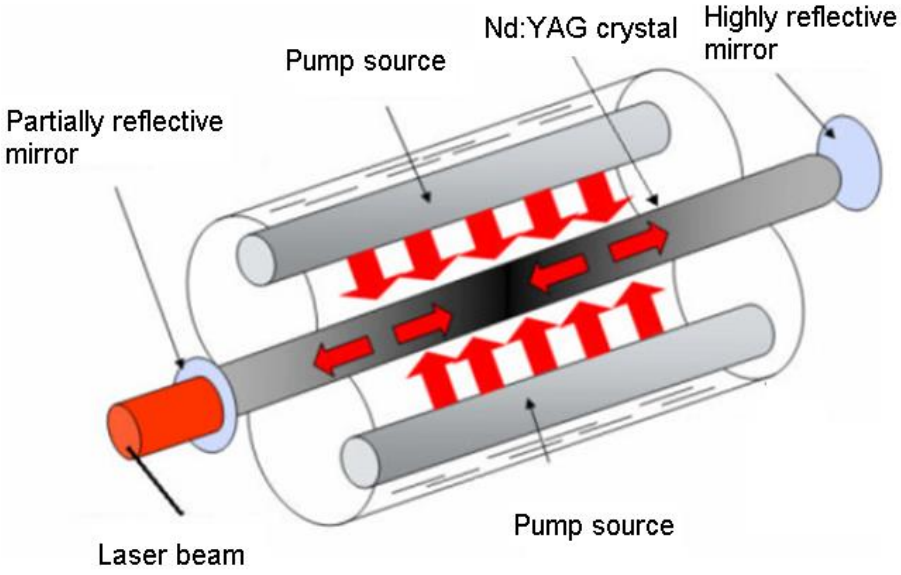

Source: modified Kavamura [44]

2.2.1 Laser welding techniques

Laser welding can be performed in two ways, conduction welding, Figure 19 (a), and keyhole welding, Figure 19 (b). The difference is in the surface of the melting pool, which in the case of the first mode remains intact during execution and in the second mode that surface is altered by the laser beam penetrating the molten region caused by a high amount of energy.

Figure 19 –Examples of (a) conduction and (b) keyhole welding

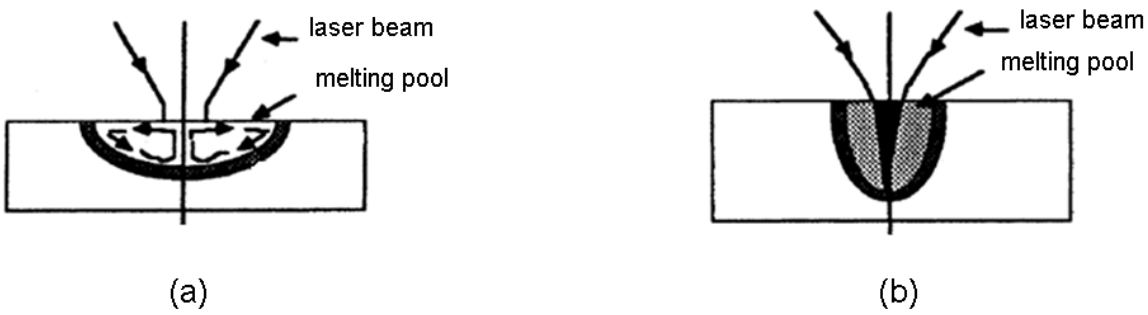

Source: modified Steen and Mazumder [47]

In conduction mode, welding is performed with low power density, usually between 0.5 MW / cm², generating a wide and shallow weld bead. In the keyhole mode, welding is done with high power density, with peak power above 1.5 MW / cm², generating a very deep and narrow weld bead, reducing the heat affected zone. In the keyhole mode, welding can be performed at high speed, at 20 in / s penetration is limited to 0.5 mm, with lower speeds penetration can reach up to 12 mm [48]. Figure 20 shows the relation between penetration depth and power density for both welding modes.

Figure 20 – Relation between penetration depth and power density

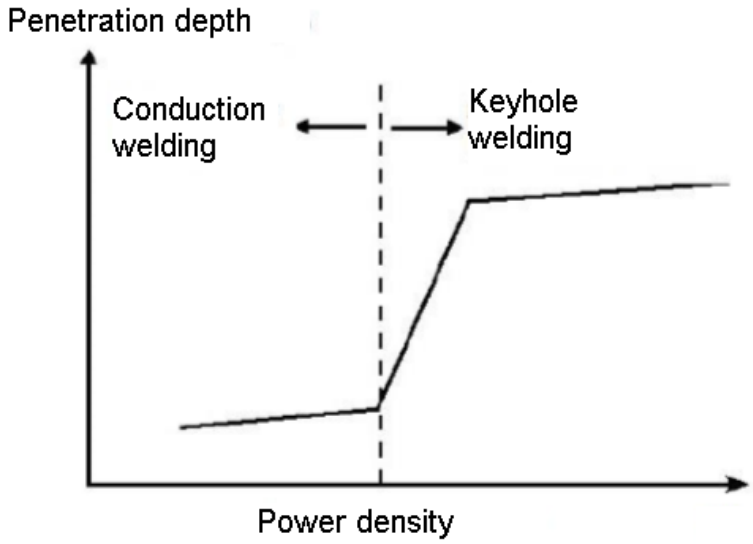

Source: America [48]

In conduction laser welding, the base material is heated by the laser beam to its melting temperature without creating vaporization [49]. The incident beam energy on the surface of the melting pool is absorbed by the material and transferred to the root of the weld by thermal conduction.

In keyhole welding the laser intensity within the focusing position is high enough to generate a high evaporation rate. With this, the recoil pressure deconstructs the melting pool allowing the laser beam to penetrate deeper into the material [47].

In both welding techniques, they can be performed with laser in pulsed or continuous mode. In the case of pulsed laser welding, the duration of the laser pulse and the intensity of the laser beam on the part to be welded are the main parameters that define whether conduction or penetration welding.

2.2.2 Differences between continuous and pulsed laser welding

In continuous mode the laser power does not vary during the welding process, the laser beam produces a continuous and regular melting pool, producing little spatter and low incidence of discontinuity. In pulsed mode, the is produced a very high peak power with short duration at relatively low average power values as shown in Figure 21. Due to this difference in energy transfer efficiency, the high peak powers generated make pulsed mode to weld a wider variety of materials than continuous mode in equivalent ranges. Pulsed mode is characterized by producing weld beads with extremely high cooling rates, minimal heat affected zone [50].

Figure 21 – Average power for continuous and pulsed laser welding

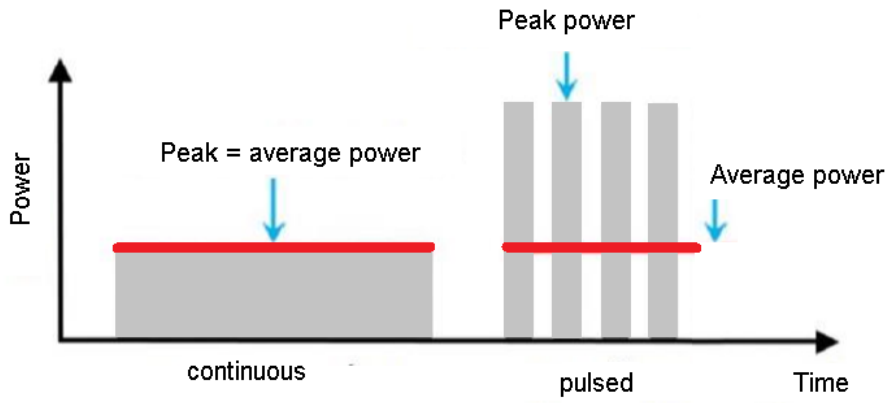

Source: Elaborated by author

2.3 RESEARCHES OF NICKEL ADDITION IN WELDING PROCESS

Many authors have studied the effects of nickel and nitrogen addition on phase balance for certain welding processes and this topic will present the top searches and their results.

Muthupandi et al. [8] studied the influence of nickel and nitrogen addition on the microstructure and mechanical properties of power laser beam processed DSS weld metals. They used an UNS 31803 DSS as base metal. First the samples were welded with Gas Tungsten Arc Welding (GTAW) using a nickel-enriched filler and a shielding gas mixture containing enriching the welds with nickel or nitrogen. The samples were re-melted using power laser beam. They concluded that the addition of nickel produced welds with acceptable ferrite-austenite balance. Figure 22 a show the microstructure of the weld metal produced with autogenous electron beam weld and Figure 22 b the microstructure of the electron beam weld metal obtained by re-melting nickel enriched GTAW weld metal.

Figure 22 – Microstructure of the weld metal for (a) autogenous EB weld (b) re-melting nickel enriched GTAW weld metal

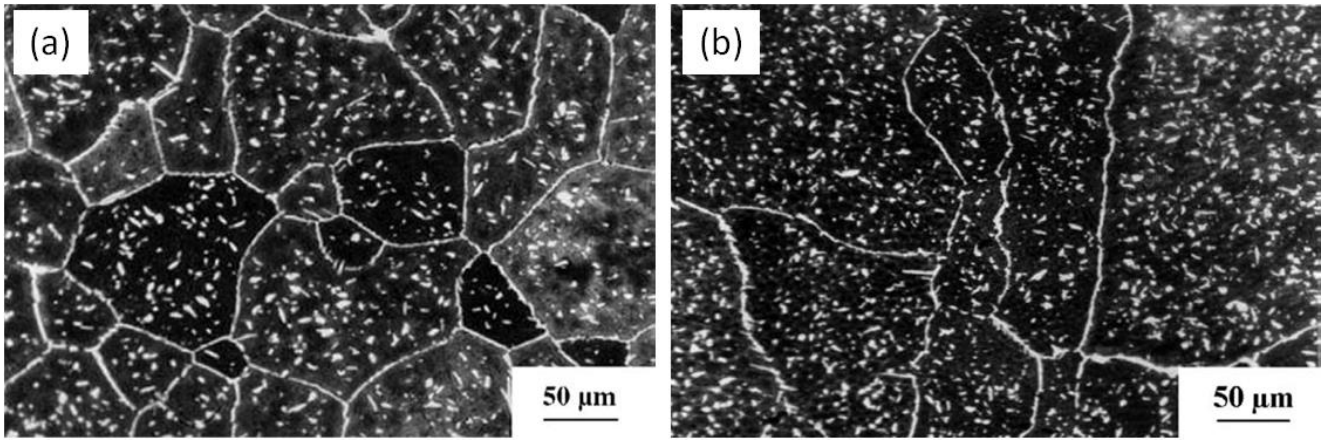

Source : Muthupandi et al. [8]

Migiakis and Papadimitriou [9] studied the effect of nitrogen and nickel on the microstructure and mechanical properties of plasma welded UNS S32760 DSS. The enrichment of both elements was made using a high Ni content filler metal and a shielding gas containing nitrogen. They concluded that nitrogen addition in protective gas and higher nickel content in the filler metal have both a positive effect. Figure 23 shows the microstructure of fusion zone for (a) without high Ni nickel filler metal and (b) with high Ni nickel filler metal

Figure 23 – Microstructure of fusion zone for (a) without high Ni nickel filler metal (b) with high Ni nickel filler metal

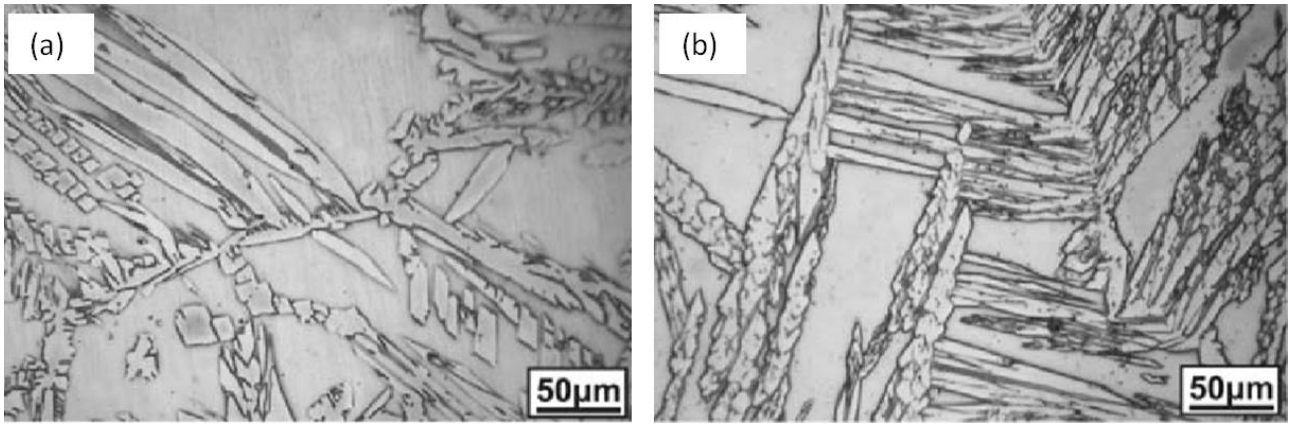

Source: Migiakis and Papadimitriou [9]

Pilhagen and Sandström [10] have investigated the role of nickel on the toughness of DSS weld metal prepared by submerged arc welding (SAW). They used an UNS 32101 DSS as base metal. They concluded that addition of nickel resulted in a weldment with appropriate ferrite content. The ductility and toughness were significantly increased. Figure 24 shows the microstructure of fusion zone for (a) low nickel content (b) high nickel content.

Figure 24 – Microstructure of fusion zone for (a) low nickel content (b) high nickel content.

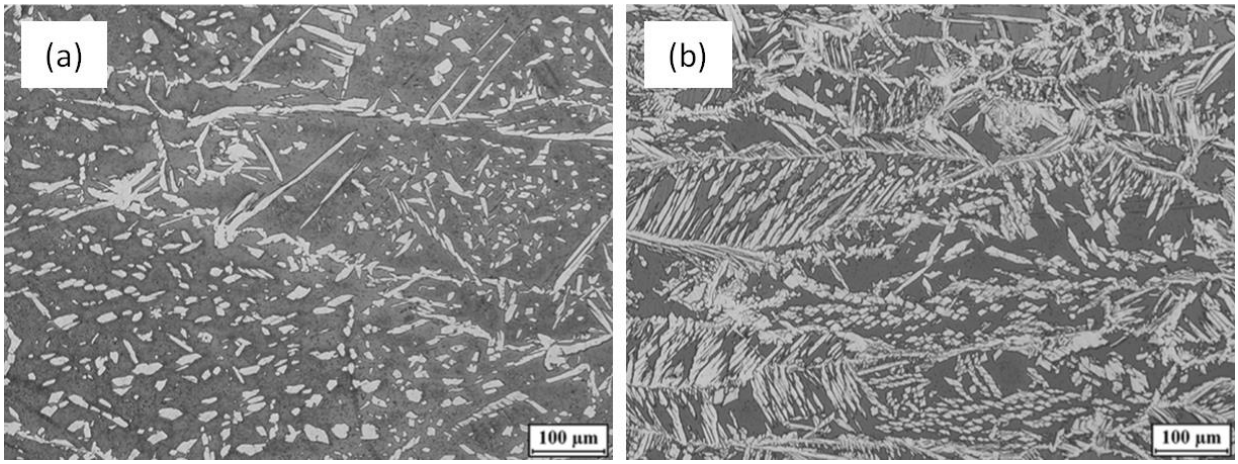

Source: Pilhagen and Sandström [10]

Tahaei et al. [11] studied the effect of the addition of nickel powder and post weld heat treatment on the metallurgical and mechanical properties of the welded UNS S32304 DSS. They concluded that both the addition of nickel powder during the welding process and the post weld heat treatment made it possible to improve the mechanical properties of the weld joints. Post weld heat treatment had the best effect in restoring the equal volume fraction of ferrite and austenite compared to the addition of nickel powder.

. Related to the Nd:YAG pulsed laser process it's hard to find results in literature. Because they are new and innovative, the first results related to this research were published in 2019 (as shown in Annex I), as a short communication. The paper demonstrated the effect on nickel addition on Nd:YAG pulsed laser welding of duplex stainless steels indicating that the addition of nickel has improved the Nd:YAG pulsed laser welding allowing to obtain balanced phases in the weld bead.

3 MATERIALS AND METHODS

This chapter describes the experimental planning of the research and the experimental procedures for welding testing and the measurement of output variables such as microstructure, mechanical properties and corrosion resistance.

3.1 EXPERIMENTAL PLANNING

The base metal was a UNS S32750 super duplex stainless steel (SDSS), in sheets of 1.5 mm thickness. The chemical composition is presented in Table 2, and the microstructure is presented in Figure 25.

Table 2 – Chemical composition of UNS S32750 (wt-%)

UNS	C	Si	Mn	P	S	Cr	Mo	Ni	Cu	N
S32750	0,018	0,29	0,63	0,02	<0,0003	25,61	3,84	6,97	0,15	0,27

Source: Elaborated by author

Figure. 25 - SEM micrograph of base material with equal proportions of austenite (light etched regions) and ferrite (dark etched regions).

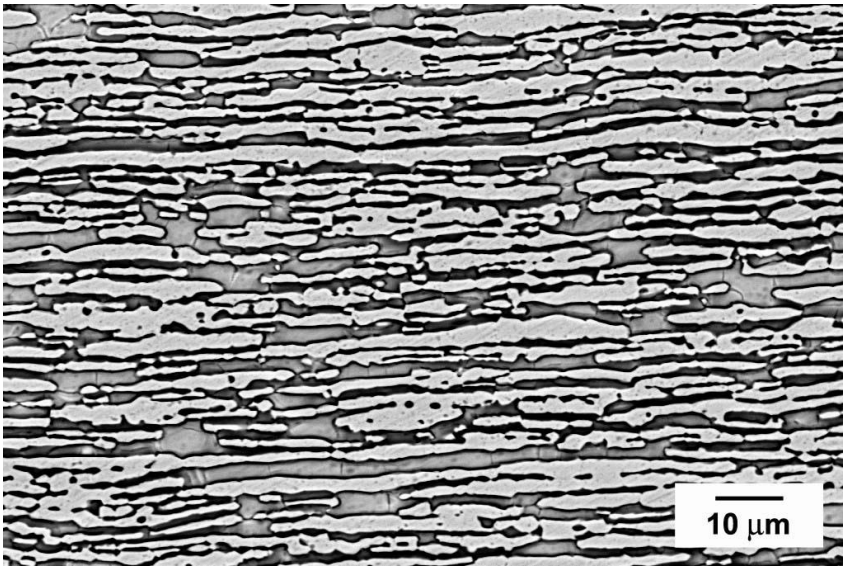

Source: Elaborated by author

Electrolytic nickel thin foil with different thickness (Table 3) was inserted between pieces of UNS S32750 base metal, providing nickel enrichment in the weld metal as presented in Figure 26. The production of the nickel foils will be explained on experimental procedure.

Figure 26 - Schematic diagram of the butt weld joint.

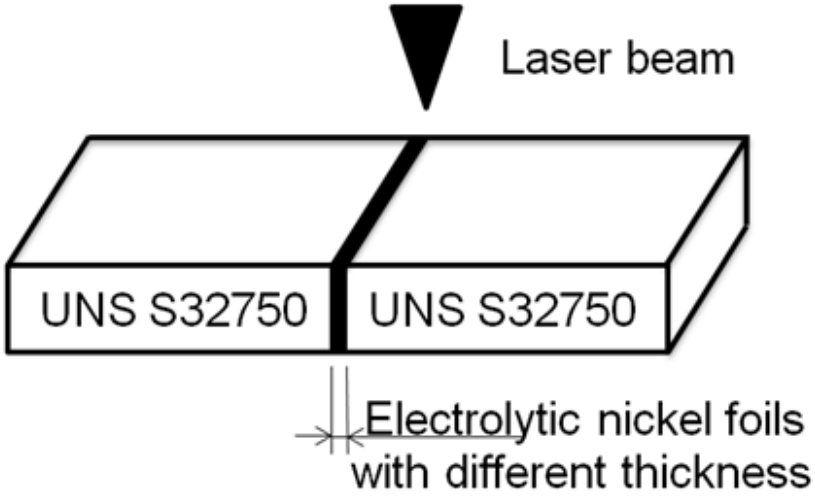

Source: Elaborated by author

A Nd:YAG pulsed laser machine model UW-150A was used as showed in Figure 27. Six conditions were evaluated, keeping the same welding conditions and varying the thickness of nickel foil added. Single-pass welding was applied. After exploratory tests, the welding parameters were selected to obtain a regular surface, without porosity, and a weld pool deeper than 50 % of the sheet thickness. The laser beam with pulse energy set at 10 J was focused on the sample surface. Table 3 summarizes the thickness of nickel foil for each conditions evaluated and the welding parameters.

Figure 27 – Nd:YAG pulsed laser machine

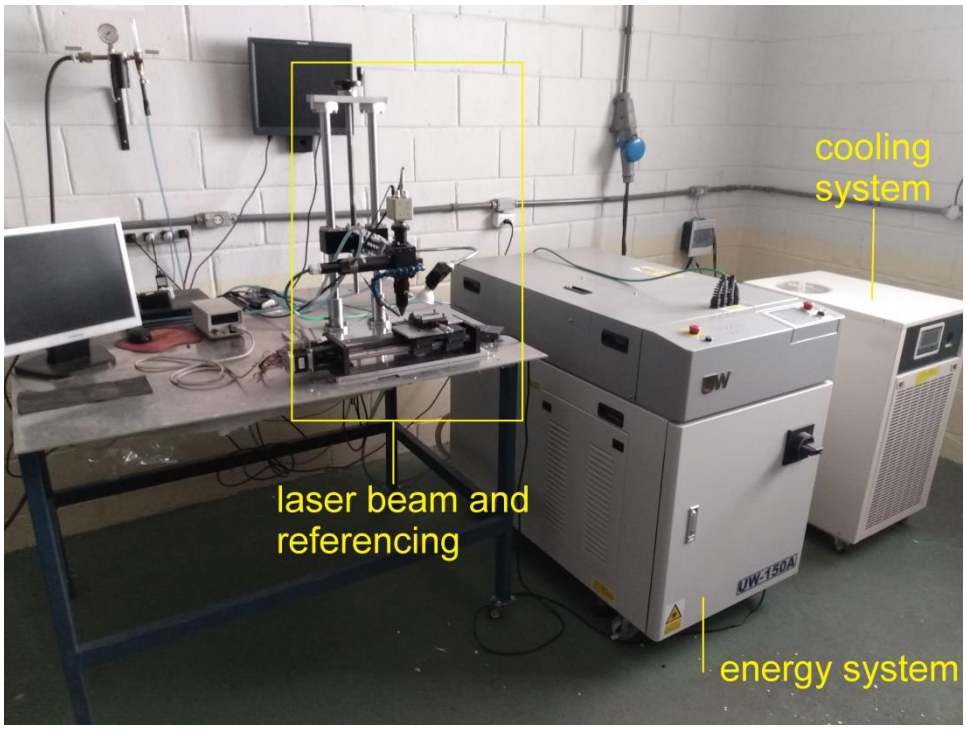

Source: Elaborated by author

. **Table 3 -** Thickness of the nickel thin foils and welding parameters.

Condition	Nickel foil thickness	Welding parameters (same for all the conditions)
AW	No nickel foil	Peak power: 2.0 kW
Ni30	30 µm	Pulse duration: 5 ms
Ni40	40 µm	Frequency: 9 Hz
Ni50	50 µm	Welding speed: 1 mm/s
Ni60	60 µm	Shielding gas: Ar
Ni70	70 µm	Flow rate: 20 l/min

Source: Elaborated by author

3.2 EXPERIMENTAL PROCEDURE

3.2.1 Welding

As already described, a Nd:YAG pulsed laser machine model UW-150A was used. The welding parameters were defined, based on the research of Franzini [51], to give an overlap rate of 90%.

In order to perform laser welding of a continuous weld bead, in pulsed mode, it is important to understand and control the overlap rate of the weld beads generated by each pulse. This type of welding is achieved by applying a linear welding speed while the pulses are emitted. These pulses create overlapping weld points, generating a weld bead very similar to that of continuous welding

Overlap rate can be understood as the difference between the two consecutive pulses distance divided by the pulse diameter. It is a very important parameter as it provides a relationship between the main parameters such as peak power, pulse duration, frequency and welding speed. As more than one pulse reaches the same area, the overlap rate will affect the total energy delivered along the weld and consequently the microstructure and mechanical properties of the weld bead [52]. The Figure 28 shows a schema of overlap rate and Equation 1 the math definition.

Figure 28 – Schema of overlap rate

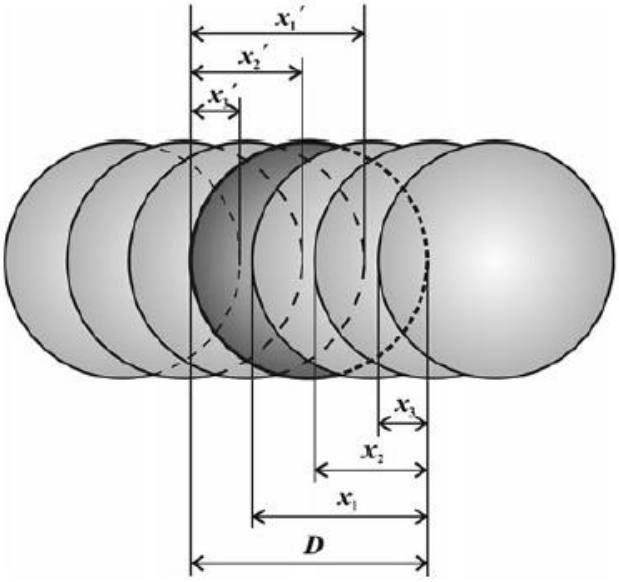

Source: Lapsanska et at. [52]

$$\text{Overlap rate} = 1 - \frac{table\ speed\left(\frac{mm}{s}\right)}{pulse\ diameter\ (mm) * frequency\ (Hz)} \quad (1)$$

As the weld bead is formed by a series of overlapping pulses, there will be variation in the effective penetration of the bead, as the pulses solidify into a conical shape, leaving voids in the deepest region of each pulse as shown in Figure 29. For this reason the welding parameter where were selected to obtain a weld pool deeper than 50 % and the laser welding were made in both side of each sample.

Figure 29 – Relation between effective penetration and overlap rate

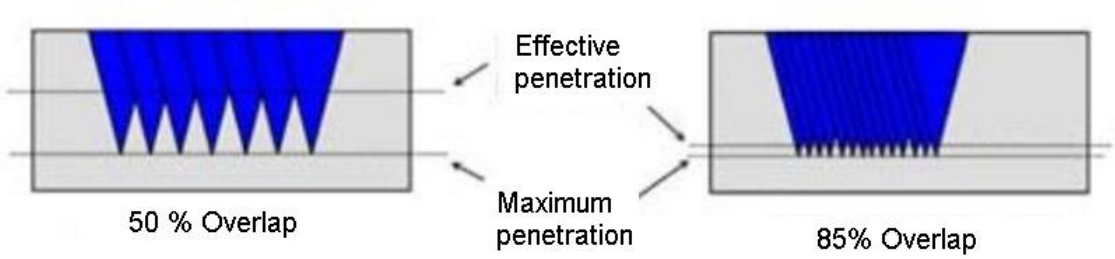

Source: América [48]

The welding parameters were kept constant for all the studied conditions, since the objective of this work was to study the effect of the nickel addition and not of the welding parameters.

Tests were made to confirm to the overlap rate for the welding parameters selected. The pulse diameter was measured and Figure 30 shows the surface of weld bead for an overlap rate of 90%.

Figure 30 – Welding surface

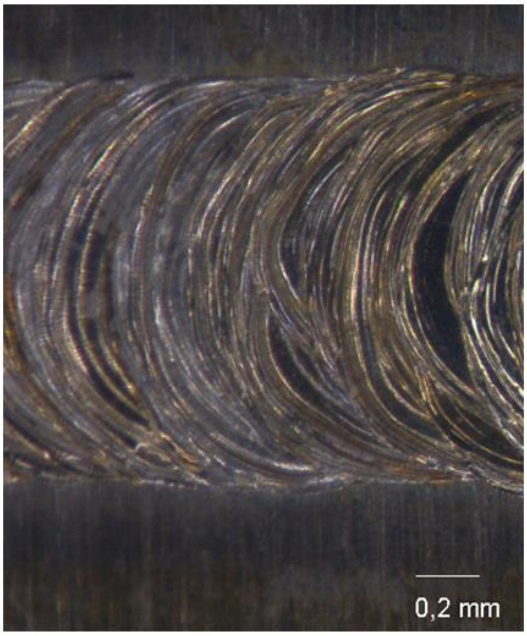

Source: Elaborated by author

3.2.2 Prodution of nickel foil

The nickel foils were obtained from an electrolytic nickel bar. Using a wire electrical discharge machining, strips were cut measuring 25.00 x 2.00 x 0.08 mm, latter sanded to the desired thickness. Finally the foils were cleaned in an ultrasonic bath. Figure 31 shows the nickel bar being cut in the wire electrical discharge machining.

Figure 31 – Cutting of electrolytic nickel bar

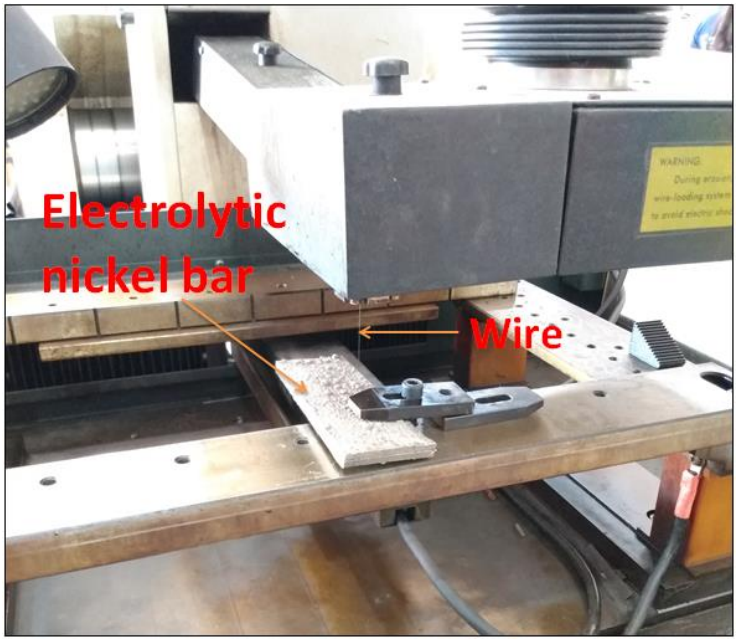

Source: Elaborated by author

Nickel foils thicknesses were verified at four points along the length using a digital micrometer (0-25) Mitutoyo, resolution 0.001 mm. Figure 32 shows the nickel foil prepared for the welding process.

Figure 32 – Nickel foil

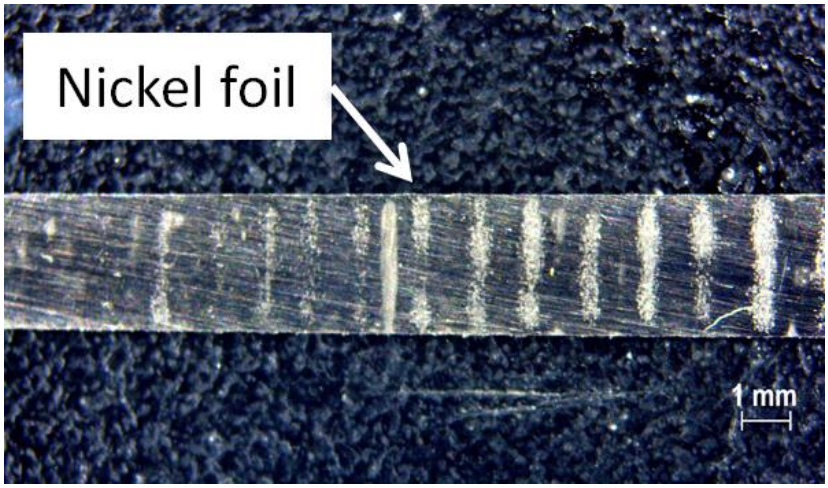

Source: Elaborated by author

3.2.3 Microstructure and microhardness

The samples were embedded in cold-curing transparent epoxy resin using a silicone mold. The samples were cut at the cross section of the weld bead. The sanding of the samples occurred manually, alternating the position by 90 ° with each sanding change. The granulation of the sandpaper followed the sequence 220, 320, 400, 600, 1000 and 1200. For the polishing, particle alumina with 1.0 and 0.3 µm, respectively, were used.

The microstructure was revealed using modified Beraha's reagent (20 ml of HCl, 80 ml of H_2O, 1,0g of $K_2S_2O_5$ and 2,0g of NH_4HF_2). To determine the austenite/ferrite ratio, several SEM micrographs (Carl Zeiss EVO LS15) in different regions of the weld bead was analysed by ImageJ freeware. For each sample ten micrographs were analysed. The micrographs were binarized (color threshold) to allow calculate the austenite/ferrite ratio as shown in Figure 33.

Figure 33 – Example of volume fraction determination (a) Ni30 SEM micrograph, (b) NI30 binarized SEM micrograph, (c) Austenite/ferrite bar graph for the micrograph

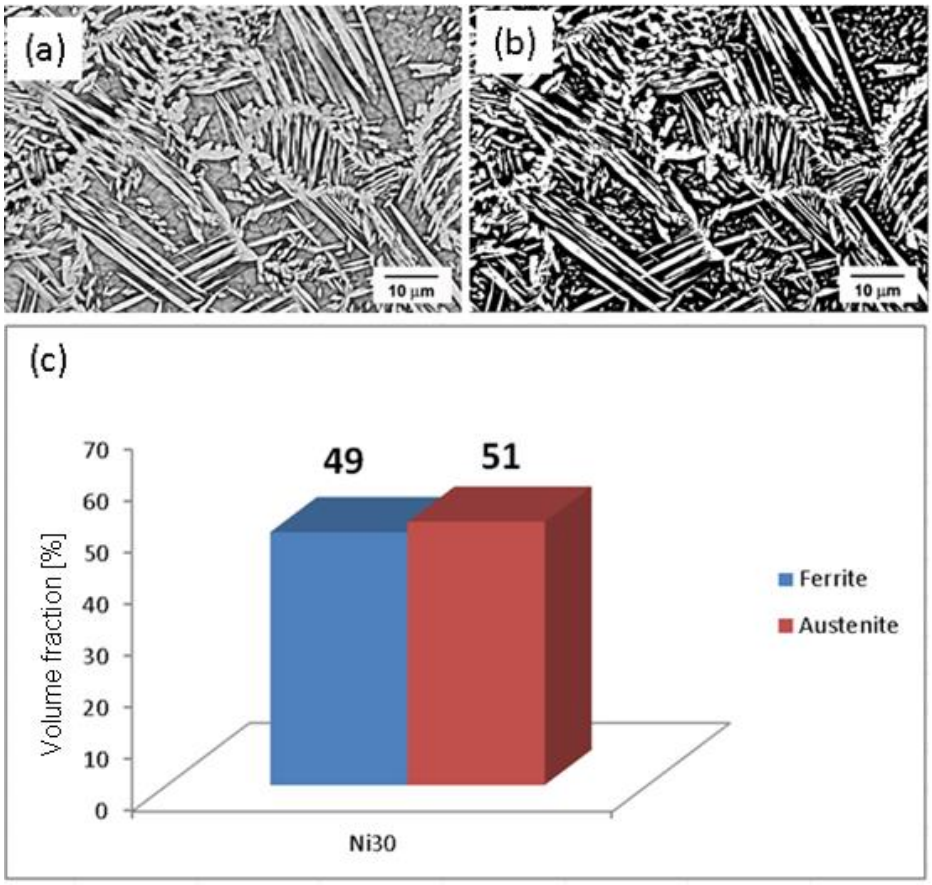

Source: Elaborated by author

Vickers microhardness tests were performed using a Dynamic Ultra Micro Hardness Tester Shimadzu DUH 211S in two directions, as shown in Figure 34. The vertical line was used to find the mean microhardness of the weld bead and the horizontal line to obtain the microhardness profile.

Figure 34 – Schema of microhardness measurement

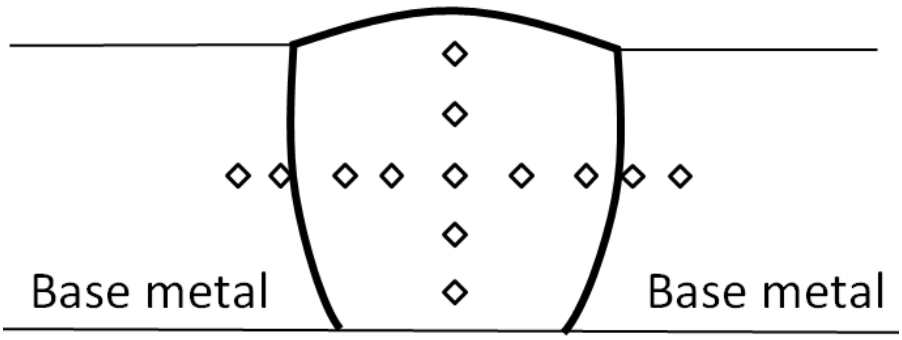

Source: Elaborated by author

Vickers scale was used and the test method used was loading / unloading. The method consists of increasing the force to a predetermined value, keeping it constant for a certain time and after that time, the unloading occurs. The load used was 100 mN.

3.2.4 Tensile tests

The tensile tests were performed in a universal testing machine EMIC DL 30.000. The samples were prepared in a wire electrical discharge machining Eletrocut NOVIK following the standart MB-4 of “Associação Brasileira de Normas Técnicas” (ABNT). For each condition were two samples were tested. Figure 35 shows the design of the tensile samples and Table 4 the dimensions.

Figure 35 – Design of tensile samples

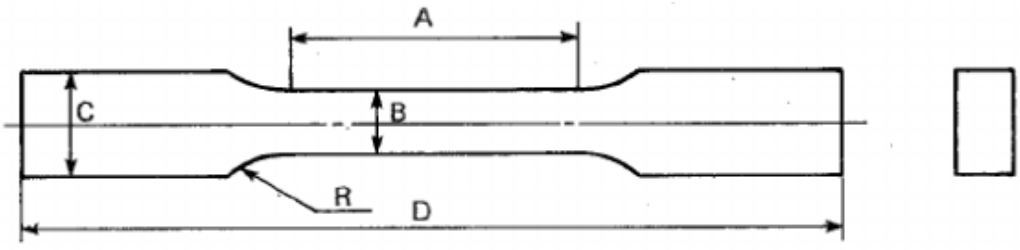

Source: Souza [53]

Table 4 – Tensile sample dimensions

Sample	A (mm)	B (mm)	C (mm)	D (mm)	R (mm)
Thin sheet	75	12,5	20	200	20

Source: Souza [53] modified

3.2.5 Critical pitting temperature (CPT)

The Critical Pitting Temperature (CPT) criterium was used to evaluate the corrosion resistance, following the ASTM G150 standard. CPT test was chosen to correlate the microstructure modifications to the corrosion properties [54].

The CPT tests were performances at Corrosion Laboratory of the Department of Industrial Engineering (University of Padua), as part of an international cooperation established between Estate University of São Paulo – UNESP and University of Padua. The samples were painted with a thermal-resistant varnish letting exposed an area of 1 cm², as presented in Figure 36.

Figure 36 – CPT sample

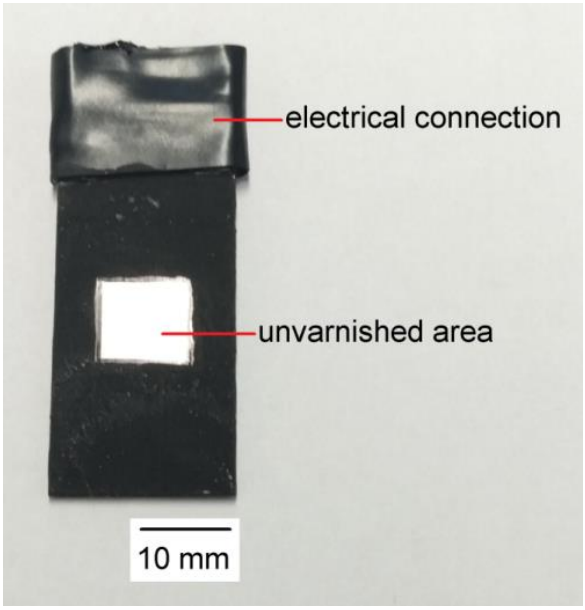

Source: Elaborated by author

A potentiostat (model AMEL 7060) equipped with two cells containing aqueous solution of NaCl (1 M) were electrically connected by a salt bridge. The standard calomel electrode (SCE) was immersed in the first cell and maintained at room temperature. The platinum counter electrode and the sample were immersed in the second cell where the temperature was raised at a rate of 1º C/min starting from 0º C until CPT was reached. CPT is defined when the current density reaches 100 µA/cm². Highest CPT values indicate greater corrosion resistance. Potential was set to 700 mV vs SCE and kept constant. The pitting locations were observed by stereomicroscopy Zeiss Stereoscan Stemi C2000. Figure 37 shows a schema of the CPT experimental apparatus.

Figure 37 – CPT experimental apparatus

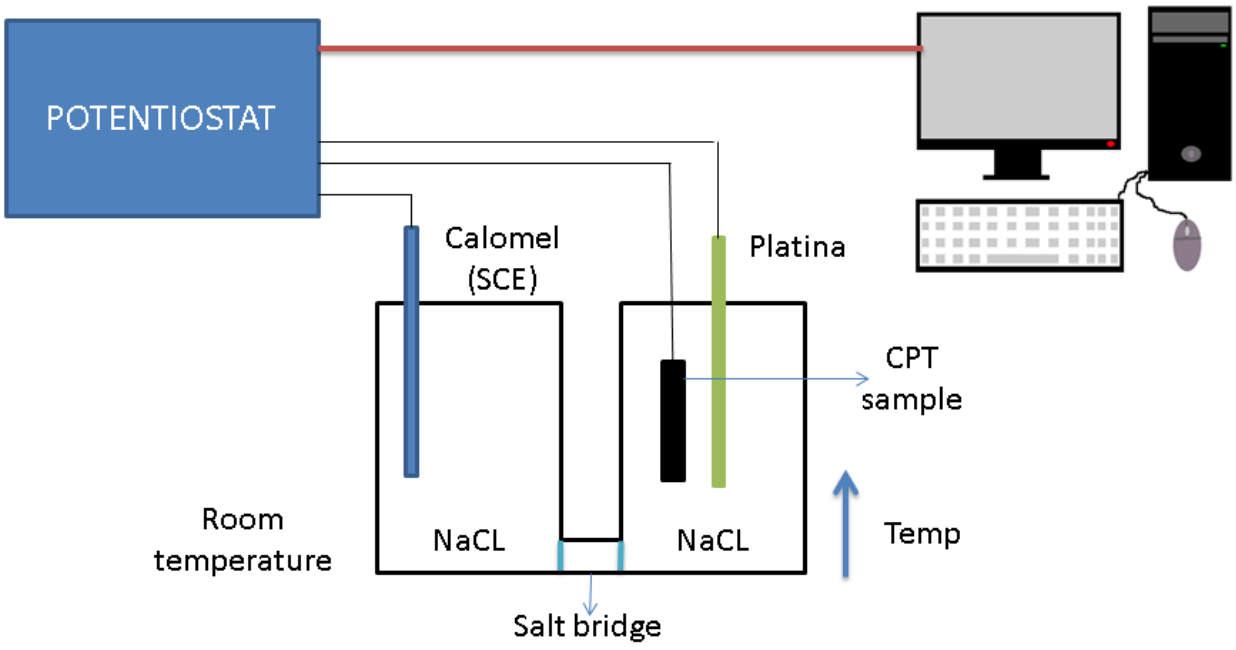

Source: Elaborated by author

4 RESULTS AND DISCUSSION

The results are presented in four topics: microstructure, microhardness, tensile strength and critical pitting temperature.

4.1 MICROSTRUCTURE

The results present, qualitatively and quantitatively, the effect of nickel addition on the fusion zone microstructure of joints welded by Nd:YAG pulsed laser by an examination of the microstructures and austenite/ferrite ratio.

The microstructures of the weld bead for all the conditions are shown in Figure 38. Austenite is light and ferrite is dark. It is possible to verify that nickel modified both the amount of austenite formed and its morphology. A autogenous welding specimen (AW) has presented strongly unbalanced microstructure (Figure 38 a), containing large amount of polygonal ferrite grains with austenite decorating its boundaries, typical result of Nd:YAG pulsed laser welding. In DSS weldments, austenite is formed through diffusional solid-state transformation, which is strongly affected by the cooling rates and heat input of thermal cycle. Under high cooling rates, given by pulsed laser, there is not enough time for completing austenite formation, which results in a predominantly ferritic microstructure [38].

Figure 38 - SEM micrographs of fusion zone for (a) AW, (b) Ni30, (c) Ni40, (d) Ni50, (e)Ni60 and (f) Ni70. Austenite is light and ferrite is dark. Beraha's etching

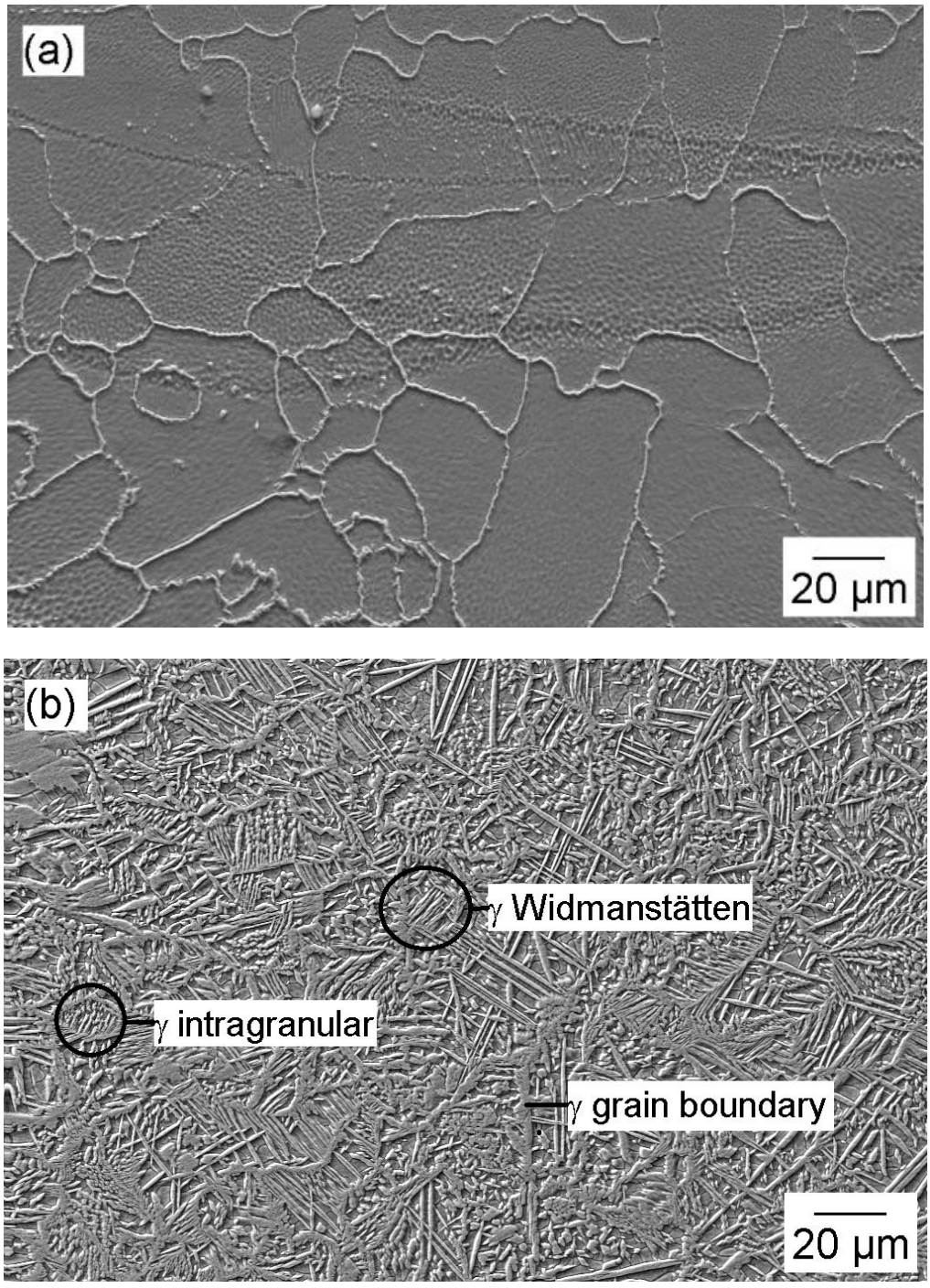

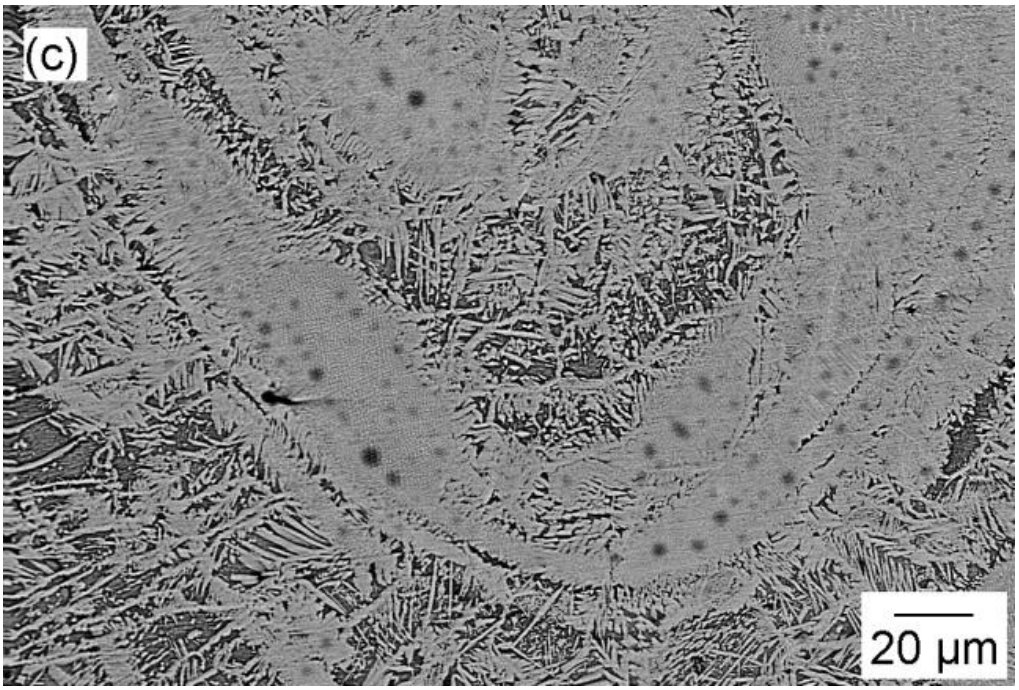
(c)
20 µm

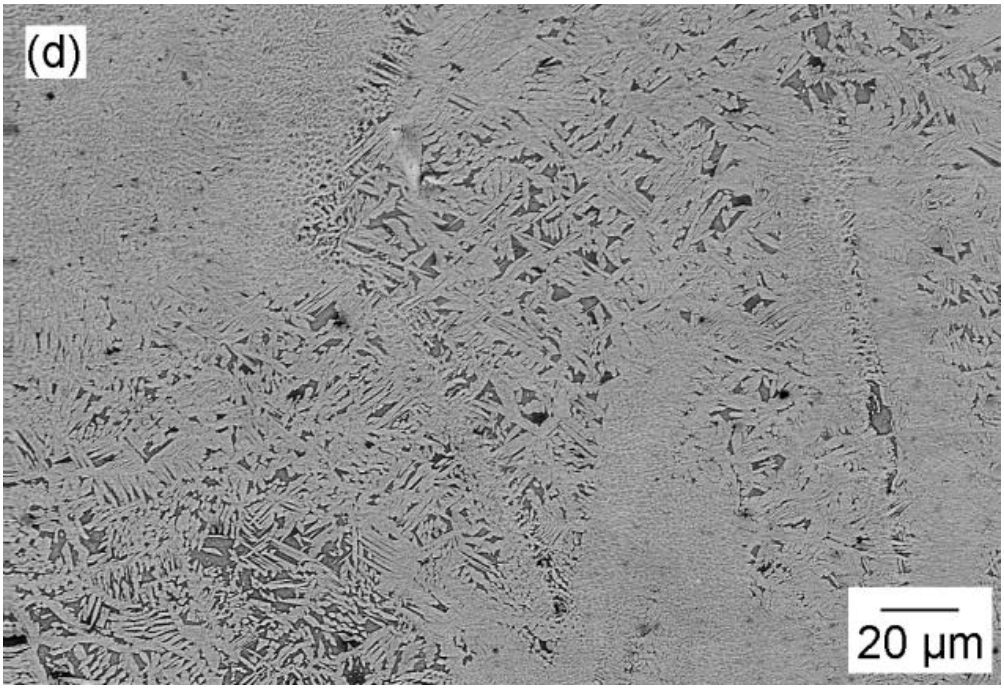
(d)
20 µm

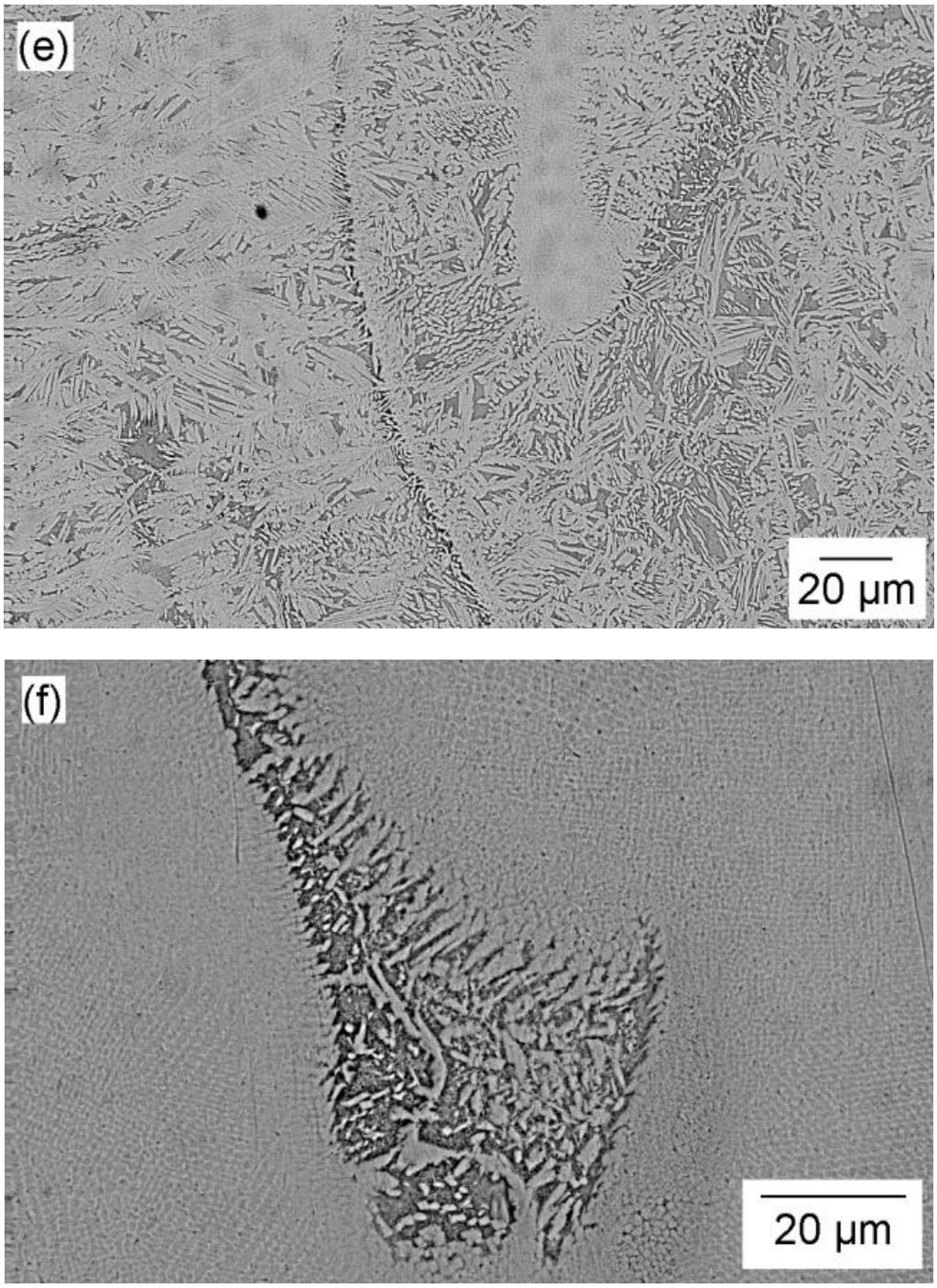

Source: Elaborated by author

Additions of nickel have promoted effective increasing of the austenite in the DSS weld metal. The Ni30 condition (Figure 38 b) resulted in well balanced ferrite-austenite microstructure, where austenite was found at the prior ferrite grain boundaries (allotriomorphic) and also inside them (idiomorphic). Higher amounts of austenite have been found with increasing of thickness of nickel foil

applied for the conditions Ni40 (Figure 38 c), Ni50 (Figure 38 d), Ni60 (Figure 38 e) and Ni70 (Figure 38 f), this late being practically all composed by austenite due to massive concentration of stabilizer elements. The phase balance in DSS is very important to maintain mechanical resistance and corrosion properties, as obtained on the Ni30 condition.

SEM analyses have identified different austenite morphologies in DSS weld metals. Allotriomorphic austenite and Widmanstätten side-plates have been identified growing into the grain from the grain boundaries; and ideomorph (intragranular) austenite. The grain boundary allotriomorphs and Widmanstätten austenite form at high temperatures, while intragranular austenite forms at lower temperatures under increased cooling rates [55].

Comparing the AW and Ni30 condition, the micrograph of the AW condition shows little presence of austenite in the form of grain boundary allotriomorphs and acicular intragranular austenite. The resulting microstructure, which is predominantly ferrite, is quite unbalanced. In the micrograph of the Ni30 condition, the austenite is visible in the earlier described forms, and in larger quantity than in the AW condition, resulting in a visibly-balanced microstructure. The sample in the AW condition presented a high content of ferrite due to the rapid cooling which it peculiar to Nd:YAG pulsed laser welding. The great amount of intragranular austenite in the Ni30 condition resulted from the thermal cycle (high cooling rate) associated with the austenite formation potential of nickel.

In the Ni30 condition the austenite/ferrite distribution was very homogeneous along the weld bead. In the other conditions, with increased addition of nickel, such homogeneous distribution was not obtained, which can affect the properties of the weld bead.

The quantitative effect of nickel on the laser welding process can be observed in Table 5 which shows the volume fraction of austenite and ferrite for the base material and for all the conditions.

Table 5 - Phase balance on weld bead

	VOLUME FRACTION	
	FERRITE %	**AUSTENITE %**
BASE METAL	50.2±0.4	49.8±0.4
AW	92.4±0.5	7.6±0.5
Ni30	48.2±0.4	51.8±0.4
Ni40	30.2±0.7	69.8±0.7
Ni50	21.1±1.2	78.9±1.2
Ni60	18.7±1.0	81.3±1.0
Ni70	4.6±1.2	95.4±1.2

Source: Elaborated by author

The volume fraction showed that the Ni30 condition was the one that most approached the volume fraction of the base metal, presenting a balanced ferrite/austenite microstructure. Comparing the AW and Ni30 condition, the addition of nickel increased the proportion of austenite from approximately 8% (AW) to 52% (Ni30). This effect was a direct consequence of the addition of nickel considering that the welding parameters were kept constant.

The AW condition presented a ferrite volume fraction of approximately 93% while the Ni70 condition presented an austenite volume fraction of approximately 95%. A higher amount of austenite will increase the corrosion resistance of the weld bead, but a decrease in the mechanical resistance since this function is developed by the ferrite.

The microstructures in the transition region between the base metal and weld bead for all the conditions are shown in Figure 39. For all conditions with nickel addition, although the amount of austenite in the fusion zone is greater than 50%, in the heat affected zone (HAZ) the amount of ferrite was higher than that of austenite. Even for the Ni30 condition, although the microstructure in the fusion zone is balanced, the HAZ presented an unbalanced microstructure with a higher amount of ferrite.

Figure 39 - SEM micrographs of transition region between base material and fusion zone for (a) AW, (b) Ni30, (c) Ni40, (d) Ni50, (e) Ni60 and (f) Ni70. Austenite is light and ferrite is dark. Beraha's etching

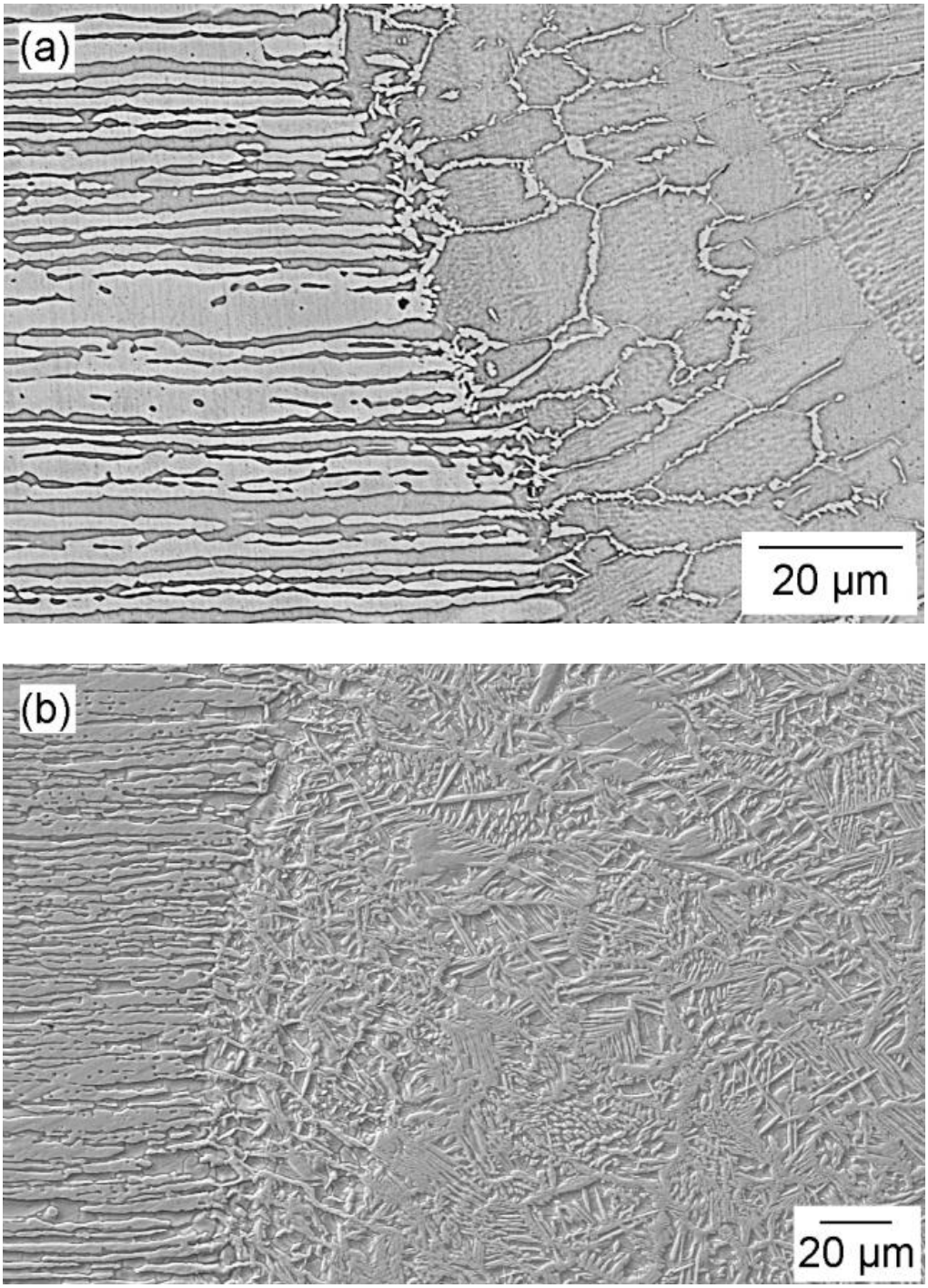

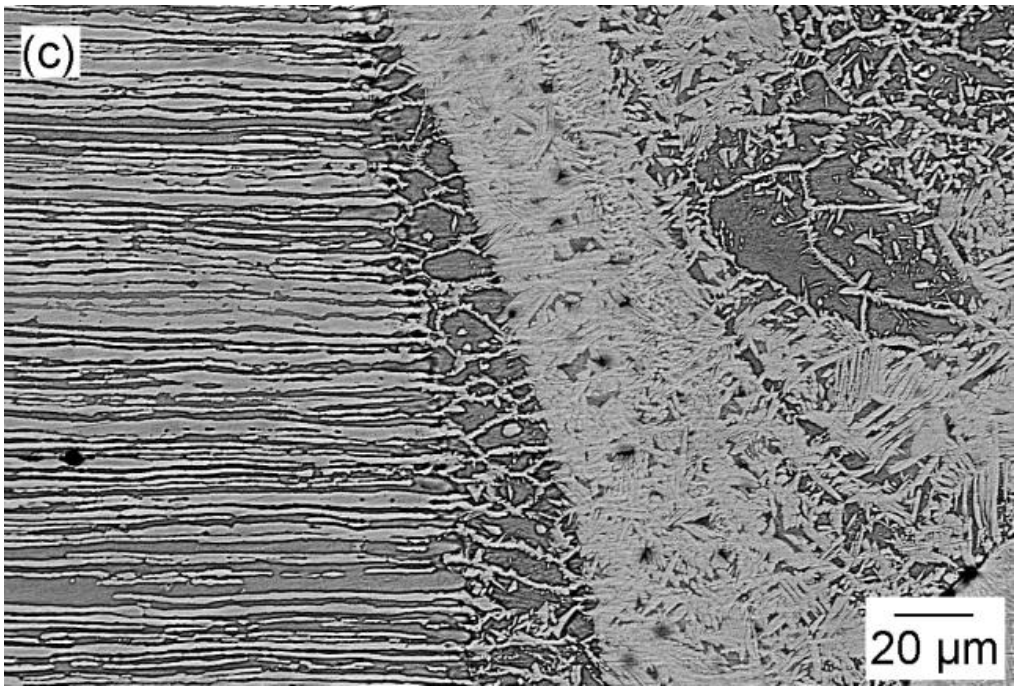
(c)
20 µm

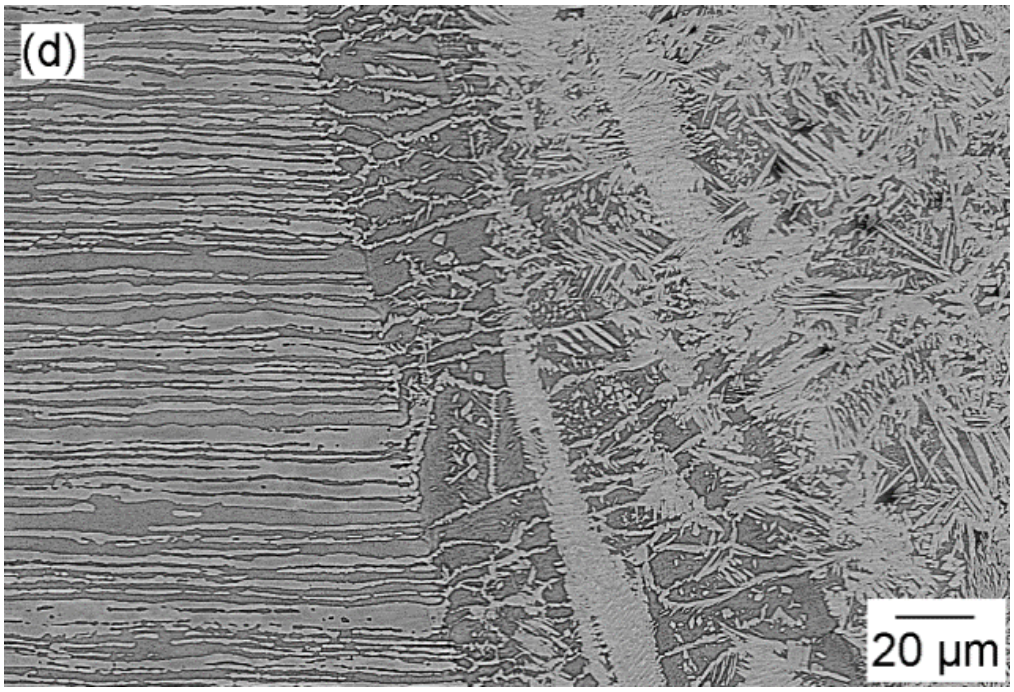
(d)
20 µm

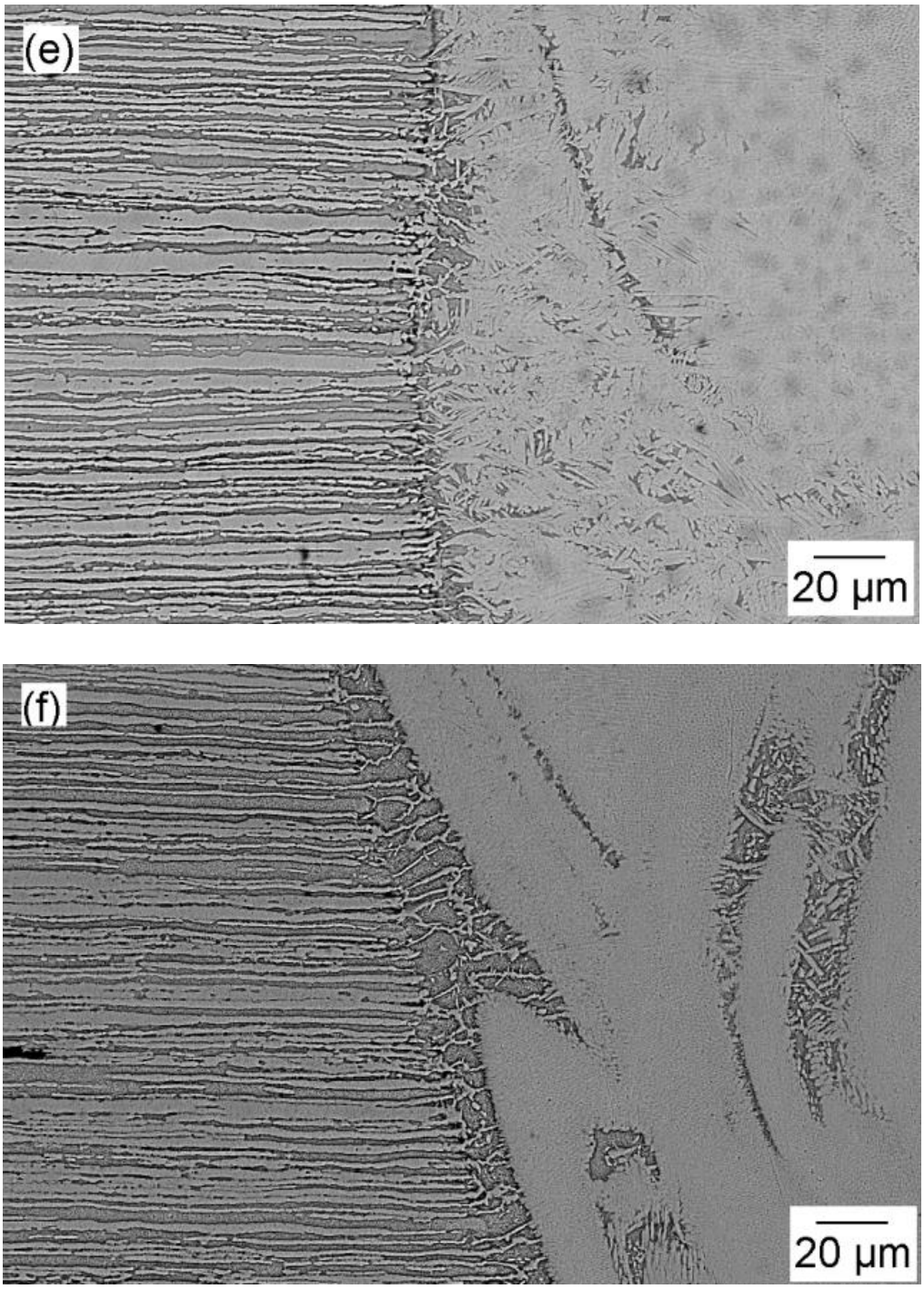

Source: Elaborated by author

The temperature reached in the HAZ is not high enough to melt the material but it modifies the phase balance. In the HAZ, the austenite fraction is slightly lower than at the weld center, which occurs because the cooling rate from the temperature range reached above γ-δ solvus (were the predominant structure is ferrite) is higher in this region, without enough time for more

austenite formation upon cooling. The unbalanced microstructure will affect the corrosion resistance of the HAZ.

In some welding processes like Submerged Arc Welding (SAW) or Gas Tungsten Arc Welding (GTAW), which may be followed by an isothermal heat treatment, secondary phases can precipitate in a temperature range between 700ºC and 950ºC [41,56]. The low heat input and the associated high cooling rate of Nd:YAG pulsed laser welding do not favour the formation of these phases.

To confirm the absence of secondary phases the samples were carefully analyzed by SEM with backscattered electron detector. In this case, the samples were not etched. Secondary phases should appear as a lighter spot located between ferrite grains and at austenite–ferrite phase boundaries, while chromium nitrides should appear as dark chains at ferrite/ferrite grain boundaries. No secondary phase was detected. Figure 40 shows the micrographs for all the condition.

Figure 40 - SEM (back-scattered electron) micrograph for (a) Ni30, (b) Ni40, (c) Ni50, (d) Ni60 and (e) Ni70. Dark line from top to bottom of image was added to point out the boundary between the two zones shown on the image

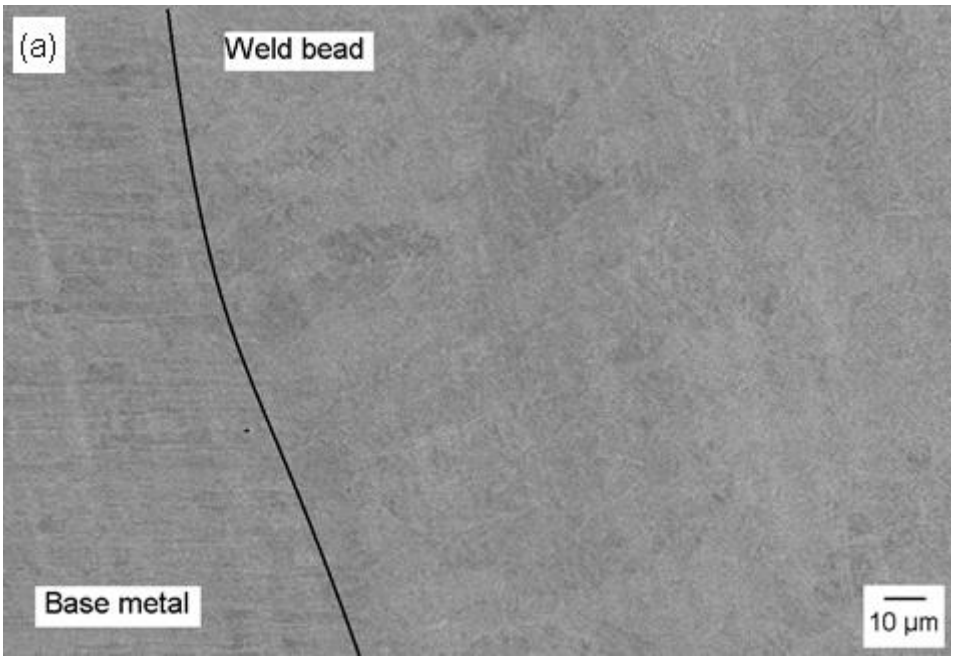

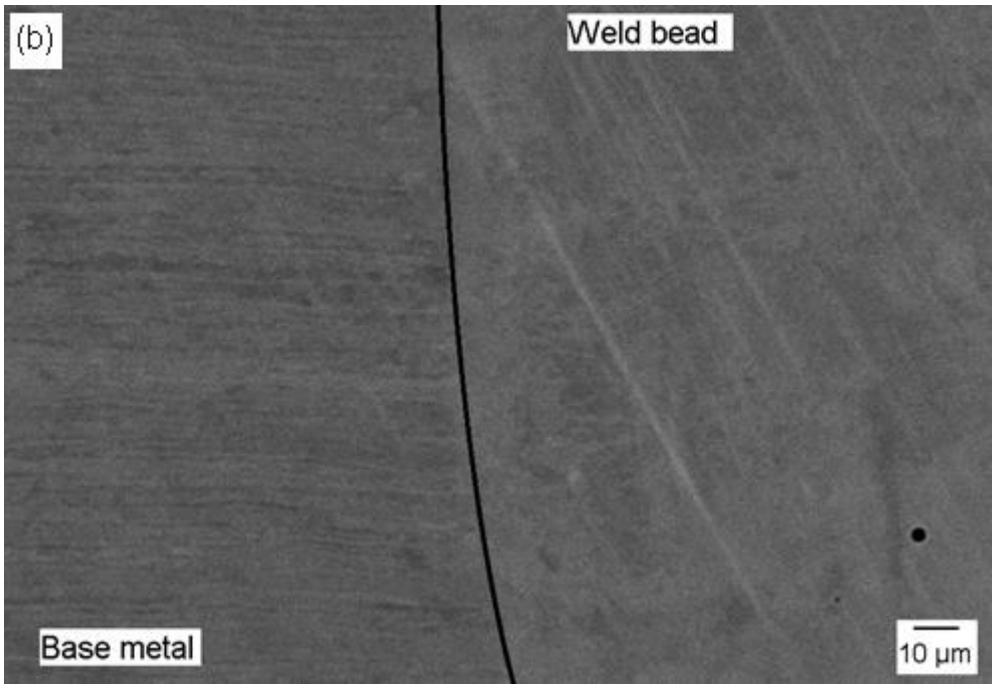
(b)
Weld bead
Base metal
10 µm

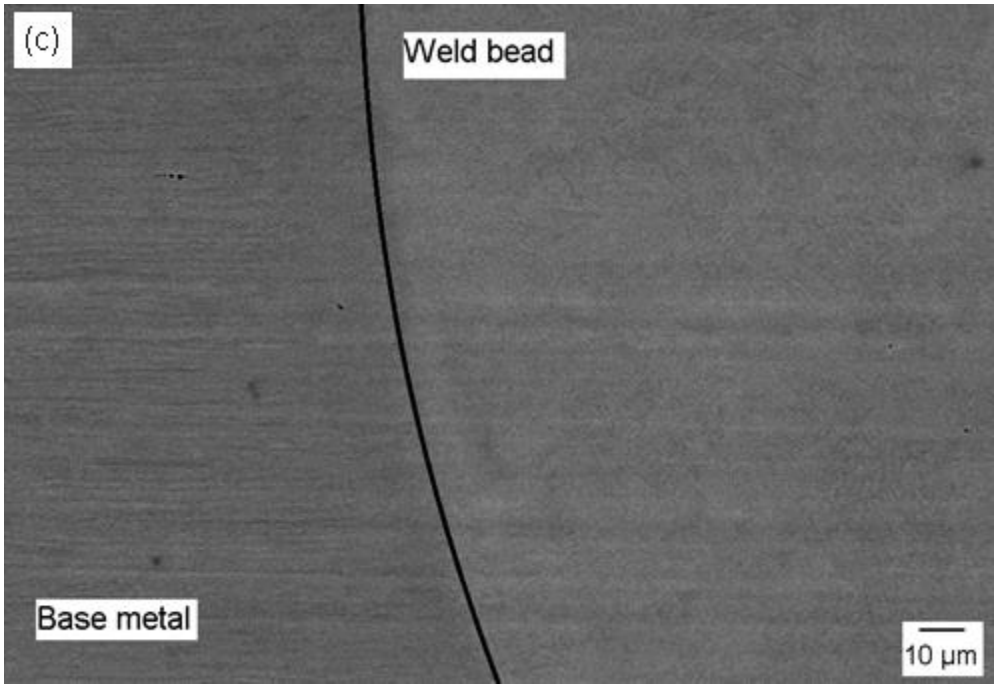
(c)
Weld bead
Base metal
10 µm

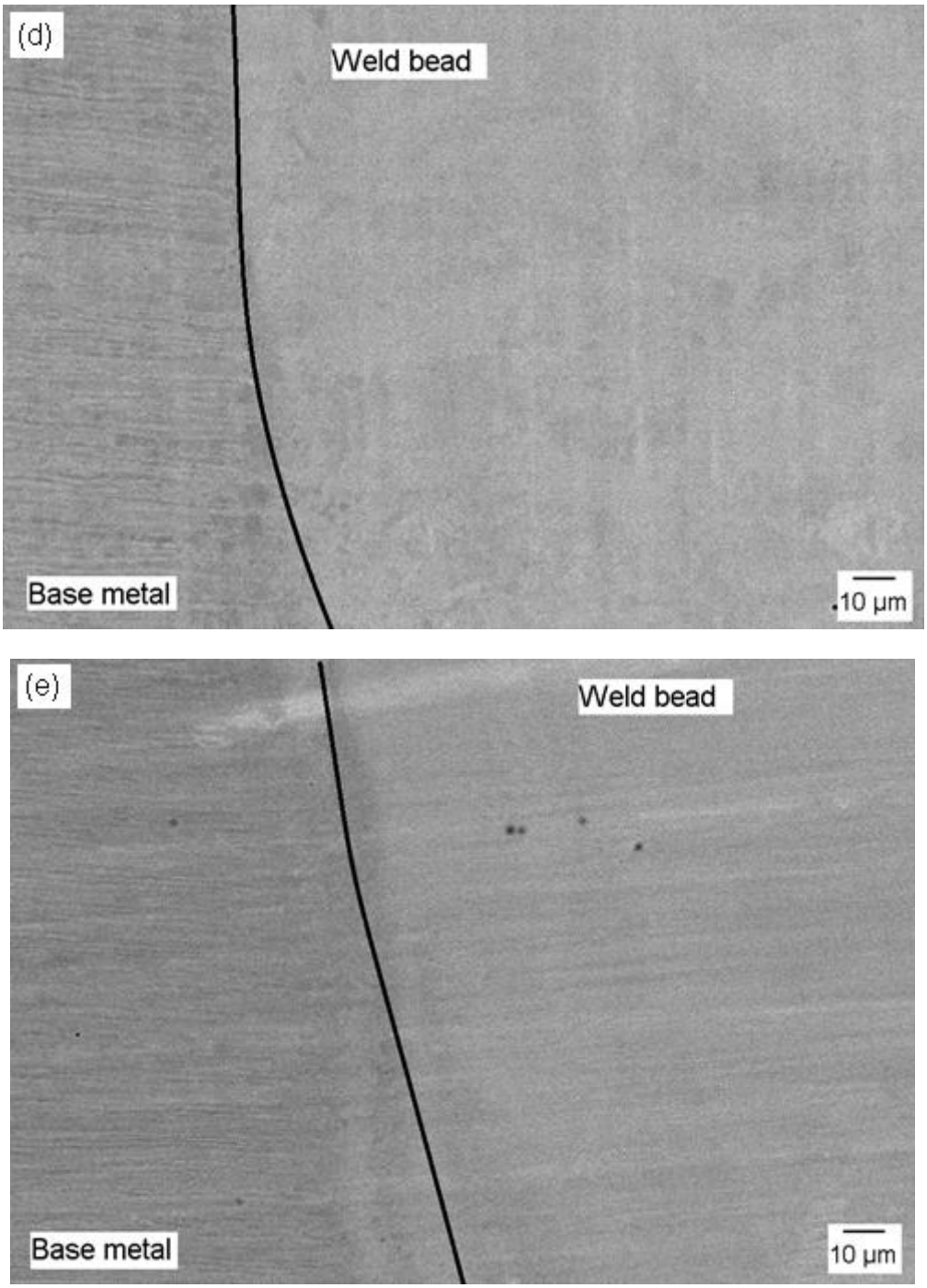

Source: Elaborated by author

Once Ni30 was the condition that achieved the phase balance, it was performed an Energy-dispersive X-ray spectroscopy (EDS) analysis to determinate the amount (wt. %) of nickel on the weld bead. Two regions were analyzed, base metal and weld bead. As expected the amount of nickel increased on the weld bead. Higher amount of nickel will expands austenite

field increasing the austenite volume fraction. Figure 41 shows the regions analyzed and Table 6 the amount of nickel and tree other elements (Fe, Cr, Mo).

Figure 41 – Regions for energy-dispersive X-ray (EDS) analysis on Ni30 condition

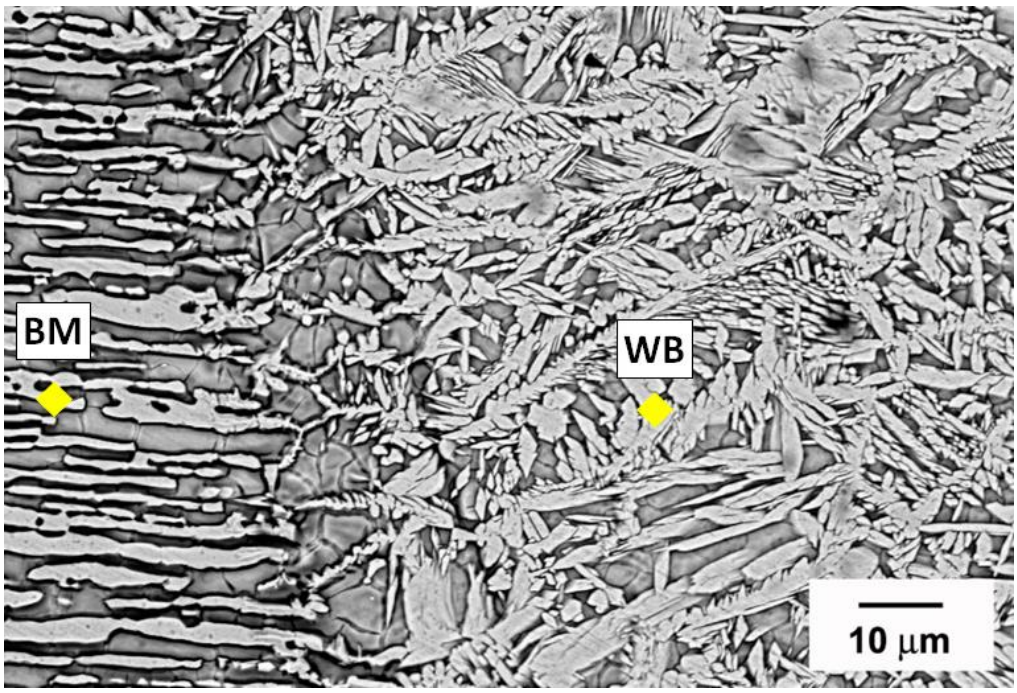

Source: Elaborated by author

Table 6 – Fe, Cr, Mo and Ni on the base metal and weld bead (wt. %)

Base Metal (BM)				Weld bead (WB)			
Fe	**Cr**	**Mo**	**Ni**	**Fe**	**Cr**	**Mo**	**Ni**
62.09	26.29	4.23	7.39	58.30	25.13	4.23	12.33

Source: Elaborated by author

4.2 MICROHARDNESS

The microhardness profile for all conditions is shown in Figure 42. As expected, a decrease in hardness is observed as the austenite volume fraction increases. For Ni50, Ni60, and Ni70 conditions the microhardness values are very close as the resulting microstructure is mainly austenitic, with some minor biphasic regions (austenite and ferrite).

Figure 42 - Microhardness profile

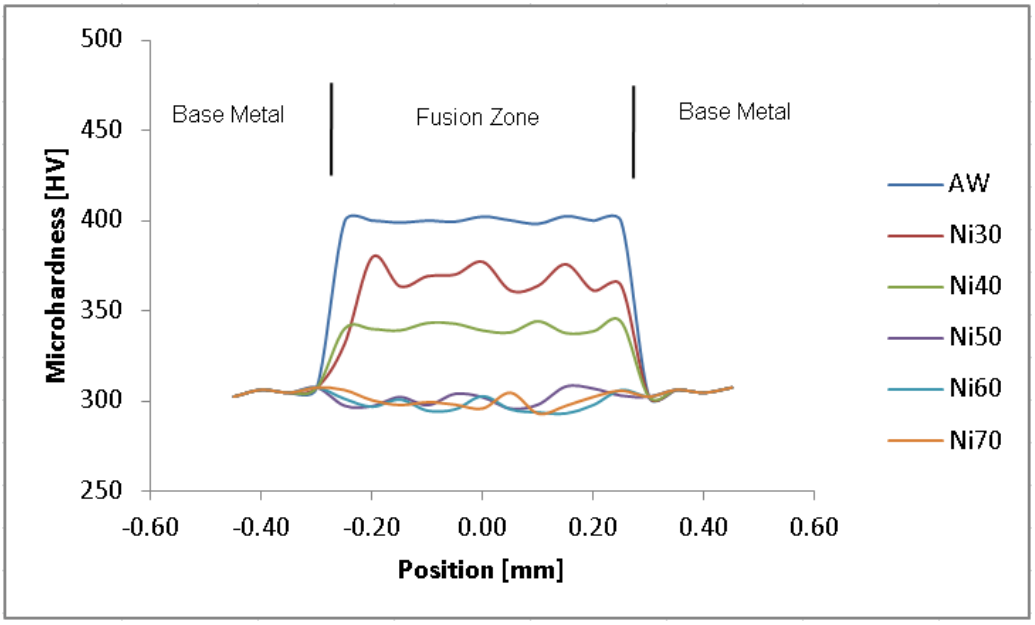

Source: Elaborated by author

The mean microhardness for the weld bead for each condition is shown in Table 7. The mean value of microhardness in the fusion zone for the AW condition was 400 ± 2 HV while for the Ni30 condition it was 365 ± 9 HV. As the AW condition presented a predominantly ferritic microstructure the microhardness in the fusion zone was higher. Although for the Ni30 condition the volume fraction are very close to those of the base material, the microhardness value was approximately 20% higher. The large amount of intragranular austenite and its arrangement along the fusion zone created dislocations thus raising the hardness, an effect also observed by Tahaei et al

[11]. It can be envisaged that the Ni30 condition could provide a weld bead with more toughness in comparison to AW.

Table 7 - Microhardness

Condition	Base Metal [HV]	Fusion Zone [HV]
Aw	307 ± 4	400 ± 2
Ni30	307 ± 4	365 ± 9
Ni40	307 ± 4	342± 3
Ni50	307 ± 4	303 ± 5
Ni60	307 ± 4	298 ± 3
Ni70	307 ± 4	298 ± 4

Source: Elaborated by author

4.3 TENSILE STRENGTH

The graphs Stress-Strain for all the conditions are shown in Figure 43.

Figure 43 - Stress x Strain curves

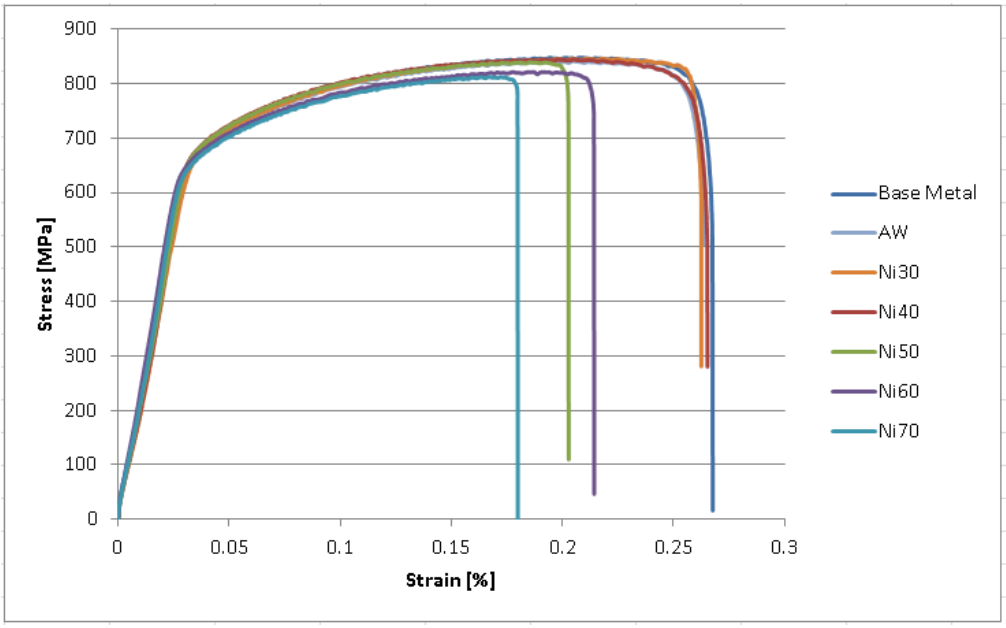

Source: Elaborated by author

The results of the tensile tests are presented in Table 8 and Figure 44 shows the tensile test specimens. For AW, Ni30 and Ni40 conditions the tensile strengths were equal since the fracture occurred in the base material (as presented in Figure 44). For these conditions the weld bead presented higher resistance than the base metal. For Ni50, Ni60 and Ni70 conditions, there were a little reduction in the tensile strengths, and the fractures occurred in the weld bead. As already mentioned, the weld bead hardness values for these conditions were slightly lower than that of the base metal justifying the observed slight decrease in tensile strength.

Table 8 - Results of tensile tests

Condition	Tensile Strength U.T.S [MPa]	Elongation [%]	Location of fracture
Base Metal	845 ± 9	26.8 ± 1.0	Base Metal
AW	845 ± 9	26.4 ± 1.0	Base Metal
Ni30	845 ± 8	26.3 ± 1.0	Base Metal
Ni40	845 ± 8	26.4 ± 1.0	Base Metal
Ni50	840 ± 11	20.3 ± 1.0	Weld bead
Ni60	822 ± 10	21.4 ± 1.0	Weld bead
Ni70	812 ± 11	18.0 ± 1.0	Weld bead

Source: Elaborated by author

Comparing the tensile strength for the Ni70 condition (which showed lower tensile strength) and the base metal, it was observed that the influence of the nickel on the tensile strength was not very large, since there was only a drop of 4% in resistance. Saravanan et. al. [57] in their study on the effect of heat input on microstructure and mechanical properties in SDSS laser welding also observed a small decrease in tensile strength in a microstructure with a higher proportion of austenite (consequently lower hardness), which behavior is similar to those presented in this research.

Figure 44 - Tensile test specimens

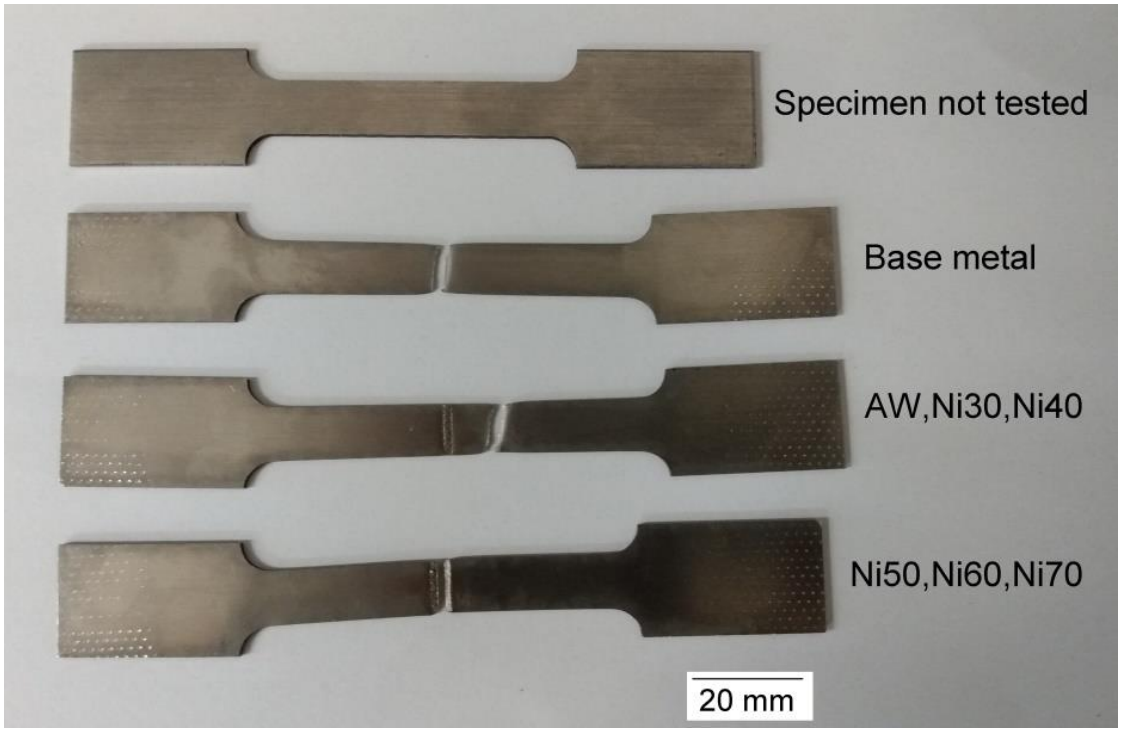

Source: Elaborated by author

Figure 45 shows the fractography for the base metal and for the Ni50 condition (once that Ni50, Ni60 and Ni70 have the same fracture behavior). The fracture surface for the base metal (Fig. 45 a) is free of cleavage with a visible necking area (Fig. 45 c) characterizing a ductile fracture. For the Ni50 condition (Fig. 45 b) it is possible to verify the presence of dimples but also some cleavage marks, the necking (Fig 45 d) is very small indicating little deformation before the fracture.

Based on tensile strength results the conditions Ni30 and Ni40 presented good weldability because the fracture occurred out of the welded region. For the conditions Ni50, Ni60 and Ni70 the facture was brittle and occurred on the weld bead.

Figure 45 - SEM fractographs of samples for: (a) Base metal, (b) Ni50, (c) Base metal and (d) Ni50

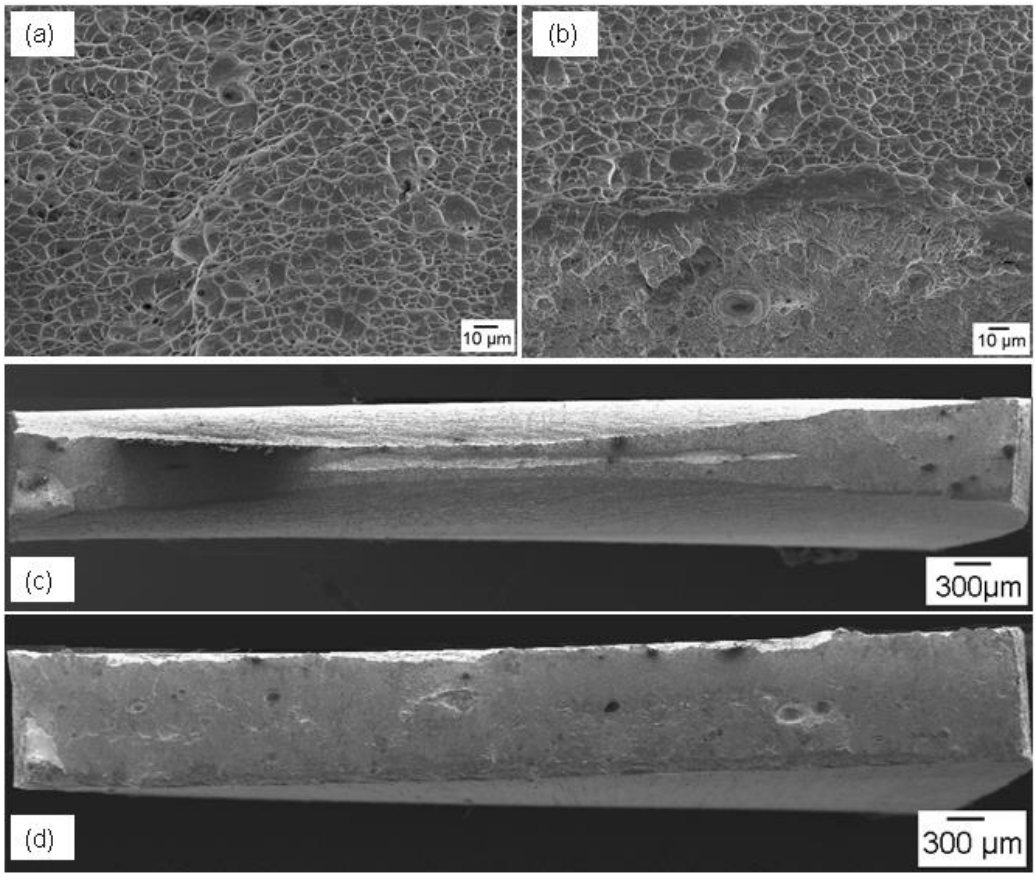

Source: Elaborated by author

4.4 CRITICAL PITTING TEMPERATURE

The results of the CPT tests are presented in Fig. 46 and Table 9.

Figure 46 - CPT curves

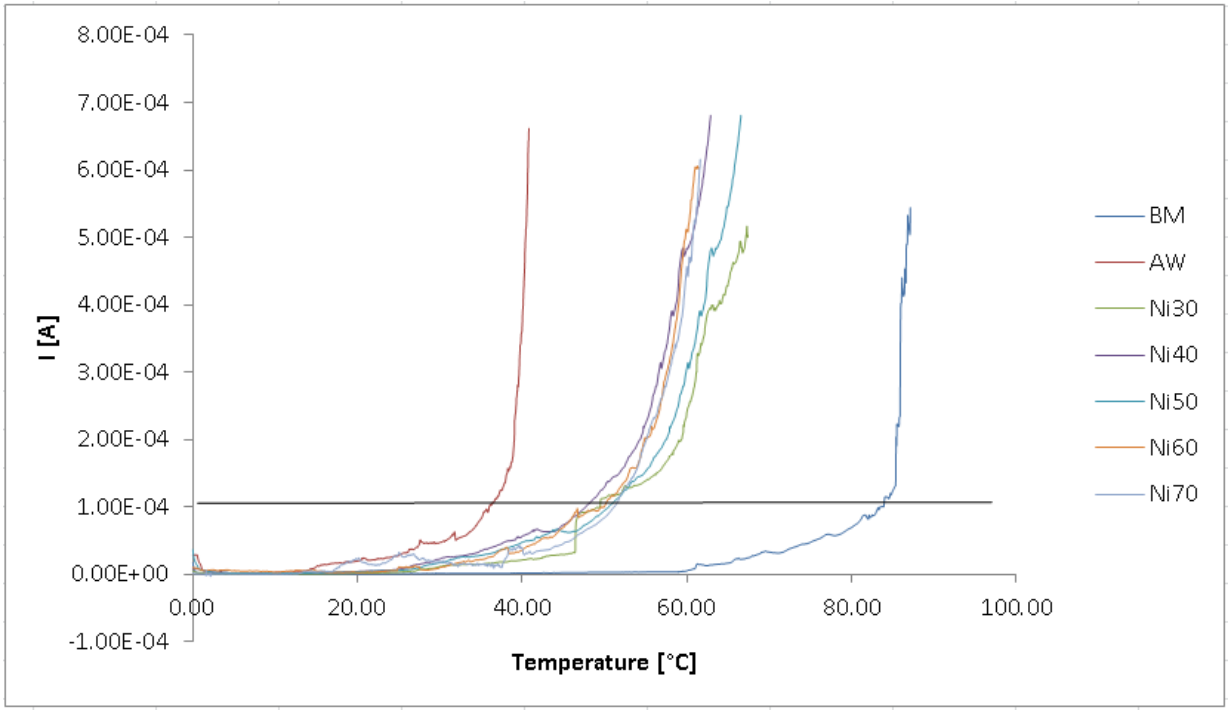

Source: Elaborated by author

Table 9 - CPT results

	CPT [°C]
Base Metal	83.5 ± 1.2
AW	36.0 ± 1.5
Ni30	49.5 ± 1.1
Ni40	49.0 ± 1.3
Ni50	50.5 ± 1.2
Ni60	50.0 ± 1.0
Ni70	51.0 ± 1.2

Source: Elaborated by author

The AW condition showed the lowest CPT (36ºC), a reduction of approximately 48°C in relation to the base metal, since it is the condition with the highest volume fraction of ferrite. Austenite content seems to be in direct relation with the corrosion resistance and the AW condition presented only 7.6% austenite in the phase balance.

The CPTs for nickel addition conditions were approximately the same regardless of the amount of nickel added. The higher the amount of austenite, the greater the resistance of the weld bead to corrosion. However, in all conditions with addition of nickel the pitting occurred outside the weld bead, that is in the HAZ, while the AW samples showed the pitting occurring in the weld bead. Figure 47 a and 47 b show the location of pitting for AW condition and for Ni30 condition respectively.

Figure 47 - Pits location after CPT tests for (a) AW and (b) Ni30

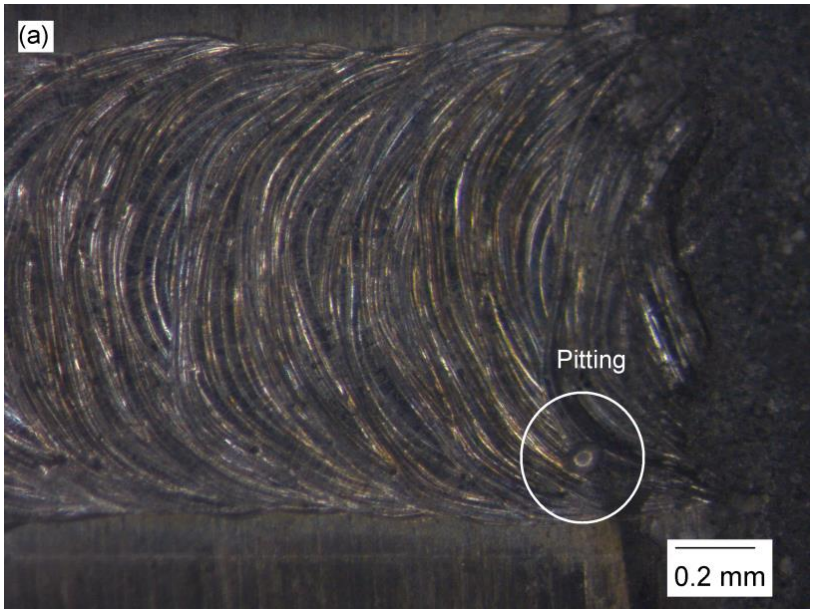

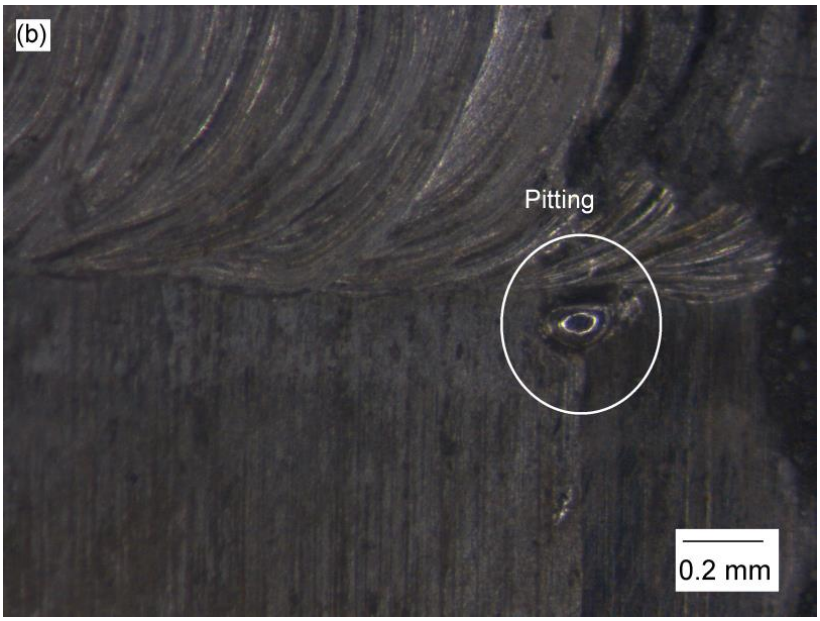

Source: Elaborated by author

As observed in Fig. 39, all conditions with nickel addition, although in the fusion zone the volumetric fraction of austenite is higher than 50%, the HAZ presents an unbalanced microstructure with greater amount of ferrite. This predominance of ferrite negatively affected the corrosion resistance of the HAZ, being the region where the pittings occurred.

Even if for the condition with addition of nickel the CPT´s were lower in relation to the base metal, it presented an increase of approximately 14 °C in relation to the autogenous welding, a significant increase in corrosion resistance.

5 CONCLUSIONS

The following conclusions could be drawn:

- Ni30 condition achieved the phase balance and consequently good mechanical properties and corrosion resistance were obtained;
- The addition of electrolytic nickel affected the formation of austenite both quantitatively and qualitatively, modifying its morphology and volume fraction;
- Compared to autogenous welding, the welds performed with nickel addition showed an higher corrosion resistance in terms of increase of CPTs.
- The CPTs for the different nickel addition examined were approximately the same regardless the amount of nickel added;
- For the AW condition the pitting occurred on the weld bead and for for all the conditions with addition of nickel it occurred outside the weld bead in the HAZ, likely because this region presents an unbalanced microstructure with higher amount of ferrite;
- For the Ni30 condition, although the volumetric fraction of austenite in the fusion zone was close to that of the base material, the hardness was higher, since the morphology and arrangement of the austenite along the fusion zone affected the hardness of the region. On the other hand, hardness decreased with further increase of nickel added;
- For the conditions Ni30 and Ni40 the tensile strength was equal to that of the base metal, the fracture was ductile and occurred out of the welded region. The Ni50, Ni60 and Ni70 condition presented a slight decrease in tensile strength, the fracture was brittle and occurred on the weld bead.

5.1 FURTHER WORKS

As further works are recommended:

- Conduct a study similar to this however with others austenite-forming elements;
- Perform nickel enrichment through an electrochemistry process.
- Perform a pré-weld heat treatment or/and pós-weld heat treatment as an option to optimize the phase balance on the HAZ.

REFERENCES

[1] Zhang, Ziying, Hui Zhao, Huizhen Zhang, Jun Hu, and Jiarui Jin. “Microstructure Evolution and Pitting Corrosion Behavior of UNS S32750 Super Duplex Stainless Steel Welds after Short-Time Heat Treatment.” Corrosion Science 121 (2017): 22–31. https://doi.org/10.1016/j.corsci.2017.02.006.

[2] Ramkumar, K. Devendranath, G. Thiruvengatam, S.p. Sudharsan, Debidutta Mishra, N. Arivazhagan, and R. Sridhar. “Characterization of Weld Strength and Impact Toughness in the Multi-Pass Welding of Super-Duplex Stainless Steel UNS 32750.” Materials & Design 60 (2014): 125–35. https://doi.org/10.1016/j.matdes.2014.03.031.

[3] Saravanan, S., K. Raghukandan, and N. Sivagurumanikandan. “Pulsed Nd: YAG Laser Welding and Subsequent Post-Weld Heat Treatment on Super Duplex Stainless Steel.” Journal of Manufacturing Processes 25 (2017): 284–89. https://doi.org/10.1016/j.jmapro.2016.12.015.

[4] Tan, Hua, Zhiyu Wang, Yiming Jiang, Yanze Yang, Bo Deng, Hongmei Song, and Jin Li. “Influence of Welding Thermal Cycles on Microstructure and Pitting Corrosion Resistance of 2304 Duplex Stainless Steels.” Corrosion Science 55 (2012): 368–77. https://doi.org/10.1016/j.corsci.2011.10.039.

[5] Arun, D., K. Devendranath Ramkumar, and R. Vimala. “Multi-Pass Arc Welding Techniques of 12 Mm Thick Super-Duplex Stainless Steel.” Journal of Materials Processing Technology 271 (2019): 126–43. https://doi.org/10.1016/j.jmatprotec.2019.03.031.

[6] Ventrella, Vicente Afonso, José Roberto Berretta, and Wagner De Rossi. “Pulsed Nd:YAG Laser Seam Welding of AISI 316L Stainless Steel Thin Foils.” Journal of Materials Processing Technology 210, no. 14 (2010): 1838–43. https://doi.org/10.1016/j.jmatprotec.2010.06.015.

[7] Hu, Yu, Yonghua Shi, Xiaoqin Shen, and Zhongmin Wang. “Microstructure Evolution and Selective Corrosion Resistance in Underwater Multi-Pass 2101 Duplex Stainless Steel Welding Joints.” Metallurgical and Materials Transactions A 49, no. 8 (2018): 3306–20. https://doi.org/10.1007/s11661-018-4686-0.

[8] Muthupandi, V., P. Bala Srinivasan, V. Shankar, S.k. Seshadri, and S. Sundaresan. “Effect of Nickel and Nitrogen Addition on the Microstructure and

Mechanical Properties of Power Beam Processed Duplex Stainless Steel (UNS 31803) Weld Metals." Materials Letters 59, no. 18 (2005): 2305–9. https://doi.org/10.1016/j.matlet.2005.03.010.

[9] Migiakis, K., and G. D. Papadimitriou. "Effect of Nitrogen and Nickel on the Microstructure and Mechanical Properties of Plasma Welded UNS S32760 Super-Duplex Stainless Steels." Journal of Materials Science 44, no. 23 (2009): 6372–83. https://doi.org/10.1007/s10853-009-3878-9.

[10] Pilhagen, Johan, and Rolf Sandström. "Influence of Nickel on the Toughness of Lean Duplex Stainless Steel Welds." Materials Science and Engineering: A 602 (2014): 49–57. https://doi.org/10.1016/j.msea.2014.01.093.

[11] Tahaei, Ali, Argelia Fabiola Miranda Perez, Mattia Merlin, Felipe Arturo Reyes Valdes, and Gian Luca Garagnani. "Effect of the Addition of Nickel Powder and Post Weld Heat Treatment on the Metallurgical and Mechanical Properties of the Welded UNS S32304 Duplex Stainless Steel." Soldagem & Inspeção 21, no. 2 (2016): 197–208. https://doi.org/10.1590/0104-9224/si2102.09.

[12] Zhang, Zhiqiang, Hongyang Jing, Lianyong Xu, Yongdian Han, Lei Zhao, and Chao Zhou. "Effects of Nitrogen in Shielding Gas on Microstructure Evolution and Localized Corrosion Behavior of Duplex Stainless Steel Welding Joint." Applied Surface Science 404 (2017): 110–28. https://doi.org/10.1016/j.apsusc.2017.01.252.

[13] Lo, K.h., C.h. Shek, and J.k.l. Lai. "Recent Developments in Stainless Steels." Materials Science and Engineering: R: Reports 65, no. 4-6 (2009): 39–104. https://doi.org/10.1016/j.mser.2009.03.001.

[14] ASM Handbook. 1990. Properties and selection: Irons, Steel and High-Perfomance Alloys. USA: ASM International.

[15] Lima, Daniela Bianchi Ponce Leon de. "Avaliação Da Soldabilidade Do Aço Inoxidável Superduplex UNS S32750," 2006. ttps://acervodigital.ufpr.br/handle/1884/7358.

[16] ISSF. "Statistics Stainless Steel 2019." ISSF Website. Accessed May 6, 2020. https://www.worldstainless.org/statistics/stainless-steel-meltshop-production/2019/.

[17] ABINOX. “ESTATÍSTICAS ANUAIS: AÇO INOX: ABINOX - Associação Brasileira Do Aço Inoxidável.” ABINOX. Accessed May 6, 2020. https://www.abinox.org.br/site/aco-inox-estatisticas-anuais.php.

[18] Verma, Jagesvar, and Ravindra Vasantrao Taiwade. “Effect of Welding Processes and Conditions on the Microstructure, Mechanical Properties and Corrosion Resistance of Duplex Stainless Steel Weldments—A Review.” Journal of Manufacturing Processes 25 (2017): 134–52. https://doi.org/10.1016/j.jmapro.2016.11.003.

[19] Bai, Yang, Tong He, and Yandong Liu. “Effects of Sn Microalloying on Cold Rolling and Recrystallization Textures and Microstructure of a Ferritic Stainless Steel.” Materials Characterization 137 (2018): 142–50. https://doi.org/10.1016/j.matchar.2018.01.022

[20] Yan, Haitao, Hongyun Bi, Xin Li, and Zhou Xu. “Microstructure, Texture and Grain Boundaries Character Distribution Evolution of Ferritic Stainless Steel during Rolling Process.” Journal of Materials Processing Technology 209, no. 5 (2009): 2627–31. https://doi.org/10.1016/j.jmatprotec.2008.06.012.

[21] Phaniraj, M.p., Dong-Ik Kim, and Young Whan Cho. “Effect of Grain Boundary Characteristics on the Oxidation Behavior of Ferritic Stainless Steel.” Corrosion Science 53, no. 12 (2011): 4124–30. https://doi.org/10.1016/j.corsci.2011.08.020.

[22] Neri, M.a, and R Colás. “Analysis of a Martensitic Stainless Steel That Failed Due to the Presence of Coarse Carbides.” Materials Characterization 47, no. 3-4 (2001): 283–89. https://doi.org/10.1016/s1044-5803(01)00189-9.

[23] Khodabakhshi, F., M.h. Farshidianfar, A.p. Gerlich, M. Nosko, V. Trembošová, and A. Khajepour. “Effects of Laser Additive Manufacturing on Microstructure and Crystallographic Texture of Austenitic and Martensitic Stainless Steels.” Additive Manufacturing 31 (2020): 100915. https://doi.org/10.1016/j.addma.2019.100915.

[24] Kumar, Nikhil, Manidipto Mukherjee, and Asish Bandyopadhyay. “Study on Laser Welding of Austenitic Stainless Steel by Varying Incident Angle of Pulsed Laser Beam.” Optics & Laser Technology 94 (2017): 296–309. https://doi.org/10.1016/j.optlastec.2017.04.008.

[25] Tomashchuk, I., D. Grevey, and P. Sallamand. “Dissimilar Laser Welding of AISI 316L Stainless Steel to Ti6–Al4–6V Alloy via Pure Vanadium Interlayer.”

Materials Science and Engineering: A 622 (2015): 37–45. https://doi.org/10.1016/j.msea.2014.10.084.

[26] Leite, Carla Gabriela Silva, Eli Jorge Da Cruz Junior, Mattia Lago, Andrea Zambon, Irene Calliari, and Vicente Afonso Ventrella. “Nd: YAG Pulsed Laser Dissimilar Welding of UNS S32750 Duplex with 316L Austenitic Stainless Steel.” Materials 12, no. 18 (2019): 2906. https://doi.org/10.3390/ma12182906.

[27] Kang, D.h., and H.w. Lee. “Study of the Correlation between Pitting Corrosion and the Component Ratio of the Dual Phase in Duplex Stainless Steel Welds.” Corrosion Science 74 (2013): 396–407. https://doi.org/10.1016/j.corsci.2013.04.033.

[28] Nakhaie, Davood, and Mohammad Hadi Moayed. “Pitting Corrosion of Cold Rolled Solution Treated 17-4 PH Stainless Steel.” Corrosion Science 80 (2014): 290–98. https://doi.org/10.1016/j.corsci.2013.11.039.

[29] Nasiłowska, Barbara, Zdzisław Bogdanowicz, and Michał Wojucki. “Shot Peening Effect on 904 L Welds Corrosion Resistance.” Journal of Constructional Steel Research 115 (2015): 276–82. https://doi.org/10.1016/j.jcsr.2015.08.041.

[30] Liou, Horng-Yih, Rong-Iuan Hsieh, and Wen-Ta Tsai. “Microstructure and Pitting Corrosion in Simulated Heat-Affected Zones of Duplex Stainless Steels.” Materials Chemistry and Physics 74, no. 1 (2002): 33–42. https://doi.org/10.1016/s0254-0584(01)00409-6.

[31] Kang, D.h., and H.w. Lee. “Study of the Correlation between Pitting Corrosion and the Component Ratio of the Dual Phase in Duplex Stainless Steel Welds.” Corrosion Science 74 (2013): 396–407. https://doi.org/10.1016/j.corsci.2013.04.033

[32] Terada, Maysa, Mitiko Saiki, Isolda Costa, and Angelo Fernando Padilha. “Microstructure and Intergranular Corrosion of the Austenitic Stainless Steel 1.4970.” Journal of Nuclear Materials 358, no. 1 (2006): 40–46. https://doi.org/10.1016/j.jnucmat.2006.06.010.

[33] Modenesi, Paulo J. Soldabilidade Dos Aços Austeníticos. São Paulo, SP: SENAI, 2001.

[34] Bhadeshia, H. K. D. H., and R. W. K. Honeycombe. Steels: Microstructure and Properties. Amsterdam: Butterworth-Heinemann, 2017.

[35] Rostfria stål. Stockholm: SIS, 1983.

[36] Pohl, Michael, Oliver Storz, and Thomas Glogowski. “Effect of Intermetallic Precipitations on the Properties of Duplex Stainless Steel.” Materials Characterization 58, no. 1 (2007): 65–71. https://doi.org/10.1016/j.matchar.2006.03.015.

[37] Jarvis, B.L., and Tanaka, M. New Developments in Advanced Welding. Boca Raton, FL: CRC Press, 2005.

[38] Mohammed, Ghusoon, Mahadzir Ishak, Syarifah Aqida, and Hassan Abdulhadi. “Effects of Heat Input on Microstructure, Corrosion and Mechanical Characteristics of Welded Austenitic and Duplex Stainless Steels: A Review.” Metals 7, no. 2 (2017): 39. https://doi.org/10.3390/met7020039.

[39] M, Mohammed Asif, Kulkarni Anup Shrikrishna, P. Sathiya, and Sunkulp Goel. “The Impact of Heat Input on the Strength, Toughness, Microhardness, Microstructure and Corrosion Aspects of Friction Welded Duplex Stainless Steel Joints.” Journal of Manufacturing Processes 18 (2015): 92–106. https://doi.org/10.1016/j.jmapro.2015.01.004.

[40] Da Cruz Junior, Eli J., Otacilio D. Franzini, Irene Calliari, and Vicente A. Ventrella. “Effects of Nickel Addition on the Microstructure of Laser-Welded UNS S32750 Duplex Stainless Steel.” Metallurgical and Materials Transactions A 50, no. 4 (2019): 1616–18. https://doi.org/10.1007/s11661-019-05115-1.

[41] Singh, Jastej, and A.s. Shahi. “Metallurgical, Impact and Fatigue Performance of Electron Beam Welded Duplex Stainless Steel Joints.” Journal of Materials Processing Technology 272 (2019): 137–48. https://doi.org/10.1016/j.jmatprotec.2019.05.010.

[42] Pettersson, Niklas, Rachel F. A. Pettersson, and Sten Wessman. “Precipitation of Chromium Nitrides in the Super Duplex Stainless Steel 2507.” Metallurgical and Materials Transactions A 46, no. 3 (2015): 1062–72. https://doi.org/10.1007/s11661-014-2718-y.

[43] Gennari, Claudio, Luca Pezzato, Enrico Piva, Renato Gobbo, and Irene Calliari. “Influence of Small Amount and Different Morphology of Secondary Phases on Impact Toughness of UNS S32205 Duplex Stainless Steel.” Materials Science and Engineering: A 729 (2018): 149–56. https://doi.org/10.1016/j.msea.2018.05.063.

[44] Kavamura, Haroldo Akira. “Aplicação De Solda Laser Em Carrocerias Automotivas: Estudo Comparativo Entre a Solda Laser e a Solda Ponto Por resistência,” 2007.

[45] “Advanced Materials and Lab Equipment Supplier.” MSE Supplies LLC. Accessed May 6, 2020. https://www.msesupplies.com/products/ndyag-nd-doped-yttrium-aluminium-garnet-laser-crystal.

[46] Katayama, Seiji. Handbook of Laser Welding Technologies. Cambridge: Woodhead publ., 2013.

[47] Steen, W. M., and Jyotiromoy Mazumder. Laser Material Processing. London: Springer, 2010.

[48] América, Amada Miyachi. Laser Welding Fundamentals. Califórnia, 2016. https://dev.amadamiyachi.com/wp-content/uploads/2019/12/Laser-Welding-Fundamentals.pdf.

[49] Benter, Christian., Petring, Dirk, Poprawe, Reinhart. 2005. “Investigation of the transition from heat conduction to deep penetration welding with high power diode lasers”. Laser in Manufacturing 2005 – Proceedings of the Third International WLT-Conference on Lasers in Manufacturing, pp. 67-71, Munich, Germany.

[50] Jin, Xiangzhong, Lijun Li, and Yi Zhang. “A Heat Transfer Model for Deep Penetration Laser Welding Based on an Actual Keyhole.” International Journal of Heat and Mass Transfer 46, no. 1 (2003): 15–22. https://doi.org/10.1016/s0017-9310(02)00255-7.

[51] Franzini, Otacilio Donizete. “Aplicação De Laser Pulsado Nd:YAG Na Soldagem Do Aço Super Duplex UNS S32750,” 2016.

[52] Lapsanska, Hana, Hana Chmelickova, and Miroslav Hrabovsky. “Effect of Beam Energy on Weld Geometric Characteristics in Nd:YAG Laser Overlapping

Spot Welding of Thin AISI 304 Stainless Steel Sheets." Metallurgical and Materials Transactions B 41, no. 5 (2010): 1108–15. https://doi.org/10.1007/s11663-010-9399-8.

[53] Souza, Sergio Augusto de. Ensaios Mecanicos De Materiais Metalicos: Fundamentos Teoricos e Praticos. São Paulo (SP): E. Blucher, 1982.

[54] Gennari, Claudio, Mattia Lago, Balint Bögre, Istvan Meszaros, Irene Calliari, and Luca Pezzato. "Microstructural and Corrosion Properties of Cold Rolled Laser Welded UNS S32750 Duplex Stainless Steel." Metals 8, no. 12 (2018): 1074. https://doi.org/10.3390/met8121074.

[55] Muthupandi, V., P. Bala Srinivasan, S.k. Seshadri, and S. Sundaresan. "Effect of Weld Metal Chemistry and Heat Input on the Structure and Properties of Duplex Stainless Steel Welds." Materials Science and Engineering: A 358, no. 1-2 (2003): 9–16. https://doi.org/10.1016/s0921-5093(03)00077-7.

[56] Vach, Marián, Terézia Kuníková, Mária Dománková, Peter Ševc, Ľubomír Čaplovič, Peter Gogola, and Jozef Janovec. "Evolution of Secondary Phases in Austenitic Stainless Steels during Long-Term Exposures at 600, 650 and 800 °C." Materials Characterization 59, no. 12 (2008): 1792–98. https://doi.org/10.1016/j.matchar.2008.04.009.

[57] Saravanan, S., N. Sivagurumanikandan, and K. Raghukandan. "Effect of Heat Input on Microstructure and Mechanical Properties of Nd: YAG Laser Welded Super Duplex Stainless Steel-Numerical and Experimental Approach." Optik 185 (2019): 447–55. https://doi.org/10.1016/j.ijleo.2019.03.145.

[58] Rose, Ian, and Clive Whittington. NICKEL PLATING HANDBOOK. Brussels: Nickel Institute, 2014.

A1 - PAPERS AND CONFERENCES

Listed below are the published papers and papers presented at conferences during the doctorate degree.

Papers

E.J. da Cruz Junior, O.D. Franzini, I. Calliari, V. A. Ventrella, Effects of Nickel Addition on the Microstructure of Laser-Welded UNS S32750 Duplex Stainless Steel, Metall. and Mat. Trans. A, 50 (2019) 1616-1618. https://doi.org/10.1007/s11661-019-05115-1

C. G. S. Leite, E. J. da Cruz Junior, M. Lago, A. Zombon, I. Calliari, V. A. Ventrella, Nd:YAG Pulsed Laser Dissimilar Welding of UNS S32750 Duplex with 316L Austenit Stainless Steel, Materials, 12 (2019). https://doi.org/10.3390/ma12182906

Conferences

CRUZ JUNIOR, ELI; VENTRELLA, VICENTE AFONSO. APLICAÇÃO DE LASER PULSADO Nd:YAG NAS SOLDAGENS AUTÓGENA E COM ADIÇÃO DE NÍQUEL EM AÇOS INOXIDÁVEIS DUPLEX UNS S32750. In: **COBEF 2019**, 2019. 10º Congresso Brasileiro de Engenharia de Fabricação, 2019

DA CRUZ JUNIOR, ELI JORGE; VIDEIRA, A. M. ; CALLIARI, IRENE ; VENTRELLA, VICENTE A. . COMPARISON BETWEEN AUTOGENOUS WELDING AND WITH ADDITION OF NICKEL ON Nd:YAG PULSED LASER WELDED UNS S32750 DUPLEX STAINLESS STEEL. In: **ESSC & DUPLEX, 2019**, Viena. ESSC & DUPLEX, 2019. v. 1. p. 1-6

VIDEIRA, A. M. ; DA CRUZ JUNIOR, ELI J. ; LAGO, MATTIA ; IRENE CALLIARI ; VENTRELLA, VICENTE A. . Nd-YAG LASER PULSED WELDING: EFFECTS ON THE SUPERDUPLEX STAINLESS STEEL UNS S32750. In: **ESSC & DUPLEX 2019**, 2019, Viena. ESSC & DUPLEX, 2019. v. 1. p. 1-6

CARVALHO, L. V. M. ; DA CRUZ JUNIOR, ELI J. ; VENTRELLA, VICENTE A. . ANÁLISE DA ADIÇÃO DE NÍQUEL ELETROLÍTICO NA SOLDAGEM LASER DO AÇO SUPERDUPLEX UNS S32750. In: **74º Congresso Anual da ABM**, 2019, São Paulo. 74º Congresso Anual da ABM, 2019. v. 1. p. 1-6.

A2 – PRELIMINARY RESULTS (WATTS BATH)

The objective of this thesis was to study the effect of using electrolytic nickel foil, as an addition metal, on the microstructure, mechanical properties and corrosion resistance of UNS S32750 DSS welded by the Nd:YAG pulsed laser. The results were good, indicating that the technique worked.

Thinking of an industrial application, the use of nickel foils would be difficult, once that the production of nickel foils demands a lot of time and resources and still the limitations on the dimensions an shapes of the foils. One of further works proposed was to perform nickel enrichment through an electrochemistry process.

The Watts Bath is one of the techniques to perform nickel electroplating. In order to validate the technique, as one of the ways to obtain balanced phases in DSS laser welding, this annex presents some preliminary results of a new research involving the application of Nd:YAG pulsed laser welding on DSS with nickel addition through Watts Bath technique.

A2.1 METHODOLOGY

The electrodeposition process involves passing an electric current between two electrodes immersed in an electrolyte. The positively charged electrode is the anode and the negatively charged electrode is the cathode. The electrolyte contains electrically charged particles or ions. Generally in nickel electroplating (Watts Bath), the anodes are composed of electrolytic nickel. The electrolyte contains soluble nickel salts [58].

The base metal (UNS S32750), in sheets of 1.5 mm thickness was subjected to Watts Bath to perform the nickel enrichment on the surface to be welded. The welding parameters were the same presented on the thesis. Three different layer´s thickness (15 µm, 25 µm and 35 µm) were obtained controlling the time of Watts Bath process. More details about the Watts Bath will be

presented in a further work. Figure 48 shows an optical micrograph of the layer (15 µm) of nickel electrodeposited on the base metal.

Figure 48 – Nickel layer electrodeposited

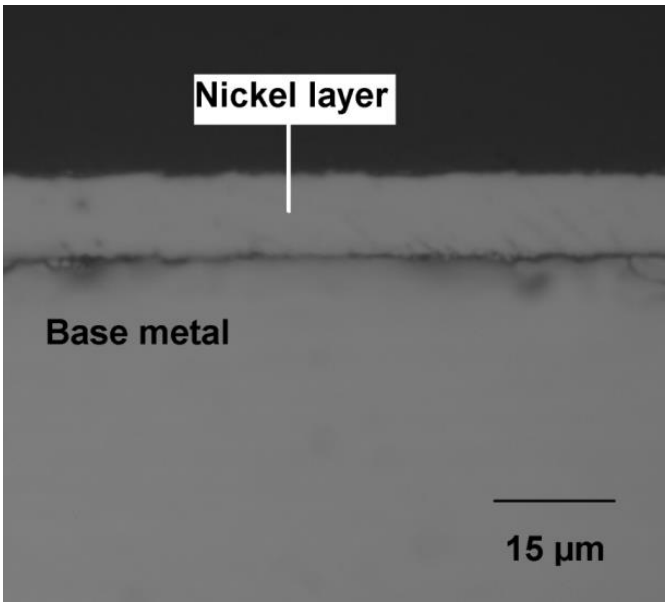

Source: Elaborated by author

For welding, it was used one piece of UNS S32750 with the nickel electrodeposited layer (on the desire thickness) and another without, as presented in Figure 49.

Figure 49 – Schematic diagram of welding pieces

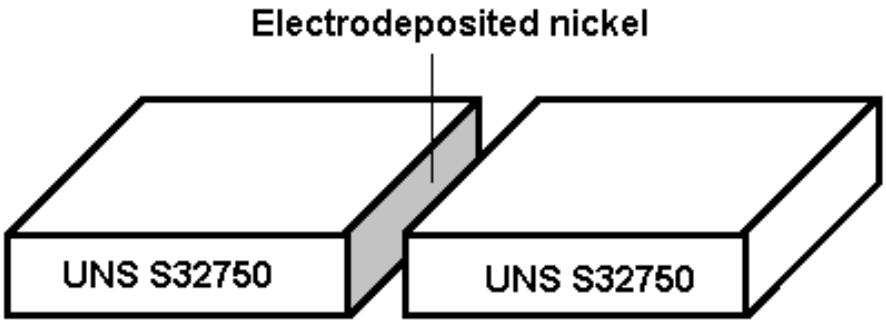

Source: Elaborated by author

A2.2 RESULTS AND DISCUSSION

The microstructures of the weld bead for the condition with 15 µm electrodeposited nickel layer are shown in Figure 50. Austenite is light and ferrite is dark.

Figure 50 – SEM micrographs of fusion zone for 15 µm

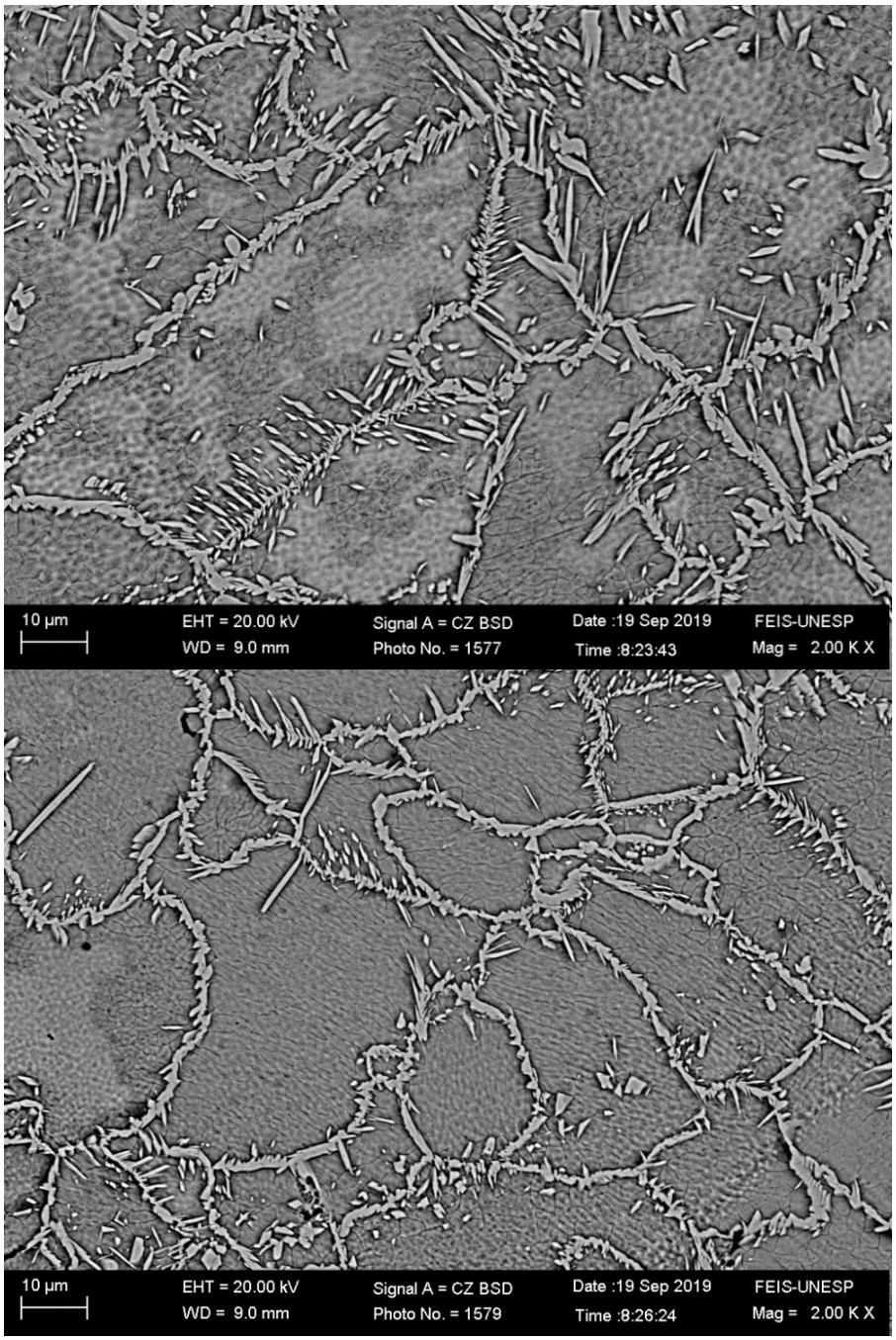

Source: Elaborated by author

As expected, there was an increase in the austenite amount in comparison to autogenous welding. Using the same technique, presented in this work, to determine the volume fraction, this condition presented 25.0 ± 1.6 % of austenite. Nickel promoted the increase of austenite on the weld bead but not enough to achieve balanced phases.

The microstructure in the transition region between the base metal and weld bead for this condition is shown in Figure 51. It is possible to verify that the base metal presents a balanced microstructure (ferrite/austenite) while the weld bead a predominantly ferritic microstructure.

Figure 51 – SEM micrographs of transition region between fusion zone and base material for 15 µm

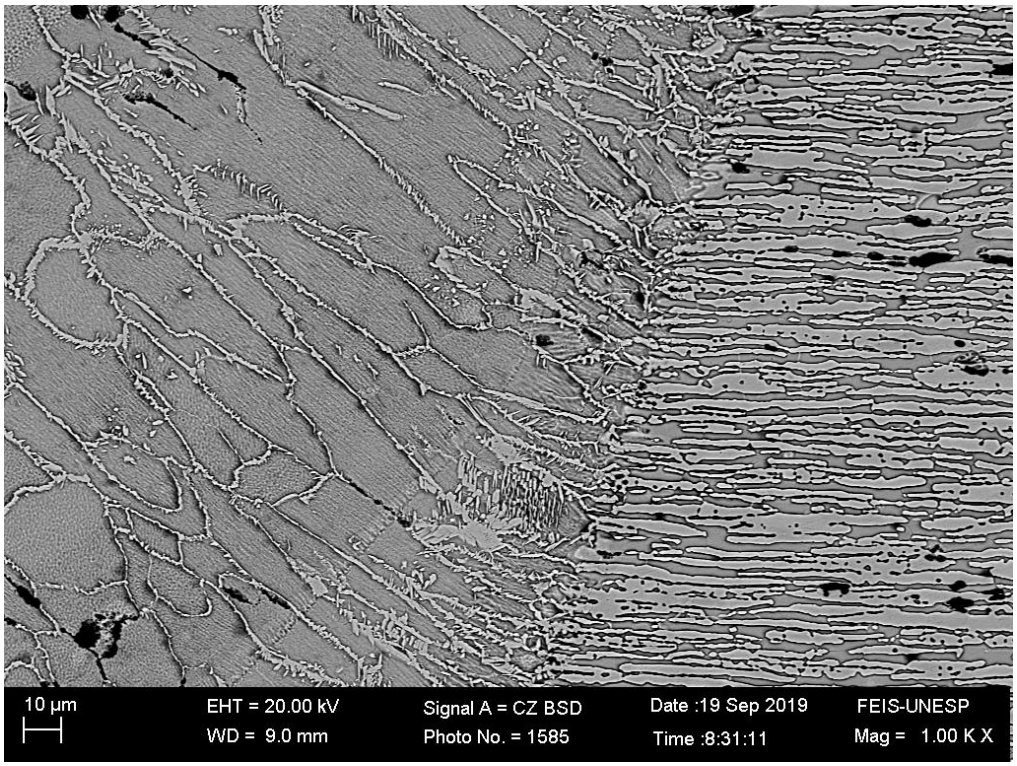

Source: Elaborated by author

It was performed an Energy-dispersive X-ray spectroscopy (EDS) analysis to determinate the amount (wt. %) of nickel on the weld bead. A line

analysis was made passing through the base metal and weld bead. Figure 52 shows the amount of Mo, Cr an Ni. The amounts of Mo and Cr remained constant and Ni increased to approximately 9 % (wt. %) on the weld bead.

Figure 52 – Mo, Cr and Ni on the base metal and weld bead (wt. %) for 15 µm.

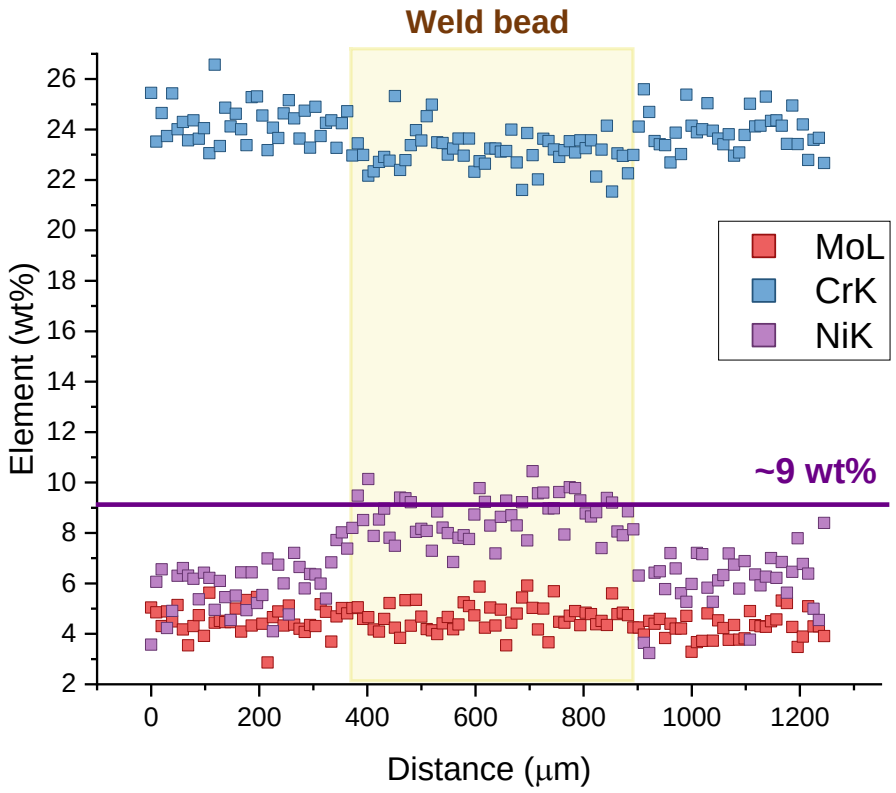

Source: Elaborated by author

The microstructures of the weld bead for the condition with 25 µm electrodeposited nickel layer are shown in Figure 53.

Figure 53 – SEM micrographs of fusion zone for 25 µm

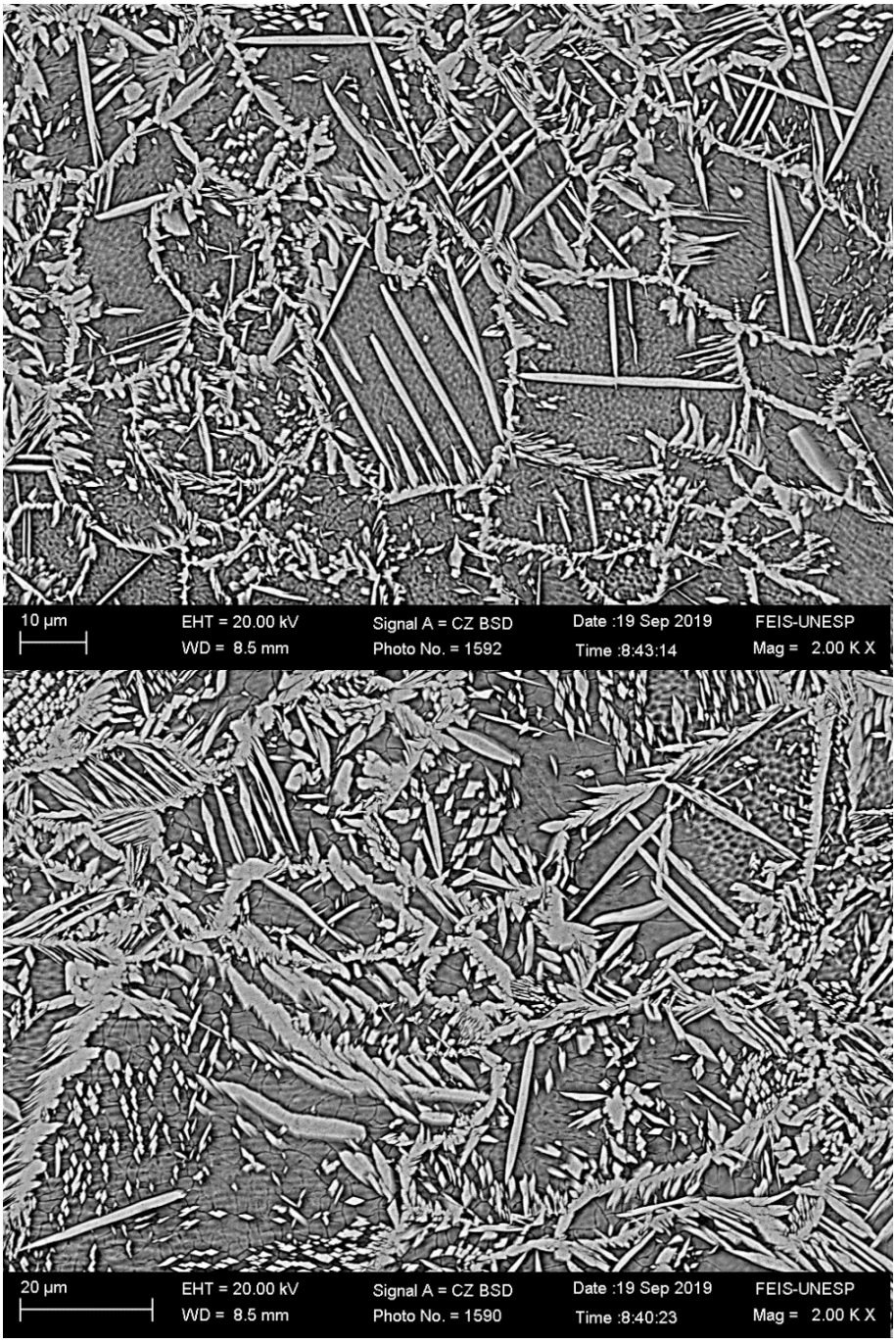

Source: Elaborated by author

The volume fraction of austenite was higher than that obtained using the 15 µm electrodeposited nickel layer. This condition presented 43.2 ± 2.3 % of austenite, the nickel amount was almost enough to achieve an well balanced microstucture.

The microstructure in the transition region between the base metal and weld bead for this condition is shown in Figure 54.

Figure 54 – SEM micrographs of transition region between fusion zone and base material for 25 µm

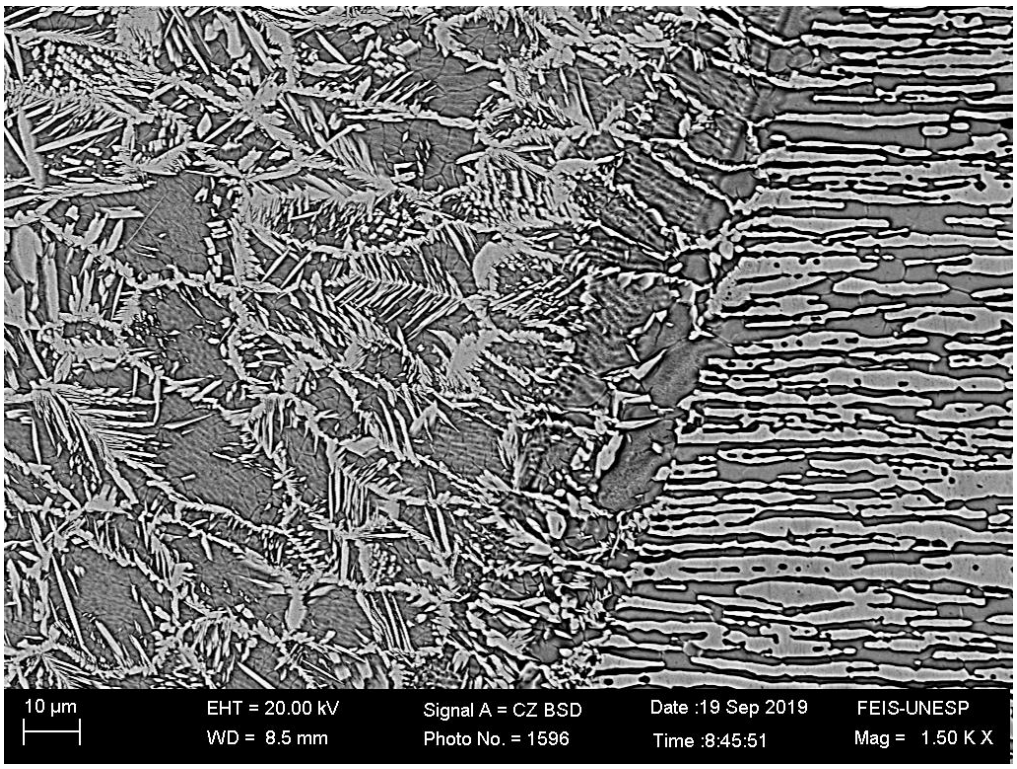

Source: Elaborated by author

As with the conditions presented in the thesis (using the electrolytic nickel foil), although the amount of austenite in the fusion zone is close to 50%, in the heat affected zone (HAZ) the amount of ferrite was higher than that of austenite

Figure 55 shows the amount of Mo, Cr and Ni (Energy-dispersive X-ray spectroscopy). The amounts of Mo and Cr remained constant and Ni increased to approximately 15 % (wt. %) on the weld bead.

Figure 55 – Mo, Cr and Ni on the base metal and weld bead (wt. %) for 25 µm

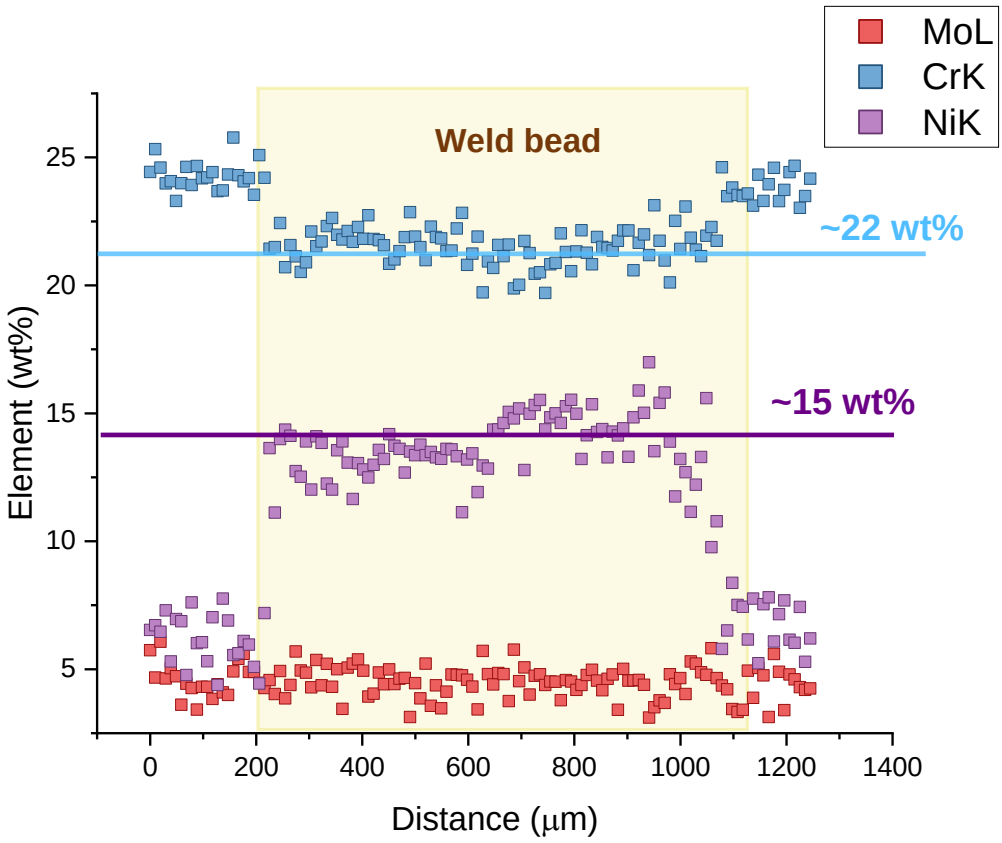

Source: Elaborated by author

The microstructure of the weld bead for the condition with 25 µm electrodeposited nickel layer are shown in Figure 56.

Figure 56 – SEM micrographs of fusion zone for 35 µm

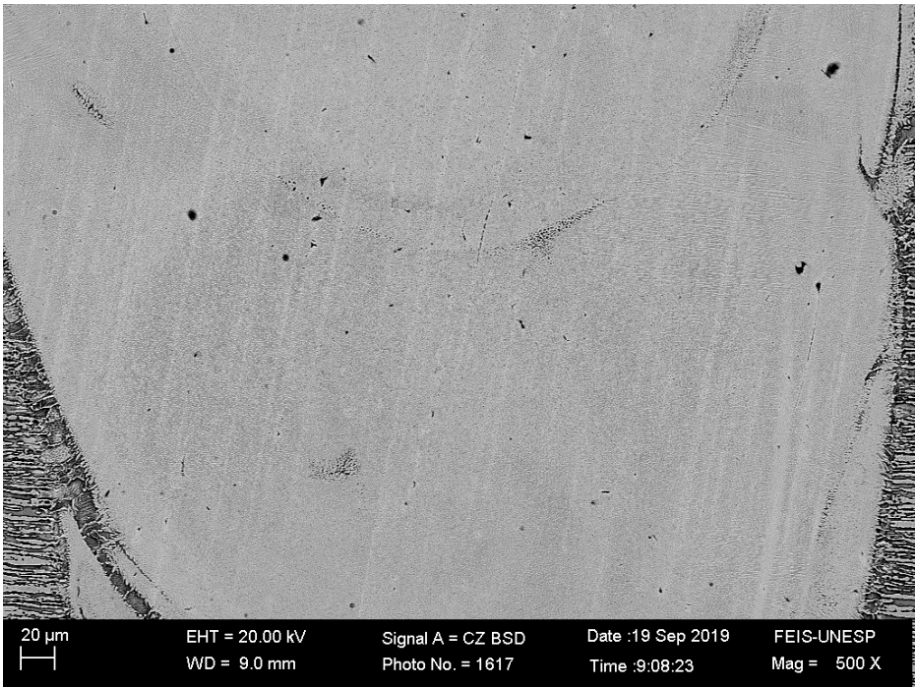

Source: Elaborated by author

The condition presented almost only austenite on the microstructure, being difficult determinate the volume fraction of ferrite. Comparing with the conditions using nickel foil, for a smaller nickel layer a predominantly austenitic structure was achieved. This will be one of the topics to be studied in the continuation of this research.

The microstructure in the transition region between the base metal and weld bead for this condition is shown in Figure 57. It is possible to verify that the base metal presents a balanced microstructure while the weld bead only austenite.

Figure 57 – SEM micrographs of transition region between base material and fusion zone for 35 µm

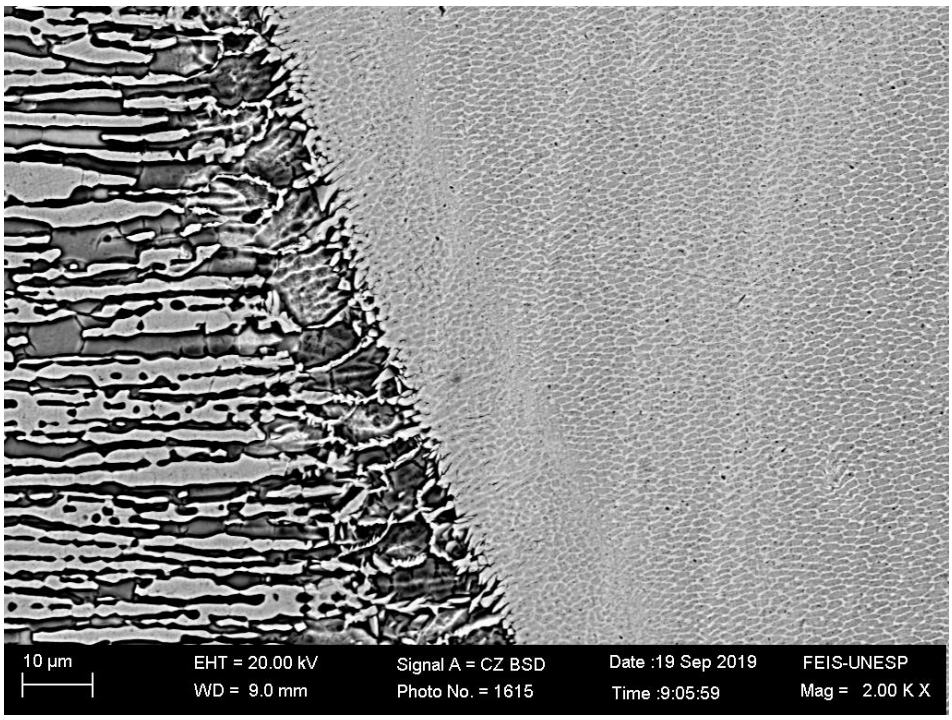

Source: Elaborated by author

A2.3 CONCLUSION

The following conclusions could be drawn:

- The Watts Bath can be used as a way to perform the nickel enrichment on DSS laser welding.
- The condition with 25 µm electrodeposited nickel layer was the one that came closest to the phase balance.
- The amount of austenite formed was different when comparing a certain thickness of nickel foil and the same thickness of the electrodeposited layer. This topic will be deeper studied in further works.